

# UNIVERSITY OF SALERNO

---

Department of Chemistry and Biology  
"Adolfo Zambelli"



*PhD Doctoral Course in Chemistry*  
XIV Cycle

## Sustainable Catalysis by Polymer Supported Gold Nanoparticles

**PhD Student**

Dr. Annarita Noschese

Matr. 8880700202

**Supervisor**

Prof. Alfonso Grassi

**Co-Supervisor**

Dr. Jose A. Lopez-Sanchez  
(*University of Liverpool*)

**Coordinator**

Prof. Gaetano Guerra

*Academic Year 2014/2015*







## **Table of Contents**

Table of Contents.....	1
Abstract.....	5
Abbreviations.....	7

### **CHAPTER 1: General Properties of Gold Nanoparticles**

1.1: Nanomaterials and Gold Nanoparticles.....	15
1.2: Properties of Gold Nanoparticles.....	18
1.2.1: Size and Shape.....	20
1.2.2: Oxidation state.....	22
1.3: Sustainable Catalysis by Gold Nanoparticles.....	23

### **CHAPTER 2: Synthesis and Characterization of Gold Nanoparticles**

2.1: A general introduction.....	29
2.2: Gold Nanoparticles protected with stabilizers.....	29
2.3: Gold Nanoparticles stabilized onto inorganic supports.....	31
2.3.1: Co-precipitation.....	34
2.3.2: Impregnation method.....	34
2.4: Gold Nanoparticles embedded in Organic Polymers.....	35
2.4.1: Synthesis of polymer protected AuNPs.....	35
2.5: Gold Nanoparticles onto Porous Supports.....	39
2.5.1: Gold Nanoparticles embedded in a Porous Polymer Support (AuNPs-sPSB).....	41
2.6: Methods for the Characterization of Gold Nanoparticles.....	44
2.6.1: UV-Vis spectroscopy.....	44
2.6.2: X-ray analysis.....	45
2.6.3: TEM and SEM analysis.....	46
2.6.4: N <sub>2</sub> adsorption analysis.....	46

2.7: Oxidation reactions catalyzed by AuNPs-sPSB .....	47
2.8: Aim of the PhD project .....	48

### **CHAPTER 3: Synthesis and Characterization of the AuNPs-sPSB catalyst**

3.1 The general synthetic route .....	53
3.2: Synthesis of the polymorphic forms of the AuNPs-sPSB catalyst: the <b>Au-C<math>\delta</math></b> , <b>Au-C<math>\beta</math></b> , <b>Au-C<math>\gamma</math></b> , <b>Au-C<math>\epsilon</math></b> catalysts .....	54
3.3: Morphological Characterization of the <b>Au-C<math>\delta</math></b> , <b>Au-C<math>\beta</math></b> , <b>Au-C<math>\gamma</math></b> , <b>Au-C<math>\epsilon</math></b> catalysts.....	55
3.4: Concluding remarks.....	61

### **CHAPTER 4: Oxidation Reactions catalyzed by AuNPs-sPSB**

4.1: Introduction.....	65
4.1.1: Oxidation reactions catalyzed by Gold Nanoparticles .....	68
4.1.2: Mechanistic hypothesis on alcohol oxidation and oxidative esterification of alcohols catalyzed by Gold Nanoparticles .....	70
4.2: Cinnamyl alcohol oxidative esterification catalyzed by AuNPs-sPSB	77
4.2.1: Cinnamyl alcohol oxidation.....	80
4.2.2: The reaction solvent .....	85
4.2.3: Cinnamyl alcohol oxidative esterification .....	86
4.2.4: Esterification with different alkyl alcohols.....	90
4.2.5: Esterification of <i>p</i> -substituted cinnamyl alcohols.....	93
4.2.6: Side reactions .....	96
4.3: Aerobic oxidation of amino-alcohols.....	98
4.4: Concluding remarks.....	100

## **CHAPTER 5: Nitroarenes Reduction catalyzed by Gold Nanoparticles**

5.1: Introduction.....	105
5.1.1: Nitrobenzene reduction catalyzed by Gold Nanoparticles.....	106
5.1.2: Mechanistic hypothesis on the NB reduction catalyzed by Gold Nanoparticles and other noble metals .....	108
5.1.3: Nitrobenzene reduction with nitroreductases .....	111
5.2: Co-crystals formed by nitroarenes and nanoporous forms of syndiotactic polystyrene.....	113
5.3: Nitroarenes reduction by AuNPs-sPSB.....	114
5.3.1: NB reduction catalyzed by <b>Au-C<math>\delta</math></b> , <b>Au-C<math>\beta</math></b> , <b>Au-C<math>\gamma</math></b> and <b>Au-C<math>\epsilon</math></b> . 114	
5.3.2: NB reduction with <b>Au-C<math>\epsilon</math></b> on varying the reaction conditions... 118	
5.3.3: Reduction of <i>p</i> -substituted nitroarenes .....	128
5.3.4: Mechanism of NB reduction with the <b>Au-C<math>\epsilon</math></b> catalyst .....	130
5.4: Concluding remarks.....	131

## **CHAPTER 6: Gold Colloids immobilized on Polymeric Support**

6.1: Catalytic activity of immobilized Gold Colloids.....	135
6.2: Sol-immobilization technique: preliminary results .....	137
6.2.1: Synthesis and characterization of gold colloids before and after immobilization on PPO .....	138
6.2.1: Synthesis of PVA stabilized gold colloids and immobilization on PPO.....	141
6.2.2: Synthesis of P123 stabilized gold colloids and immobilization on PPO.....	144
6.3: Concluding remarks.....	148

## **CONCLUDING REMARKS.....149**

## CHAPTER 7: Experimental Section

7.1: General Procedure and Materials.....	153
7.2: Instruments and Samples Preparation .....	154
7.2.1: AAS and ICP-OES.....	154
7.2.2: WAXD analysis.....	154
7.2.3: TEM and SEM analysis.....	155
7.2.5: GC analysis.....	155
7.2.6: NMR analysis.....	156
7.2.7: UV-Vis analysis .....	156
7.3: General procedures for the synthesis of the AuNPs-sPSB catalyst... 156	
7.3.1: Synthesis of the AuNPs-sPSB catalyst and Au-C $\delta$ , Au-C $\beta$ , Au-C $\gamma$ and Au-C $\epsilon$ .....	157
7.4 General procedure for the synthesis of the colloidal gold solutions.. 157	
7.5: General procedure for the immobilization of the gold colloidal solutions on PPO .....	157
7.6:General procedures adopted for the catalytic tests .....	157
7.6.1: General procedure for the oxidation of cinnamyl alcohols .....	157
7.6.2: General procedure for direct esterification of cinnamyl alcohol 158	
7.6.3: General procedure for direct esterification of cinnamaldehyde. 158	
7.6.4: General procedure the aerobic cleavage of double bond of cinnamaldehyde .....	159
7.6.5: General procedure for nitroarenes reduction.....	160



University of Salerno  
Department of Chemistry and Biology  
"Adolfo Zambelli"

*PhD Doctoral Course in Chemistry*  
XIV Cycle

# Sustainable Catalysis by Polymer Supported Gold Nanoparticles

## Abstract

Gold Nanoparticles are nanomaterials whose properties are completely different from the ones of the bulk material. Nowadays many chemists have been using them as catalysts which work under mild conditions and respect the principles *green* and *sustainable* chemistry. The increasing need for new heterogeneous catalysts to be applied in industrial processes encourages the finding of efficient and selective catalytic systems.

The aim of the current PhD project is the synthesis of gold nanoparticles (AuNPs) supported onto a porous polymer matrix, consisting of syndiotactic polystyrene-*co*-*cis*-1,4-polybutadiene (sPSB) and the use of this hybrid material in redox reactions.

Aerobic oxidative esterification of cinnamyl alcohol and nitroarenes reduction to amines were chosen as benchmark reactions to assess the activity and selectivity of the AuNPs-sPSB catalyst.

In cinnamyl alcohol oxidation and esterification, a large number of products can be obtained, coming from oxidation, dehydrogenation or

reduction pathways, but the catalytic system here presented resulted highly selective towards cinnamaldehyde and alkyl cinnamates. The synthetic protocol was successfully extended to *p*-substituted cinnamyl alcohols, and information about the effects of Electron Withdrawing or Electron Donating Groups on the esterification of cinnamyl alcohol were achieved.

Nitroarenes reduction to aniline derivatives is a complex multistep reaction, since the main intermediates are azoxybenzene and azobenzene. Once again, the AuNPs-sPSB catalyst was selective in the aniline formation. Different reaction pathways have been proposed for this reaction; under the reaction conditions here used the *condensation route* proposed by Haber was detected.

The access of reagents to the catalytic active site is facilitated by the presence of nanoporous polymeric matrix, whose role is to determine which species are able to permeate the polymeric matrix in order to reach the AuNPs. Different kinetic studies confirmed this initial hypothesis.

In addition to the AuNPs-sPSB catalyst, gold colloids were immobilized on a polymeric support in order to investigate a different synthetic approach for the achievement of gold nanoparticles. Different supports have been tested, *e.g.* polyvinyl alcohol, polyvinylpyrrolidone, cetrimonium bromide and P123 (a poloxamer triblock *co*-polymer). The removal of the colloid stabilizer was evaluated through catalytic tests.

**PhD Student**

Dr. Annarita Noschese  
Matr. 8880700202

**Supervisor**

Prof. Alfonso Grassi

**Co-Supervisor**

Dr. Jose A. Lopez-Sanchez  
(*University of Liverpool*)

## Abbreviations

**AAS:** Atomic Absorption Spectroscopy

**AB:** Azobenzene

**AN:** Aniline

**AOB:** Azoxybenzene

**Au-C $\beta$ :** AuNPs-sPSB catalyst with the syndiotactic polystyrene block in the  $\beta$  phase

**Au-C $\delta$ :** AuNPs-sPSB catalyst with the syndiotactic polystyrene block in the  $\delta$  phase

**Au-C $\epsilon$ :** AuNPs-sPSB catalyst with the syndiotactic polystyrene block in the  $\epsilon$  phase

**Au-C $\gamma$ :** AuNPs-sPSB catalyst with the syndiotactic polystyrene block in the  $\gamma$  phase

**AuNPs:** Gold Nanoparticles

**AuNPs-X:** Supported Gold Nanoparticles (X stands for a generic support)

**AuNPs-sPSB:** Gold Nanoparticles supported on sPSB

**BET:** Brunauer–Emmett–Teller (theory)

**CA:** Cinnamyl Alcohol

**C<sub>crit</sub>:** Critical Saturation Concentration

**CTAB:** cetyltrimethylammonium bromide

**DFT:** Density Functional Theory

**DMABA:** *p*-dimethylamino benzyl alcohol

**DMSO:** Dimethyl sulfoxide

**E<sub>a</sub>:** Activation Energy

**EDG:** Electron Donating Group

**EPR:** Electron Paramagnetic Resonance

**EWG:** Electron Withdrawing Group

**FAD:** flavin adenine dinucleotide

***fcc*:** face centered cubic

**FMN:** flavin mononucleotide

**FT-IR:** Fourier Transform InfraRed Spectroscopy

**FTIR-ATR:** Fourier Transform Infrared spectroscopy-Attenuated Total Reflectance

**GC-MS:** Gas Chromatograph-Mass Spectrometer

**FWTH:** Full Width at Half Maximum

$\lambda_{\text{spr}}$ : SPR band

**HAB:** Hydroazobenzene

**ICP-OES:** Inductively Coupled Plasma Optical Emission Spectroscopy

**MAO:** Methylaluminoxane

**MOFs:** Metal Organic Frameworks

*mol%*: molar percentage

**MTA:** mesoporous titania

**NADH:** nicotinamide adenine dinucleotide

**NADPH:** nicotinamide adenine dinucleotide phosphate

**NB:** Nitrobenzene

**NMR:** Nuclear Magnetic Resonance (Spectroscopy)

**NSB:** Nitrosobenzene

**P123:** poly(ethylene glycol)-poly(propylene glycol)-poly(ethylene glycol)  
(20:70:20)

**PHA:** Phenylhydroxylamine

**PPO:** Polyphenylene Oxide

**PVA:** Polyvinyl alcohol

**PVP:** Polyvinylpyrrolidone

**QSEs:** Quantum Size Effects

**SAED:** Selected Area (Electron) Diffraction

**SEM:** Scanning Electron Microscopy

**SPR:** Surface Plasmon Resonance

**sPSB:** Syndiotactic polystyrene-*co*-cis-1,4-polybutadiene

**TEM:** Transmission Electron Microscopy

$T_g$ : Glass Transition Temperature

**THF:** Tetrahydrofuran

$T_m$ : Melting Temperature

**TOF:** Turnover Frequency

**UV-Vis:** ultraviolet-visible (spectroscopy)

*v/v*: volume ratio

*v%*: volume percentage

**WAXD:** Wide Angle X-Rays Diffraction

*wt%*: weight percentage

*w/w*: weight ratio



*“Two roads diverged in a wood, and I  
I took the one less travelled by,  
And that has made all the difference”*

**Robert Frost, *The Road Not Taken*, 1916**

*“Ma Nino non aver paura di sbagliare un calcio di rigore  
Non è mica da questi particolari che si giudica un giocatore.  
Un giocatore lo vedi dal coraggio, dall'altruismo e dalla fantasia.”*

**Francesco De Gregori, *La leva calcistica del '68*, 1982**



# CHAPTER 1



## GENERAL PROPERTIES OF GOLD NANOPARTICLES



## 1.1: Nanomaterials and Gold Nanoparticles

Nanomaterials are defined as systems having particles with one or more dimensions in the range of 1-100 nm. The possibility of manipulating matter at the nanometric scale has attracted the interest of the whole scientific community (chemists, biologists, physicians, engineers), causing an increase in the number of publications in this field since 1990<sup>1</sup> (**Figure 1.1**).

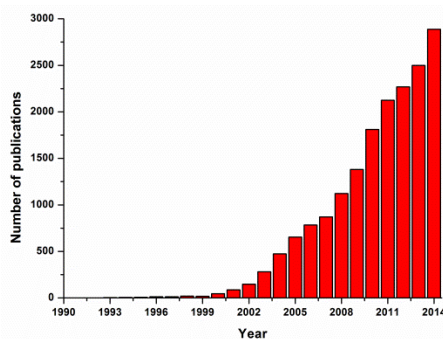


**Figure 1.1:** Number of publications per year dealing with nanomaterials (1990-2014). Source: SciFinder.

Gold Nanoparticles (AuNPs) are just one example of nanomaterials. They are characterized by a large surface-to-volume ratio and high surface energy compared to the bulk material, and for this reason are thermodynamically very unstable.

The formation of the AuNPs can be generally described with the LaMer model (**Figure 1.2**)<sup>2</sup> and can be divided in three stages: *i*) in stage I, for

<sup>1</sup> J. M. Campelo, A. A. Romero, D. Luna, R. Luque, J. M. Marinas, *ChemSusChem* **2009**, *2*, 18-45.

<sup>2</sup> **a)** K. Na, Q. Zhang, G. A. Somorjai, *J. Clust. Sci* **2014**, *25*, 83-114; **b)** C. B. Murray, C. R. Kagan, M. G. Bawendi, *Annu. Rev. Mater. Sci.* **2000**, *30*, 545-610; **c)** T. Sugimoto, F. Shiba, T. Sekiguchi, H. Itoh, *Coll. Surf. A: Physicochem. Eng. Asp.* **2000**, *164*, 183-203.

nucleation to occur, a supersaturated solution should be considered, either by directly dissolving the solute or by adding the necessary reactants to produce a supersaturated solution; *ii*) once the concentration of the reagents reaches the critical saturation concentration ( $C_{\text{crit}}$ ), the nucleation of particles starts, causing a decrease in their concentration (stage II, nucleation); *iii*) when the concentration of the reagents drops below the  $C_{\text{crit}}$ , the nucleation of new particles will cease and are only consumed for the particle growth (stage III, growth).

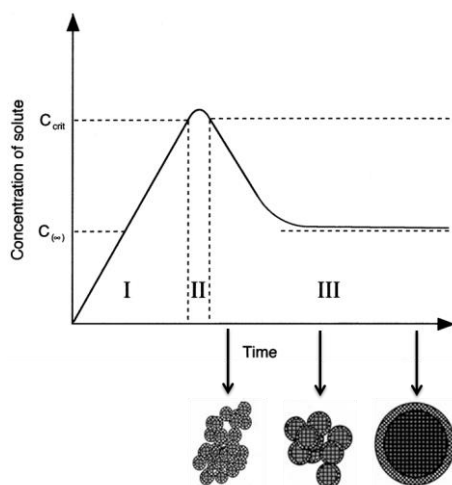


**Figure 1.2:** LaMer theoretical model for the nucleation and growth of nanoparticles.<sup>2</sup>

The final AuNPs size will depend strictly on the rate of nucleation and growth steps. Thus, to achieve an elevated number of the AuNPs having quite the same small size, an elevated number of nucleations are required in order that the metal precursor concentration reaches rapidly the level under the  $C_{\text{crit}}$ ; the rate of the growth stage will determine the final shape of the AuNPs (**Figure 1.3**).

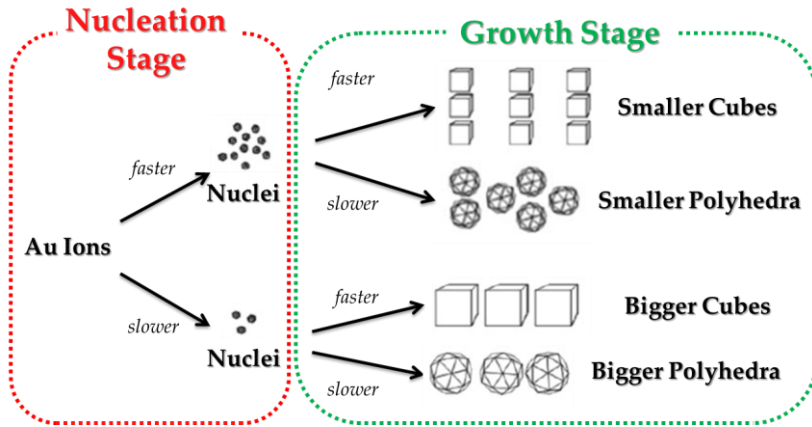


**Figure 1.3:** Influence of the rates of nucleation and growth stage in nanoparticles formation.

The first example of the use of the AuNPs is represented by Lycurgus Cup (**Figure 1.4**):<sup>3</sup> manufactured in 5<sup>th</sup> century B.C., this cup is ruby red in transmitted light and green in reflected light due to the presence of AuNPs and silver nanoparticles whose dimensions are in the range 5-60 nm.



**Figure 1.4:** Lycurgus cup observed with light **a)** in transmittance and **b)** in reflectance.

<sup>3</sup> U. Leonhardt, *Nat. Photonics* **2007**, 1, 207-208.

Lycurgus cup is a clear demonstration that AuNPs have properties completely different from the bulk material, and for this reason they find application in sensors, biosensors, diagnostic, information storage, photovoltaics, transistors, fuel cells, and as it will be later described, catalysis.

## 1.2: Properties of Gold Nanoparticles

The properties of the AuNPs which make them different from the bulk material depend on their *nano*-dimensions and are the Quantum Size Effects (QSEs) and the Surface Plasmon Resonance (SPR).<sup>4</sup>

Moving from the bulk material to *nano* size, the gap between the gold electronic states becomes larger, so the electrons can be localized and the AuNPs act as semi-conductors rather than conductors (**Figure 1.5**); all the phenomena related to this increase of separation in electronic states are called QSEs. For example, AuNPs show different colour depending on their size.

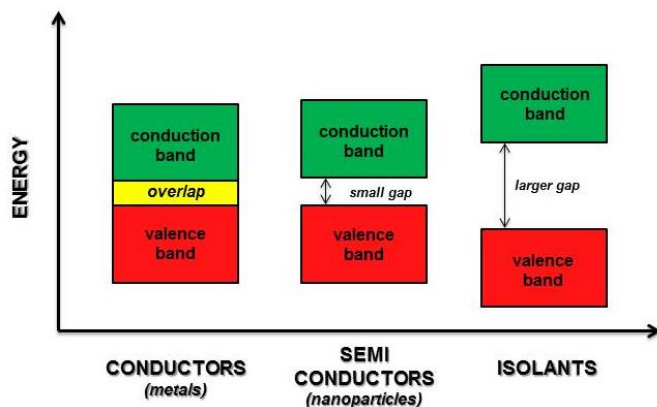


**Figure 1.5:** Separation of energetic levels of conductors, semi-conductors and isolants.

<sup>4</sup> G. Schmid, B. Corain, *Eur. J. Inorg. Chem.* **2003**, 3081-3098.

When the AuNPs interact with a strong electromagnetic radiation having a wavelength comparable to the nanoparticle dimension, the electrons located at the surface (*plasmon*) will start having a collective coherent oscillation (SPR) in the direction of the electric field of the radiation (**Figure 1.6**).<sup>5</sup> Since this is a surface property, everything that modifies the environment of the nanoparticle has consequences on the local SPR.

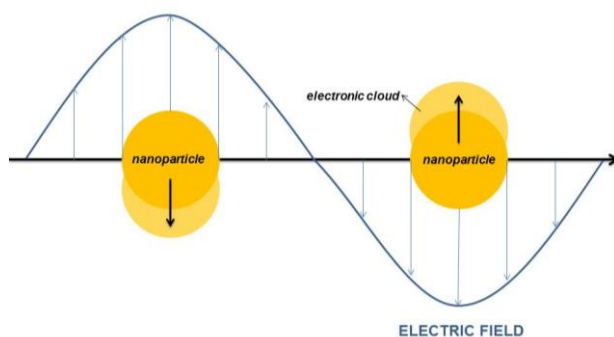


**Figure 1.6:** Resonance of the plasmon of the AuNPs.

The crystalline structure of gold is a *face centered cubic (fcc)* (**Figure 1.7**), where more than 74% of the space in the unit cell is occupied by gold atoms.<sup>6</sup> In an infinite lattice, each atom located at the corner of the cube is shared among 8 cubes, while the atoms centered on the facets of the cell are shared among only two cells. Since AuNPs are not infinite structures, the atoms on the surface will be coordinatively unsaturated and thermodynamically unstable.

<sup>5</sup> **a)** P. K. Jain, X. Huang, I. H. El-Sayed, M. A. El-Sayed, *Acc. Chem. Res.* **2008**, *41*, 1578-1586; **b)** K. A. Willets, R. P. Van Duyne, *Acc. Rev. Phys. Chem.* **2007**, *58*, 267-297.

<sup>6</sup> *Material Chemistry*, B. D. Fahlman, Springer, **2007**.

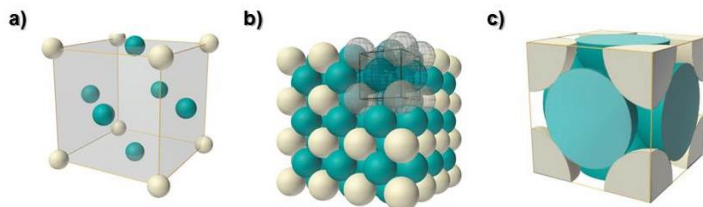


**Figure 1.7:** *fcc* lattice of gold in different representations: a) ball-and-stick model, b) aggregate of several unit cells and c) a space-filling cutaway model that shows the portion of each atom that lies within the unit cell. Source: <http://chemwiki.ucdavis.edu/>

The catalytic activity of the AuNPs arises from the sum of many factors, *e.g.* size, shape, oxidation state, type of support; obviously each of these parameters doesn't act separately, but there is always an interconnection among them.

### 1.2.1: Size and Shape

Both catalytic activity and selectivity are influenced by the AuNPs size since the energy of the surface atoms changes with the size of the AuNPs.

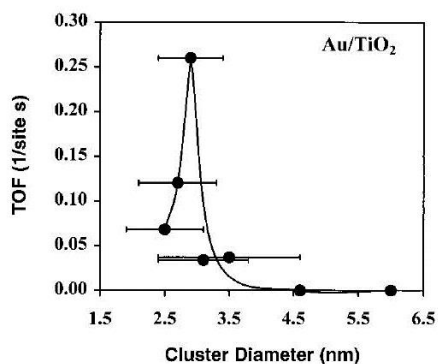


**Figure 1.8:** Relation between AuNPs size and activity in CO oxidation reaction.<sup>8</sup>

For example, Prati and co-workers<sup>7</sup> demonstrated that the catalytic activity of AuNPs supported on carbon in glycerol oxidation decreases with the increasing of the AuNPs size. The importance of the AuNPs size has been underlined also by Goodman *at al.* in CO oxidation.<sup>8</sup>

High values of TOF were achieved by reducing the size of the AuNPs

<sup>7</sup> N. Dimitratos, J.-A. Lopez-Sanchez, D. Lennon, F. Porta, L. Prati, A. Villa, *Catal. Lett.* **2006**, *108*, 147-153.

<sup>8</sup> M. Valden, X. Lai, D. W. Goodman, *Science* **1998**, *281*, 1647-1650.

supported on TiO<sub>2</sub>, as result from the inspection of **Figure 1.8**. However, the decrease in activity under  $\sim 3$  nm was not explained. Finally, Lopez and co-workers<sup>9</sup> found a  $\sim 1/d^3$  dependence of the catalytic activity *vs* the particle diameter  $d$ .

However it would be more appropriate to talk about a distribution range rather than a well-defined number, and all catalytic results should be analysed in light of that.

The shape of the AuNPs determines the energy values of the Au atoms located on different facets, edge or corner, as previously said.

The AuNPs shape can be generally modified by the amount of gold precursor, type of the support, presence of defects, confinement effects (in template synthesis) and presence of impurities.<sup>10</sup> For metal having a *fcc* crystalline structure like gold, at 0 K the equilibrium shape is a truncated octahedron (**Figure 1.9**), but this can change at the nanometric scale since surface energy and stress increase and different structures, like the icosahedral one, can become more stable. Truncated morphologies can be observable even when there is strong adhesion of the AuNPs to the support.<sup>11</sup>

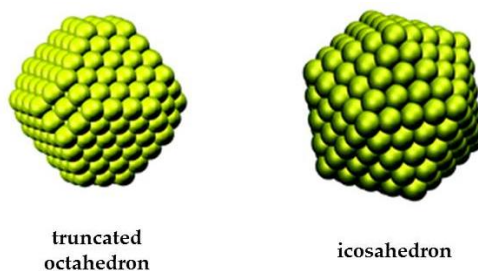


**Figure 1.9:** Different possible shapes for gold nanoparticles.

<sup>9</sup> N. Lopez, T. V. W. Janssens, B. S. Clausen, Y. Xu, M. Mavrikakis, T. Bligaard, J. K. Nørskov, *J. Catal.* **2004**, *223*, 232-235.

<sup>10</sup> C. R. Henry, *Progr. Surf. Sci.* **2005**, *80*, 92-116.

<sup>11</sup> *Advances in Catalysis*, B. Gates, F. Jentoft, *Elsevier*, **2012**.

### 1.2.2: Oxidation state

In general, gold can assume three oxidation states, I, III and obviously 0, but the real nature of surface gold atoms under catalysis conditions is still under discussion. It has been demonstrated that the oxidation state depends from both experimental conditions (temperature, pressure) and interactions between the oxide-based support.<sup>12</sup>

The presence of defects on the surface of the support can enhance the catalytic activity for the presence of strong interactions between the AuNPs and the support itself. Guzman and Gates investigated this issue by considering CO oxidation catalyzed by AuNPs supported on highly defected MgO.<sup>13</sup> The catalyst was prepared by treating the inorganic support with

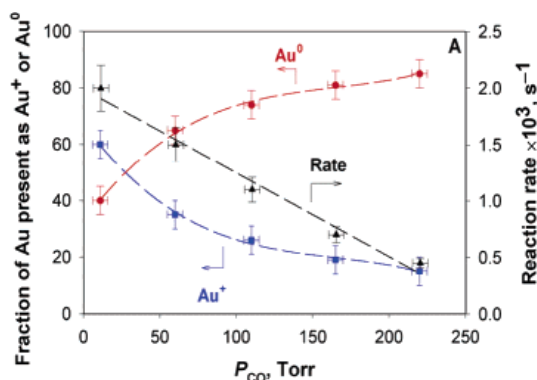


**Figure 1.10:** Effect of CO pressure on Au(I) and Au(0) concentration and on the rate of CO oxidation.<sup>13</sup>

Au(III)(dimethylacetylacetonate) followed by in situ reduction with a mixture of CO (used both as reducing agent and reagent) and  $O_2$  at 373K. The presence of Au(III) is excluded by inspection of X-ray Absorption Near Edge Structure spectra (XANES) and only of Au(I) and Au(0) species were detected. The relative mole ratio of Au(I) and Au(0)

depends on the amount of CO and  $O_2$  used in the reduction step/reaction; the catalytic activity was related to the amount of Au(I) during the reaction, that diminished when the amount of CO was increased (**Figure 1.10**).

<sup>12</sup> S. Laursen, S. Linic, *Phys. Rev. Lett.* **2006**, 97, 026101.

<sup>13</sup> J. Guzman, B. C. Gates, *J. Chem. Am. Soc.* **2004**, 126, 2672-2673.

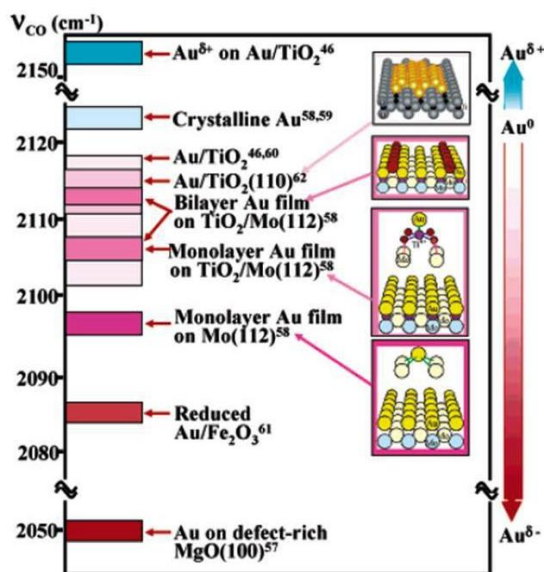


**Figure 1.11:** Stretching frequencies for CO adsorbed on different gold heterogeneous catalysts.<sup>14</sup>

Chen and Goodman analysed the nature of AuNPs supported on different metal oxides by Infra-Red spectroscopy (IR): by the inspection of the stretching frequency of CO adsorbed on the metal it is possible to understand the electron density on the AuNPs surface, since  $\nu_{\text{CO}}$  shifts to lower frequency when CO is adsorbed onto electron-rich gold, whereas  $\nu_{\text{CO}}$  shifts to higher values, when an electron-deficient gold species is present (Figure 1.11).<sup>14</sup>

### 1.3: Sustainable Catalysis by Gold Nanoparticles

Gold has been generally considered as an inert metal until Haruta<sup>15</sup> and Hutchings<sup>16</sup> reports on the catalytic activity of the AuNPs in low tempera-

<sup>14</sup> M. Chen, D. W. Goodman, *Acc. Chem. Res.* **2006**, *39*, 739-746.

<sup>15</sup> M. Haruta, T. Kobayashi, H. Sano, N. Yamada, *Chem. Lett.* **1987**, *16*, 405-408.

<sup>16</sup> G. J. Hutchings, *J. Catal.* **1985**, *96*, 292-295.

ture aerobic oxidation of CO to CO<sub>2</sub> and in hydrochlorination of acetylene, respectively.

Since then, the *gold rush* started, and nowadays many catalytic processes involving the use of AuNPs have been developed.

The first definition of *catalyst* was given by Berzelius in 1836; according to this, a catalyst is a "soluble and insoluble simple and compound bodies that have the property of exercising on other bodies an action very different from chemical affinity, and that remain unaltered through the reaction"<sup>17</sup>. However, this definition illustrates only partially the main role of a catalyst: it is able to increase the rate of reaction since it finds a reaction pathway different from the non-catalyzed reaction and characterized by a lower activation energy (**Figure 1.12**).<sup>18</sup> The catalyst is completely restored at the end of the catalytic cycle.

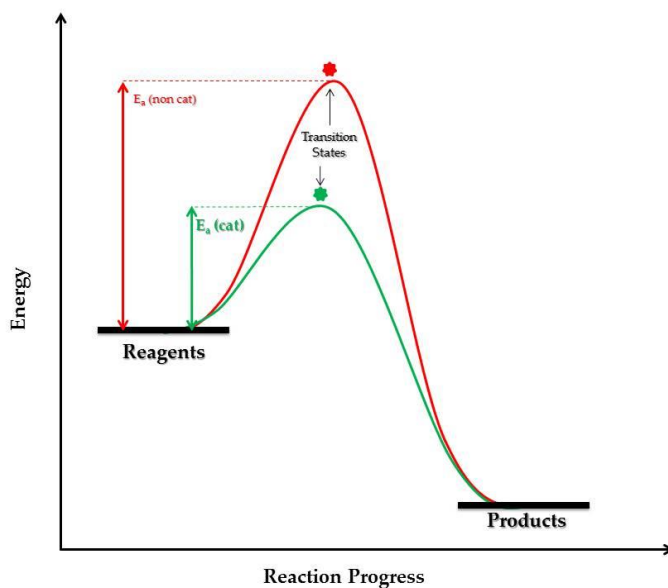


**Figure 1.12:** Generic reaction energy diagram for a non-catalyzed (red) and for a catalyzed (green) reaction, characterized by a lower activation energy.

<sup>17</sup> B. Lindstrom, L.J. Pettersson, *CATTECH* **2003**, 7, 130.

<sup>18</sup> *Kinetic and Mechanism*, J. W. Moore, R. G. Pearson, Wiley, 1981.

The use of supported AuNPs catalysts (*heterogeneous catalysts*) offers many advantages compared to *homogeneous catalysts*. In fact they have a higher thermal stability, are cheaper and can be easily recovered from the reaction medium.

Actually many different chemical transformations involve the use of heterogeneous AuNPs based catalysts, *e.g.* alkane and alcohol oxidation, alkene epoxidation, direct synthesis of hydrogen peroxide, carbon-carbon coupling reactions, hydrogenation reactions and hydrochlorination of alkyne.<sup>19</sup>

These reactions are generally carried out under mild reaction conditions, *e.g.* atmospheric pressure, room temperature, in aqueous media or under solvent-free conditions, thus the principles of *green and sustainable chemistry* defined by Anastas and Warner are respected.<sup>20</sup> In addition to that, AuNPs can be manipulated under air and they are not sensitive to moisture.

The importance of AuNPs based catalysts in industrial applications is proved by the high number of patents actually present in this field owned by companies like Johnson Matthey, 3M, Degussa and Toyota.<sup>21</sup> The development of these heterogeneous AuNPs based catalysts is a key point for the economic development if it is considered that around the 80% of all industrial processes actually involve a catalytic step, and it is foreseen that the catalyst market will reach the value of 27.59 billion dollars by 2020, corresponding to a catalysts production of 7.803 kilo tons.<sup>22, 23</sup>

---

<sup>19</sup> a) C. Della Pina, E. Falletta, M. Rossi, *Chem. Soc. Rev.* **2012**, *41*, 350-369; b) S. E. Davis, M. S. Ide, R. J. Davis, *Green Chem.* **2013**, *15*, 17-45; c) M. Stratakis, H. Garcia, *Chem. Rev.* **2012**, *112*, 4469-4506; d) Y. Zhang, X. Cui, F. Shi, Y. Deng, *Chem. Rev.* **2012**, *112*, 2467-2505; e) T. Mallat, A. Baiker, *Chem. Rev.* **2004**, *104*, 3037-3058.

<sup>20</sup> *Green Chemistry: Theory and Practice*, P. T. Anastas, J. C. Warner, Oxford University Press: New York, **1998**.

<sup>21</sup> C. C. Corti, R. K. Holliday, D. T. Thompson, *Top. Catal.* **2007**, *44*, 331-343.

<sup>22</sup> *Catalyst Market Analysis*, Grand View Research, Market Research & Consulting, **August 2014**.

<sup>23</sup> *Synthesis of Solid Catalysts*, K. P. de Jong, WILEY-VCH Verlag GmbH & Co. KGaA, Weinheim, **2009**.



# CHAPTER 2



## SYNTHESIS AND CHARACTERIZATION OF GOLD NANOPARTICLES



## 2.1: A general introduction

Different synthetic procedures are nowadays available to achieve AuNPs, and they are all based on the succession of three steps: 1) formation of a solution of the support; 2) addition of the gold precursor; 3) addition of the reducing agent.<sup>24</sup>

The most used gold precursor is tetrachloroauric acid ( $\text{HAuCl}_4 \cdot \text{H}_2\text{O}$ ): it is a moisture sensitive orange solid (**Figure 2.1**), therefore some precautions must be used when a gold catalyst is going to be prepared. Alternative gold precursors are  $\text{HAuCl}_4 \cdot \text{H}_2\text{O}$  are  $\text{Au}(\text{PPh}_3)(\text{NO}_3)$  and  $\text{Au}(\text{CH}_3\text{COO})_3$ .<sup>23</sup>

In general  $\text{NaBH}_4$  is used for the reduction of the gold precursor, but the formation of the AuNPs can occur also through thermal annealing after calcination of the catalyst.

The use of a support for the AuNPs is necessary to stabilize them and to minimize their surface energy, thus preventing their sintering and avoiding the loss of their catalytic properties. The stabilization can occur with capping agents in liquid phase or inorganic/polymeric supports, therefore obtaining heterogeneous catalysts.



**Figure 2.1:** A sample of  $\text{HAuCl}_4 \cdot \text{H}_2\text{O}$ .

## 2.2: Gold Nanoparticles protected with stabilizers

A *colloidal dispersion* is a system in which particles of colloidal size of any nature (e.g. solid; liquid or gas) are dispersed in a *continuous phase* of a different composition (or state).<sup>25</sup>

Hence colloidal gold is a three component system, in which the AuNPs are stabilized by a capping agent and dispersed in a solution (**Figure 2.2**).

<sup>24</sup> V. V. Pushkarev, Z. Zhu, K. An, A. Hervier, G. A. Somorjai, *Top. Catal.* **2012**, *55*, 1257-1275.

<sup>25</sup> IUPAC *Compendium of Chemical Terminology*, **1972**, 31, 605.

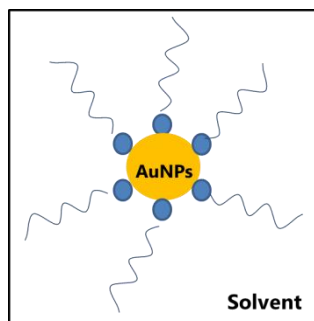


**Figure 2.2:** Schematic representation of a colloidal nanoparticle system based on gold.

This colloidal approach has been the first methodology developed to stabilize the AuNPs.

Turkevich reported in 1951 the citrate-based colloidal AuNPs synthesis,<sup>26</sup> where citrate molecules were used both as reducing and protective agent; AuNPs having an average size of 20 nm can be generally obtained. The Brust method, published in 1994, is based on the use of thiolate ligands to stabilize AuNPs;<sup>27</sup> the AuNPs obtained according to this procedure are highly stable for the presence of strong Au-S bonds.

Some of the most used stabilizers are polyvinyl alcohol (PVA) or cetyltrimethylammonium bromide (CTAB). If it is not possible to form covalent bonds (like for Brust method), the stabilization can alternatively occur with electrostatic/steric interactions, steric or a combination of both. In the electrostatic stabilization, the AuNPs are surrounded by an electrical double layer: the sintering is therefore minimized for the Coulombic repulsion. In the steric stabilization, the use of large molecules like high molecular weight polymers prevents the aggregation of AuNPs. The third option is a combination of the ones just described, and it is named electrosteric stabilization.<sup>28</sup>

To facilitate the recovery of the AuNPs, it is possible to immobilize the colloid on a support; however, the resulting catalyst will show a poor activity until the removal (at least partial) of the stabilizer. The removal of the stabilizer can occur, for example, by heat treatment.<sup>29</sup> The final AuNPs dispersion will depend basically from the presence of a high surface area

<sup>26</sup> J. Turkevich, P.C. Stevenson, J. Hillier, *Discuss. Faraday Soc.* **1951**, *11*, 55.

<sup>27</sup> M. Brust, M. Walker, D. Bethell, D.J. Schiffrin, R.J. Whyman, *J. Chem. Soc., Chem. Commun.* **1994**, 801.

<sup>28</sup> C.-J. Jia, F. Schüth, *Phys. Chem. Chem. Phys.*, **2011**, *13*, 2457–2487.

<sup>29</sup> L. Prati, A. Villa, *Acc. Chem. Res.* **2014**, *47*, 855–863.

support and by the eventual presence of functional groups on the solid material.

### **2.3: Gold Nanoparticles stabilized onto inorganic supports**

Many metal oxides have been reported as supports for the AuNPs. TiO<sub>2</sub>, SiO<sub>2</sub>, and Al<sub>2</sub>O<sub>3</sub> are often used since they have high mechanical, high porosity and high surface area (>100 m<sup>2</sup> g<sup>-1</sup>)<sup>30</sup>. Fe<sub>3</sub>O<sub>4</sub> is a superparamagnetic oxide, and its recovery from the reaction medium could be very simple just by using a permanent magnet. The surface of these oxides may contain hydroxyl groups, which could favour the adsorption of metal precursor and influence the interaction between the support and the AuNPs during the catalytic tests.

All these material have high thermal stability, thus the formation of the AuNPs can be achieved by calcination.

In addition to their use as support, metal oxides can play further roles: 1) they can furnish additional reaction sites, such as oxygen vacancies; 2) they can stabilize intermediate reaction species; 3) they can transfer electronic charge to the AuNPs. In all this cases, the effect of the support will be determined by the amount of contacts with the AuNPs.

The strength of support stabilization will have effects also on the AuNPs shape, which is basically determined by the *contact angle* defined by **Equation 2.1**, where the physical quantities  $\gamma$  represent the energies between the support and the gas phase ( $\gamma_{sg}$ ), the AuNPs and the support ( $\gamma_{ms}$ ), and between the AuNPs and the gas phase ( $\gamma_{mg}$ )<sup>31</sup> (**Figure 2.3**).

$$\cos\theta = \frac{(\gamma_{sg} - \gamma_{ms})}{\gamma_{mg}}$$

**Equation 2.1:** Contact angle definition in relation to the strength of interactions between the NPs and support.

<sup>30</sup> R. J. White, R. Luque, V. L. Budarin, J. H. Clark, D. J. Macquarrie, *Chem. Soc. Rev.* **2009**, 38, 481-494.

<sup>31</sup> *Catalysis by Gold*, G. J. Hutchings, Imperial College Press, **2006**.

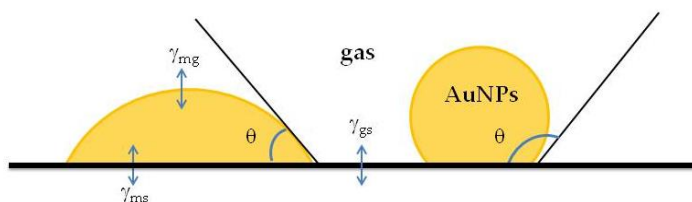


**Figure 2.3:** Interactions between the AuNPs, gas and support, and definition of contact angle.

When  $\gamma_{ms}$  is large, namely when the interaction between the AuNPs and the support is strong, the nanoparticle will *wet* the support, and its shape will be not spherical or cubo-octahedral anymore (this happens when  $\gamma_{ms}$  is small), hemispherical or truncated cubo-octahedral.

The interactions between the AuNPs and  $\text{TiO}_2$  have been recently described in details;<sup>32</sup> the gold atoms can be strongly stabilized, resulting almost *bound* to the support, so that the growth of the AuNPs is influenced by this *bond* (**Figure 2.4**). As consequence if the support has a lot of defects, defected AuNPs are obtained.

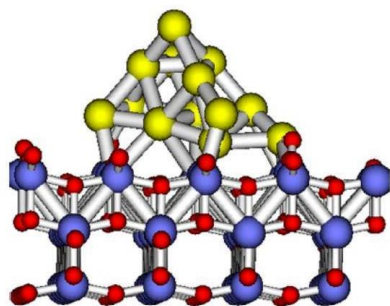


**Figure 2.4:** Model of a AuNPs growing on titania.<sup>32</sup>

For metal oxides based supports, the control of oxygen vacancies could be decisive in oxidation reactions since in their absence low catalytic activities

can be observed.<sup>33</sup> The highest oxygen vacancy is observable in  $\text{TiO}_2$  and  $\text{Fe}_2\text{O}_3$ , while the AuNPs supported on oxides like  $\text{SiO}_2$  or  $\text{Al}_2\text{O}_3$  have, in

<sup>32</sup> *New and Future Development in Catalysis – Catalysis by Nanoparticles*, S. L. Sub, Elsevier, 2013.

<sup>33</sup> J.A. Rodriguez, P. Liu, J. Hrbek, J. Evans, M. Perez, *Angew. Chem. Int. Ed.* **2007**, 1329-1332.

general, lower catalytic activity.<sup>12</sup> Alternatively, CeO<sub>2</sub> can be used as support.

The lack of oxygen in metal oxide structures can be filled by oxygen uptake from the gas phase,<sup>32</sup> thus resulting in oxygen activation. For this reason the AuNPs-CeO<sub>2</sub> catalyst results active in the low-temperature CO oxidation with O<sub>2</sub> and neat primary and secondary alcohol oxidation, both aliphatic and aromatic.<sup>34</sup>

Metal oxides can have a role also in determining the oxidation state of the atoms located on the surface of the AuNPs by pulling or giving electrons, and this effect can be measured through X-ray Photoelectron Spectroscopy (XPS) analysis. Gold shows a characteristic peak of the 4f<sub>7/2</sub> electron level and the energy of this band depends on the oxidation state (+I, +III, 0); in **Figure 2.5** an XPS spectra of the AuNPs-CeO<sub>2</sub> catalyst is reported.<sup>32</sup> The deconvolution of the experimental spectral profile (black line, **Figure 2.5**) clearly demonstrates that, in the AuNPs-CeO<sub>2</sub> catalyst some cationic gold species can be present.

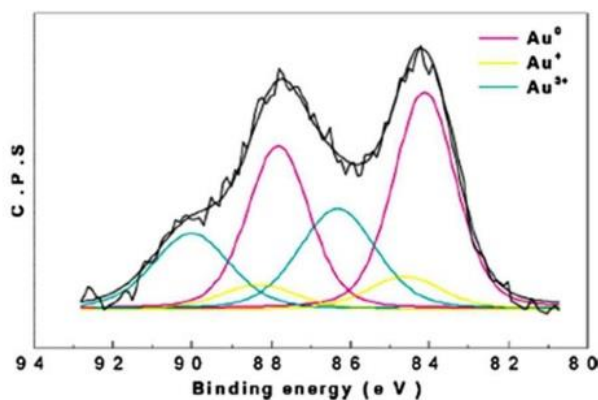


**Figure 2.5:** Deconvolution of XPS spectra of the AuNPs-CeO<sub>2</sub>.<sup>32</sup>

<sup>34</sup> A. Abad, P. Concepción, A. Corma, H. García, *Angew. Chem.* **2005**, *117*, 4134–4137.

Nowadays many different procedures for supporting AuNPs have been reported in literature; some of these are: *deposition-precipitation*, *deposition-reduction*, *chemical-vapour deposition*, however the *co-precipitation* and the *impregnation* methods are generally used.<sup>31</sup>

### **2.3.1: Co-precipitation**

The *co-precipitation* method was employed for the first time in 1987 and consists in the simultaneous precipitation of both support and gold precursors, thus achieving the direct incorporation of the AuNPs in the support.<sup>1</sup> The relative rate of precipitation of support and gold precursors is the main parameter to be controlled if this synthetic procedure is used. In these cases, since two different species are reduced, different type of salts are obtained as by-products, and if these are not completely eliminated from the solid catalyst during the final washing step, a suppressed catalytic activity could result, *e.g.* these by-products could favour the mobility of AuNPs over the solid support during the catalytic run, thus increasing their size. Nevertheless, this method allows the preparation of AuNPs dispersed in the support in a homogeneous way.<sup>23</sup>

### **2.3.2: Impregnation method**

The *impregnation* method is the simplest way to support AuNPs, and can be applied, at least in principle, to any porous material. Firstly, the support, just like a sponge, is wetted with a solution of the metal precursor, and then the solvent is slowly evaporated (*drying step*), thus concentrating the solution of the gold precursor up to saturation and crystallization conditions.<sup>23</sup> Finally, the catalyst is calcinated to produce the AuNPs.<sup>11</sup>

Two different impregnation procedures are available, depending on the volume of solution added to solid support:<sup>23</sup> if an excess of gold precursor solution is used, the method will be called *wet impregnation*. On the contrary, in the *wetness impregnation* method called also *pore volume impregna-*

tion or *dry impregnation*, the gold precursor salt is dissolved in the lowest amount of solvent.<sup>1</sup>

## **2.4: Gold Nanoparticles embedded in Organic Polymers**

In addition to metal oxides, organic polymers, under the form of powders, granules, membranes and fibers, can be used as support for the AuNPs.<sup>35, 36</sup> The advantages of polymeric supports *vs.* metal oxides are: *i*) they can be easily synthesized, thus being easily available; *ii*) they can be functionalized in order to modify the chemical environment of the AuNPs, thus influencing the selectivity of the catalyst; *iii*) they can be crosslinked, in order to prevent gold leaching; *iv*) they can be swelled in order to favour the access of the reagents to the AuNPs.<sup>37, 36, 38</sup>

### **2.4.1: Synthesis of polymer protected AuNPs**

At least in principle, all of the synthetic method described for the AuNPs supported on metal oxides can be used also with polymers; the main drawback is that these materials have lower thermal stability compared to the oxides, thus calcination steps cannot be used. In most of the cases, the final formation of the AuNPs is achieved by using different chemical agents, such as sodium formate, formaldehyde, alcohols, hydrogen gas, hydrazine and sodium borohydride.<sup>36</sup>

Hereafter four different examples of available methods to synthesize AuNPs-polymer embedded are described (**Figure 2.6**).<sup>39</sup>

Tsukuda<sup>40</sup> reported the synthesis of very small AuNPs (1.3 nm) stabilized by the amide groups of poly(*N*-vinylpyrrolidone) (PVP, **a**, **Figure 2.6**).

---

<sup>35</sup> J. Shan, H. Tenhu, *Chem. Commun.* **2007**, 4580-4598.

<sup>36</sup> S. Sarkar, E. Guibal, F. Quignard, A. K. SenGupta, *J. Nanopart. Res.* **2012**, *14*, 715.

<sup>37</sup> Y. Ofir, B. Samanta, V. M. Rotello, *Chem. Soc. Rev.* **2008**, *37*, 1814-1825.

<sup>38</sup> M. Králik, A. Biffis, *J. Mol. Catal. A Chem* **2001**, *177*, 113-138.

<sup>39</sup> T. Ishida, M. Haruta, *Angew. Chem. Int. Ed.* **2007**, *46*, 7154 - 7156.

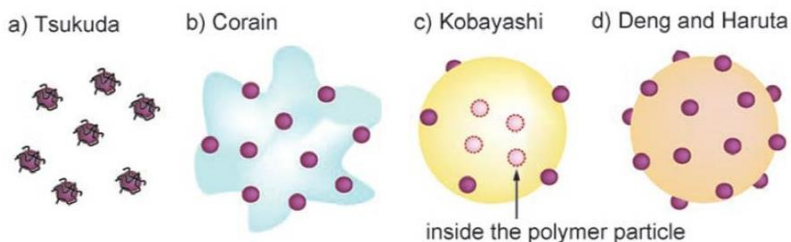


**Figure 2.6:** Four main classes of polymer stabilized metal nanoparticles: a) colloidal solutions with soluble polymers; b) AuNPs stabilized with resins; c) AuNPs embedded into a polymeric matrix; d) AuNPs located at the surface of a polymer.<sup>39</sup>

PVP and  $\text{HAuCl}_4$  were dissolved in water and then a water solution of  $\text{NaBH}_4$  was rapidly added, leading to the formation of the AuNPs. This catalyst was found to be really active in benzyl alcohol oxidation in water. Corain *et al.*<sup>41</sup> used a crosslinked *co*-polymer, namely poly-2-(methylthio)ethyl methacrylate-*N,N*-dimethylacrylamide-*N,N*-methylenebisacrylamide (4–88–8 mol%) (MTEMA-DMAA-4–8) to support AuNPs (b, Figure 2.6 and Figure 2.7).

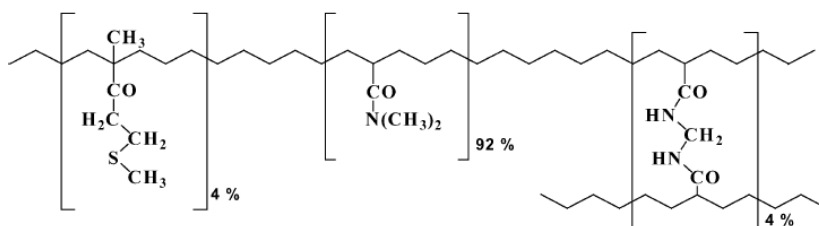


**Figure 2.7:** Structure of MTEMA-DMAA-4–8 resin.<sup>41</sup>

<sup>40</sup> H. Tsunoyama, H. Sakurai, Y. Negishi, T. Tsukuda, *J. Am. Chem. Soc.* **2005**, *127*, 9374–9375.

<sup>41</sup> **a)** C. Burato, P. Centomo, G. Pace, M. Favaro, L. Prati, B. Corain, *J. Mol. Catal. A: Chemical* **2005**, *238*, 26–34; **b)** B. Corain, C. Burato, P. Centomo, S. Lora, W. Meyer-Zaika, G. Schmid, *J. Mol. Catal. A: Chemical* **2005**, *22*, 189–195; **c)** M. Králik, V. Kratky, M. De Rosso, M. Tonelli, S. Lora, B. Corain, *Chem. Eur. J.* **2003**, *9*, 209–214.

The thioether groups present within the polymer coordinate Au(III) before the reduction step where  $\text{NaBH}_4$  is generally used. The porosity of the resin acts as a templating agent, and the AuNPs with different size can be obtained by modulating the degree of crosslinking (**Figure 2.8**). This system, stable up to  $300^\circ\text{C}$ , was used in synthesis of pentanoic acid from pentanal using mild reaction conditions.

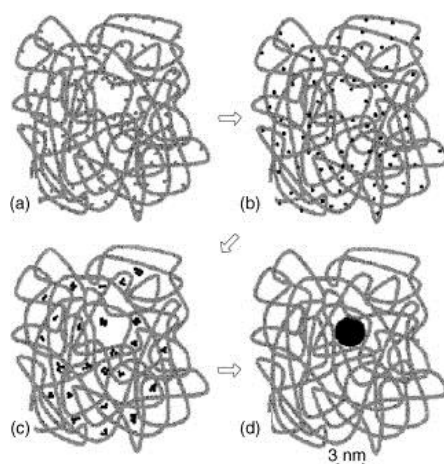


**Figure 2.8:** Template synthesis of AuNPs in a cross-linked resin: a) introduction of gold precursor; b) AuNPs formation; c) sintering of AuNPs; d) the growing process is stopped thanks to the cross-linking within the resin.<sup>41</sup>

To avoid the use of any reducing agents, Haruta *et al.*<sup>42</sup> chose an anion-exchange resin as both support and reducing agent for AuNPs (**d**, **Figure 2.6**). The final catalyst, having AuNPs located on the surface, showed really high catalytic activity in oxidation of glucose to gluconic acid, with TOF values up to  $33000 \text{ h}^{-1}$ .

<sup>42</sup> T. Ishida, M. Haruta, R. Makiyama, Patent JP 2007-082287, 2007.

Kobayashi<sup>43</sup> used a polystyrene based copolymer to support AuNPs (**c**, **Figure 2.6** and **Figure 2.9**): in this case, the stabilization occurs through interactions among the  $\pi$ -electrons of the aromatic rings of polystyrene blocks and the vacant orbital of metal atoms, and the AuNPs were located also inside the polymer. The synthetic procedure used was really simple: the polymer was dissolved in THF containing  $\text{NaBH}_4$ , and a solution of chloro(triphenylphosphine)gold(I) ( $\text{AuClPPh}_3$ ) was added; thermal treatment at  $150^\circ\text{C}$  afforded the formation of the crosslinkage by means of the epoxide and alcohol moieties within the polymer, thus resulting in AuNPs incarcerated in the polymeric matrix.

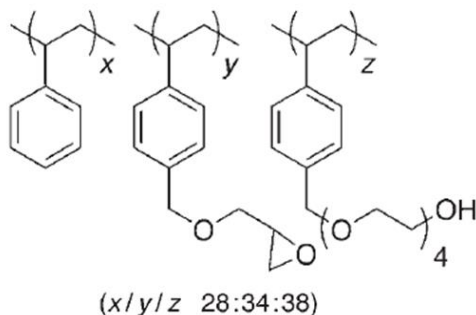


**Figure 2.9:** Polystyrene based support for AuNPs used by Kobayashi *et al.*<sup>43</sup>

The catalyst was successfully employed in the aerobic oxidation of various secondary alcohols with mild conditions and an average value of TOF equal to  $2.0 \cdot 10^4 \text{ h}^{-1}$  was achieved.

Actually, the first part of this synthesis can be generally defined as micro-encapsulation technique (**Figure 2.10**); after the reticulation process,

<sup>43</sup> H. Miyamura, R. Matsubara, Y. Miyazaki, S. Kobayashi, *Angew. Chem. Int. Ed.* **2007**, *46*, 4151–4154.

which gives to the catalyst higher stability of the AuNPs, a different catalyst is obtained and this final step of the whole synthesis has been called polymer incarceration.<sup>44</sup>

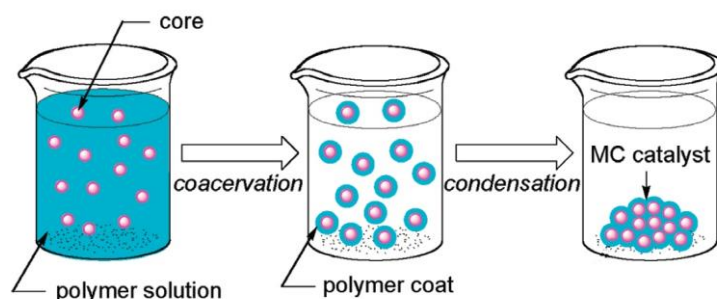


**Figure 2.10:** Schematization of Kobayashi synthesis of microencapsulated nanoparticles.<sup>43</sup>

## 2.5: Gold Nanoparticles onto Porous Supports

According to de Jongh and co.,<sup>45</sup> density, nature (size and shape of the AuNPs) and accessibility of the active site (also called “DNA”) determine the activity and stability of a catalyst. Particularly, the accessibility is a very critical parameter, since diffusion rates of reagents towards the catalytic sites affects the activity of the whole catalyst; for this reason, porous materials are generally preferred as AuNPs supports. These are defined by IUPAC as materials having pores or voids inside their structure; according to the size of their pores, these materials can be classified in: *i*) microporous, having the pore diameter of less than 2 nm; *ii*) mesoporous,

<sup>44</sup> R. Akiyama, S. Kobayashi, *Chem. Rev.* **2009**, *109*, 594–642.

<sup>45</sup> P. Munnik, P. E. de Jongh, K. P. de Jong, *Chem. Rev.* **2015**, *115*, 6687–6718.

having the pore diameters between 2 and 50 nm; *iii*) macroporous, having the pore diameters of greater than 50 nm.<sup>46</sup>

In addition to their use as support, porous materials can be used as templating agents to control the size of the AuNPs during the synthesis.<sup>30, 47</sup> The size of the pores will determine which molecules are allowed to penetrate the support, thus the presence of macro or mesoporous is generally preferred; the uptake of reagent from the reaction medium will concentrate this latter and will enhance its diffusion and the one of products too.<sup>48</sup>

The first synthesis of a mesoporous solid, namely silica and aluminosilicate based material, was achieved in 1971, but only later the porosity features were discovered.<sup>49</sup> Since then, a large number of reactions have been developed using porous materials, *e.g.* biomass transformations, conversion of synthesis gas or acylation reactions.<sup>50</sup>

For example, mesoporous silica or microporous zeolites have been successfully employed as catalysts in alkylation reactions; however, the use of these materials presents some drawbacks, like the complexity of their synthesis with templating material. McCrea and Somorjai reported for the first time the preparation metal nanoparticles (platinum, gold, silver) in the pores of mesoporous silica. This catalyst was mainly employed for dehydrogenation reactions.<sup>51</sup>

Other examples of porous materials used to support AuNPs are: metal organic frameworks (MOFs), TiO<sub>2</sub>, CeO<sub>2</sub>, SiO<sub>2</sub> or Fe<sub>3</sub>O<sub>4</sub>.

---

<sup>46</sup> **a)** *Manual of Symbols and Terminology for Physicochemical Quantities and Units - Appendix II. Definitions, Terminology and Symbols in Colloid and Surface Chemistry. Part II: Heterogeneous Catalysis*, PAC, **1971**; **b)** J. Rouquerol, *Pure and Appl. Chem.* **1994**, *66*, 1739–1758.

<sup>47</sup> G. Prieto, M. Shakeri, K. P. de Jong, P. E. de Jong, *ACS Nano* **2014**, *8*, 2522–2531

<sup>48</sup> **a)** Y. Was, D. Zhao, *Chem. Rev.* **2007**, *107*, 2821–2860; **b)** A. Corma, *Chem. Rev.* **1997**, *97*, 2373–2419.

<sup>49</sup> C. Perego, R. Millini, *Chem. Soc. Rev.* **2013**, *42*, 3956–3976.

<sup>50</sup> R. M. Martin-Aranda, J. Ceika, *Top. Catal.* **2010**, *53*, 141–153.

<sup>51</sup> N. R. Shiju, V. V. Guliants, *App. Catal. A: General* **2009**, *356*, 1–17.

### 2.5.1: Gold Nanoparticles embedded in a Porous Polymer Support (AuNPs-sPSB)

Syndiotactic polystyrene-*co*-*cis*-1,4-polybutadiene (sPSB, **Figure 2.11**) is a linear *multiblock co*-polymer, synthesized by copolymerization of styrene and 1,2-butadiene catalyzed by CpTiCl<sub>3</sub> and methylaluminoxane (MAO).<sup>52</sup> sPSB has been recently described as a novel functional support of the AuNPs (AuNPs-sPSB). Actually this catalyst has been successfully tested in the selective oxidation of different primary and secondary *benzyl-like* alcohols under very mild conditions.<sup>53</sup>

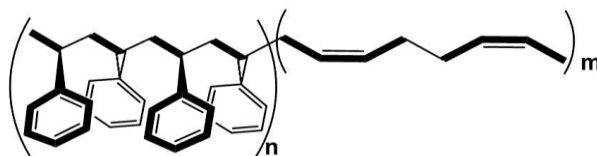


**Figure 2.11:** sPSB *co*-polymer structure, where *n* and *m* represent the length of each block.

In the sPSB support, the polystyrene blocks represent the crystalline portion of the *co*-polymer, while polybutadiene segments represent the amorphous part of the *co*-polymer, which enhance the *swelling* properties of the whole polymeric structure, an important feature to improve the diffusion of reagents during the catalytic tests.

This multiblock *co*-polymer, having a styrene content of 93% *w/w*, shows the same polymorphous behaviour of syndiotactic polystyrene. In fact this polymer, having a *T<sub>g</sub>* and *T<sub>m</sub>* respectively of 100°C and 270°C and

<sup>52</sup> M. Caprio, M. C. Serra, D. E. Bowen, A. Grassi, *Macromolecules* **2002**, *35*, 9315-9322-9315.

<sup>53</sup> A. Buonerba, C. Cuomo, S. Ortega Sánchez, P. Canton, A. Grassi, *Chem. Eur. J.* **2012**, *18*, 709 – 715.

good chemical and physical properties,<sup>54</sup> show a complex polymorphic behaviour, having five different polymorphous forms  $\alpha$ ,  $\beta$ ,  $\delta$ ,  $\epsilon$  and  $\gamma$ .<sup>55, 56</sup> Contrary to  $\alpha$ ,  $\beta$  and  $\gamma$  forms which are compact,  $\delta$  and  $\epsilon$ , characterized by the presence of a helicoidal conformation of polymer chains, have nanometric cavities with an average volume of 120-160 Å<sup>3</sup>, but in the  $\delta$  form these cavities are isolated, while in the  $\epsilon$  form they are connected one to the other, thus forming nanochannels (Figure 2.12).<sup>54, 57, 58</sup>

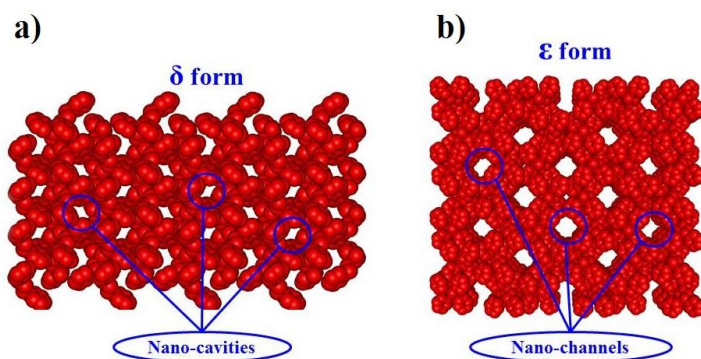


**Figure 2.12:** Crystalline structures of polymorphous forms a)  $\delta$  and b)  $\epsilon$ .

For the presence of nanoporosity,  $\delta$  and  $\epsilon$  forms of syndiotactic polystyrene are able to form *co*-crystals with guest molecules having low molecular weight.<sup>59, 60, 61</sup>

<sup>54</sup> a) G. Milano, G. Guerra, *Prog. Pol. Sci.* **2009**, *54*, 68-88; b) M. Malanga, *Adv. Mater.* **2000**, *12*, 1869-1872.

<sup>55</sup> E. M. Woo, Y. S. Sun, C.-P. Yang, *Prog. Pol. Sci.* **2001**, *26*, 945-983.

<sup>56</sup> E. Bhoje Gowd, K. Tashiro, C. Ramesh, *Prog. Pol. Sci.* **2009**, *34*, 280-315.

<sup>57</sup> P. Rizzo, C. Daniel, A. De Girolamo Del Mauro, G. Guerra, *Chem. Mater.* **2007**, *19*, 3864-3866.

<sup>58</sup> V. Petraccone, O. R. de Ballesteros, O. Tarallo, P. Rizzo, G. Guerra, *Chem. Mater.* **2008**, *20*, 3663-3668.

<sup>59</sup> G. Guerra, V. M. Vitagliano, C. De Rosa, V. Petraccone, P. Corradini, *Macromolecules* **1990**, *23*, 1539-1544.

A *clathrate* is obtained when the guest molecules are imprisoned and isolated into cavities formed between two polymer helices; in this case, the guest/monomer unit molar ratio is equal to  $1/4$ .<sup>62</sup> An *intercalate* is formed when the guest molecules are not isolated but they are contiguous inside the layers of helicoidal chains. For this reason, these structures will present a higher guest content, and the molar ratio between the guest and the monomer unit will be  $1/2$ .<sup>62</sup>

$\delta$  form is generated obtained as *co*-crystal with the solvent used for its synthesis, such as benzene or THF. When these solvents are removed by heating, supercritical CO<sub>2</sub> extraction or solvent exchange, for example with acetone, methanol or acetonitrile, empty  $\delta_e$  form is obtained.  $\delta$  and  $\delta_e$  crystalline structures will be characterized by different cell parameters, since these are slightly modified when *co*-clathrate structures are formed.<sup>55, 56</sup>

$\epsilon$  form has been discovered in 2007 by Guerra *et al.*;<sup>57</sup> it can be generally obtained from  $\gamma$  form after exposition to CHCl<sub>3</sub> and, just like  $\delta$  form, it is able to form both clathrates and intercalates.

The compact  $\alpha$  and  $\beta$  forms can be obtained, respectively, from fast or slow crystallization of the melt and they exhibit a *trans*-planar (*zig-zag*) structure.<sup>55</sup>  $\beta$  can be also formed by thermal treatment at high temperatures ( $T > 150^\circ\text{C}$ ) of  $\delta$  form,<sup>59</sup> and its formation is thermodynamically favoured comparing to  $\alpha$  form.<sup>56</sup>  $\gamma$  phase can be obtained after thermal treatment at temperatures  $\sim 130^\circ\text{C}$  starting from  $\delta$  form<sup>56</sup> or from the amorphous after treatment with bulky solvents, like 1-chlorodecane.  $\gamma$  form of syndiotactic polystyrene is its only polymorphous form whose structure has not been resolved yet.<sup>60</sup>

---

<sup>60</sup> P. Rizzo, A. R. Albuñia, G. Guerra, *Polymer* **2005**, *46*, 9549–9554.

<sup>61</sup> Y. Chatani, Y. Shimane, Y. Inoue, T. Inagaki, T. Ishioka, T. Iijysu, T. Yukinari, *Polymer* **1992**, *33*, 488–492.

<sup>62</sup> C. Daniel, N. Galdi, T. Montefusco, G. Guerra, *Chem. Mater.* **2007**, *19*, 3302–3308.

This complex polymorphous behaviour can bring many advantages in catalysis when the AuNPs-sPSB system is considered. The presence of microporous support, along with the possibility to form *co*-crystals with the polymeric matrix, can enhance the catalytic activity of the AuNPs-sPSB, as it will be later described.

## 2.6: Methods for the Characterization of Gold Nanoparticles

The characterization of the AuNPs based systems, both supported or colloidal, is essential to understand the properties of the system; with this aim, different instrumental analysis can be considered, which can be divided in two groups: 1) support analytical techniques, which give informations about the properties of the support, namely its morphology, porosity, chemical composition and eventually degree and type of functionalization, and 2) AuNPs analytical techniques, which give informations on size, shape, distribution of the nanoparticles.<sup>36</sup>

### 2.6.1: UV-Vis spectroscopy

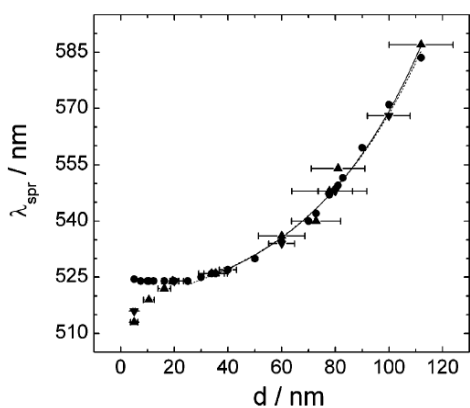


**Figure 2.13:** Position of SPR band peak  $\lambda_{\text{spr}}$  plotted as a function of the AuNPs size.<sup>64</sup>

A gold colloid can be analysed with UV-Vis spectroscopy: in fact the AuNPs show a SPR band at  $\approx 520$  nm, and the exact position of this band will depend by both their size and shape.<sup>63</sup> The position of SPR band ( $\lambda_{\text{spr}}$ ) gives informations about the average size of the AuNPs. (**Figure 2.13**).<sup>64</sup>

For AuNPs having size small-

<sup>63</sup> X. Huang, M. A. El-Sayed, *J. Adv. Res.* **2010**, *1*, 13-28.

<sup>64</sup> W. Heiss, N. T. K. Thanh, J. Aveyard, D. G. Fernig, *Anal. Chem.* **2007**, *79*, 4215-4221.

er than 35 nm, it is possible to use **Equation 2.2** to calculate the average size of the AuNPs, where  $A_{spr}$  and  $A_{450}$  are respectively the absorbances of SPR and the one at 450 nm, with  $B_1$  and  $B_2$  constants equal to 3.55 and 3.11, respectively.

$$d = \exp\left(B_1 \frac{A_{spr}}{A_{450}} - B_2\right)$$

**Equation 2.2:** Relation used to calculate the AuNPs size.

Spherical AuNPs generally show only one SPR band in the UV-Vis spectrum; if the AuNPs have different shape, *e.g.* nanorods, two SPR bands will be detected which refers to transverse and longitudinal SPR of gold nanorods.<sup>65</sup>

### 2.6.2: X-ray analysis

X-Ray Diffraction analysis (XRD analysis) gives informations about both support and the AuNPs. The region included in the  $2\theta$  values range of  $4^\circ$ – $30^\circ$  gives informations about the morphology of the polymer (if the AuNPs-sPSB catalyst is considered), while the diffraction peaks in the region  $30^\circ$ – $80^\circ$  are generally related to the gold crystalline structure. Particularly, the diffraction peaks at  $2\theta$  values equal to  $38.1^\circ$ ,  $44.4^\circ$ ,  $64.6^\circ$  and  $77.8^\circ$  are attributed, respectively, to the (111), (200), (220) and (311) planes of the *fcc* crystalline lattice of nanocrystalline gold.<sup>66</sup> Moreover, considering the Full Width at Half Maximum (FWHM) of the (111) peak, it was possible to evaluate the average size of gold crystallites with Debye-Scherrer equation.<sup>67</sup>

<sup>65</sup> **a)** M. Mlambo, P. S. Mdluli, P. Shumbula, S. Mpelane, N. Moloto, A. Skepu, R. Tshikhudo, *Mat. Res. Bull.* **2013**, *48*, 4181–4185; **b)** Z. Xiao, Q. Wu, S. Luo, C. Zhang, J. Baur, R. Justice, T. Liu, *Part. Part. Syst. Charact.* **2013**, *30*, 338–345.

<sup>66</sup> Y. Chen, X. Gu, C.-G. Nie, Z.-Y. Jiang, Z.-X. Xie, C.-Jian Lin, *Chem. Commun.* **2005**, 4181–4183.

<sup>67</sup> *Metal Nanoclusters in Catalysis and Material Science: The Issue of Size Control* (Eds.: B. Corain, G. Schmid, N. Toshima), Elsevier, Amsterdam, **2008**, pp. 131–132.

The X-ray analysis is a not destructive method, cheap and the preparation of the sample to be analysed is very simple. However, considering supported AuNPs, the evaluation of metallic crystallite size from XRD is not possible if the metal loading is < 0.5 wt% and if the size is < 2 nm, for the low intensity of diffraction peaks.

### **2.6.3: TEM and SEM analysis**

Scanning and Transmission Electron Microscopy (namely SEM and TEM) are principally employed to study the morphology of polymer and the AuNPs, respectively.<sup>68</sup>

Considering supported AuNPs, TEM analysis is used to explore size and shape of the nanoparticles and to obtain a size distribution if at least 500-1000 particles are observed.

The typical resolution of a SEM image equal to 5 nm generally allows definite images of the support and, in the presence of porosity, the diameter of the pores can be simply measured.

Both TEM and SEM analysis are expensive techniques and require a special training for their use; moreover, since they are microscopic techniques, only a portion of the whole sample is analysed, which could be not fully representative of the properties of the sample itself.

### **2.6.4: N<sub>2</sub> adsorption analysis**

The analysis of surface area of a generic porous material is realized through measurements of physical adsorption of nitrogen gas within the sample by varying the gas pressure; the obtained data are analysed using the Brunauer–Emmett–Teller (BET) theory.<sup>36, 69</sup> Different types of isotherms can be obtained according to different modality of gas sorption,

---

<sup>68</sup> *Sample Preparation Techniques in Analytical Chemistry*, ed. S. Mitra, Wiley-Interscience: Hoboken, NJ, 2003.

<sup>69</sup> **a)** S. Brunauer, P. H. Emmett, E. Teller, *J. Am. Chem. Soc.* **1938**, *60*, 309-319; **b)** W. G. McMillan, E. Teller, *J. Phys. Chem.* **1951**, *55*, 17–20.

and these are used to calculate the amount of surface area of the sample. Before the analysis, the sample should be dried under vacuum at least for 12 hours, after which the exact weight of the sample is taken to achieve an accurate calculation of surface areas.

## 2.7: Oxidation reactions catalyzed by AuNPs-sPSB

The AuNPs-sPSB has been already tested in the oxidation of different primary and secondary *benzyl-like* alcohols under mild reaction conditions (Table 2.1).<sup>53</sup> For example, using benzyl alcohol, thiophene-2-methanol, 1-indanol and  $\alpha$ -tetralol as reagents (entries 1-5, Table 2.1), the related aldehydes or ketones were achieved in high yields (76-99 mol%) and selectivities (>99 mol%). Poor results were achieved with both allyl and alkyl alcohols (entries 6-9, Table 2.1).

Table 2.1: Previous results obtained in oxidation reaction catalyzed by AuNPs-sPSB system.

Entry <sup>[a]</sup>	Substrate	Product <sup>[b]</sup>	t [h]	Yield [mol%]	Selec. [mol%]
1	Benzyl alcohol	Benzaldehyde	6	>99	97
2	Thiophene-2-methanol	2-formylthiophene	7	76	>99
3	1-indanol	1-indanone	1	>99	>99
4	$\alpha$ -tetralol	$\alpha$ -tetralone	6	86	>99
5	furfuryl alcohol	furfural	6	30	>99
6	geraniol	geranial	21	29	>99
7	1-butanol	-	24	-	-
8	1-hexanol	-	24	-	-
9	cyclohexanol	cyclohexanone	24	10	>99

[a] Reaction conditions: alcohol=0.51 mmol, catalyst=0.200 g, solvent=H<sub>2</sub>O/CHCl<sub>3</sub> (1:1, total volume 6 mL), KOH=0.51 mmol, T=35°C, P<sub>O2</sub>=1 bar. Yields and selectivities determined by NMR spectroscopy or GC-MS analysis when using anisole as the internal standard.

The high selectivities achieved towards the aldehyde or ketone (reaction products) were remarkable comparing to other polymer-supported AuNPs.<sup>40, 43,<sup>70</sup>, <sup>71</sup></sup>

Kinetic studies on 1-phenylethanol oxidation to acetophenone revealed that the reaction is a pseudo-first order reaction respect to the alcohol. The nanoporous  $\epsilon$  form of syndiotactic polystyrene within the sPSB co-polymer used as support for the AuNPs was formed in situ with the solvent mixture  $H_2O/CHCl_3$ . The presence of the porous crystalline domains in the support enhances the diffusion of the alcohols towards the AuNPs, whereas the presence of polybutadiene blocks increases the swelling of the polymeric matrix.

## **2.8: Aim of the PhD project**

The continuous need of new *green* and *sustainable* industrial chemical processes encourages the discovery and development of new catalytic heterogeneous systems, which are able to operate under mild conditions furnishing good results in terms of activity and selectivity. The AuNPs-sPSB catalyst was previously successfully tested in the selective aerobic oxidation of *benzyl*-like alcohols. The use of the sPSB *co*-polymer as support offered some advantages: 1) sPSB copolymer retains the same polymorphism as syndiotactic polystyrene when the styrene blocks are long more than nine units, thus  $\alpha$ ,  $\beta$ ,  $\gamma$ ,  $\delta$  and  $\epsilon$  forms of syndiotactic polystyrene can be obtained within the copolymer; 2) using a porous support, namely sPSB with syndiotactic polystyrene in  $\delta$  or  $\epsilon$  forms, it is possible to enhance the access of reagents to the catalytic site as previously described; 3) the presence of polybutadiene double bonds represent a possible site of

---

<sup>70</sup> **a)** H. Tsunoyama, T. Tsukuda, H. Sakurai, *Chem. Lett.* **2007**, *36*, 212 – 213; **b)** H. Tsunoyama, N. Ichikuni, H. Sakurai, T. Tsukuda, *J. Am. Chem. Soc.* **2009**, *131*, 7086 –7093.

<sup>71</sup> **a)** M. Conte, H. Miyamura, S. Kobayashi, V. Chechik, *J. Am. Chem. Soc.* **2009**, *131*, 7189–7196; **b)** C. Lucchesi, T. Inasaki, H. Miyamura, R. Matsubara, S. Kobayashi, *Adv. Synth. Catal.* **2008**, *350*, 1996 – 2000.

further copolymer functionalizations;<sup>72</sup> 4) the polybutadiene domains enhance the swelling of the polymers.<sup>53</sup>

Moreover, a different approach for the synthesis of gold based catalysts was explored during a research period spent at the University of Liverpool under the supervision of Dr. J. Lopez-Sanchez. This was based on the synthesis of preformed gold colloids and immobilization on a polymeric matrix. Gold colloids generally have small nanoparticles dimension but suffers of poor catalytic activity since they are completely covered by the colloid stabilizer. To facilitate their recovery from the reaction medium, it is possible to immobilize them but it is necessary to remove the stabilizer. Catalytic tests can help in understanding if the removal has been successfully accomplished.

---

<sup>72</sup> **a)** A. Buonerba, V. Speranza, P. Canton, C. Capacchione, S. Milione, A. Grassi, *RSC Adv.* **2014**, *4*, 60158-60167; **b)** A. Buonerba, V. Speranza, A. Grassi, *Macromolecules* **2010**, *46*, 778-784.



# CHAPTER 3



## SYNTHESIS AND CHARACTERIZATION OF THE AUNPS-SPSB CATALYST



### 3.1 The general synthetic route

The sPSB used in this study has a styrene content of 88 *mol%*, (corresponding to 93 *wt%*), which corresponds to a crystallinity of 32%; the polybutadiene content is sufficient to guarantee a good swelling of the *co*-polymer.<sup>53</sup>

The general synthetic procedure to support of AuNPs on sPSB used in this project has been reported in literature for the first time in 2012.<sup>53</sup> Briefly, the sPSB copolymer was dissolved in THF, and the mixture was stirred for 24 h at room temperature and then heated to reflux for 1 h to complete the swelling of the polymer. Later, a HAuCl<sub>4</sub> solution was added at room temperature; the resulting slurry was kept under agitation for 24h to guarantee a good dispersion of gold precursor into the polymeric matrix, and then heated to reflux for 1 h. After the addition of the selected gold precursor the solution colour changed from white to pale yellow. A THF solution of sodium triethylborohydride was added at 25 °C producing a rapid change of the color from pale yellow to red. The polymer was rapidly precipitated in a plenty of methanol, recovered by filtration, washed with fresh methanol and dried in vacuo at room temperature (**Figure 3.1**). The use of THF was sufficient to guarantee an optimal final dispersion of the AuNPs within sPSB since it conveniently dissolves all the reagents.<sup>53</sup>

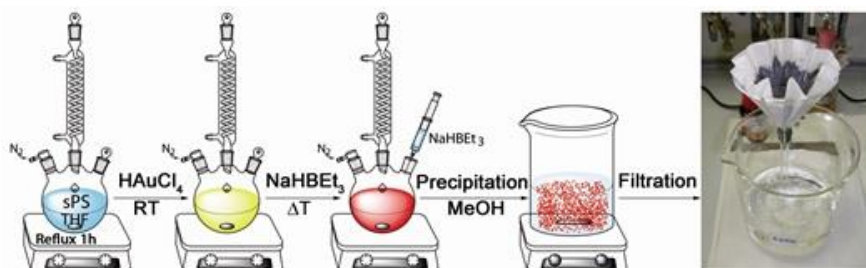


**Figure 3.1:** Schematic representation for the synthesis of the AuNPs-sPSB catalyst.<sup>53</sup>

The final rapid coagulation in methanol avoids the growth in size of the AuNPs through ripening: in this way, the AuNPs are *embedded* into the polymeric matrix and this is sufficient to stop their increase in size. Due to the absence of specific functional groups like sulphur atoms which stabilize the AuNPs by means of covalent bonds, it can be assumed that in this case the stabilization occurs through the formation of strong interactions with the aromatic moieties of polystyrene blocks, as previously reported by Kobayashi.<sup>43</sup> Finally, to remove all the polar by-products such as borates and chloride anions deriving from the reduction step for the formation of the AuNPs, deep catalyst washing with methanol is required. The final pale purple colour of the AuNPs-sPSB is strictly related to the AuNPs size and to their SPR.

To verify the effectiveness of the embedding process, the methanol washing solution was analysed by atomic absorption spectroscopy (AAS), and no gold leaching was found. The final gold content within the polymer was evaluated by inductively coupled plasma optical emission spectroscopy (ICP-OES) on the digested catalyst. After treatment with sulphuric acid, hydrogen peroxide and aqua regia, and a gold content of 2 wt% was assessed. The synthetic procedure here described allows *pre-fixing* the desired gold content, since it is completely embedded into the polymeric matrix and the AAS analysis on its leaching was negative.

### **3.2: Synthesis of the polymorphic forms of the AuNPs-sPSB catalyst: the Au-C $\delta$ , Au-C $\beta$ , Au-C $\gamma$ , Au-C $\epsilon$ catalysts**

The AuNPs-sPSB catalyst directly coming from the synthetic procedure just described presents polystyrene blocks in  $\delta$  form (Au-C $\delta$ ); to obtain the other polymorphous forms, some thermal annealing or solvent treatments were necessary (Table 3.1). Compact Au-C $\beta$  sample was obtained treating Au-C $\delta$  at 170°C for 5 hours; analogously, thermal treatment of

**Au-C $\delta$**  but at 135°C for 2 hours afforded the formation of **Au-C $\gamma$**  compact catalyst sample.

**Table 3.1:** AuNPs-sPSB catalysts characterization.

Catalyst <sup>[a]</sup>	Treatment		Cryst. Form
	Thermal Annealing	Solvent	
<b>Au-C<math>\delta</math></b>	-	-	$\delta$
<b>Au-C<math>\beta</math></b>	170°C; 5 h	-	$\beta$
<b>Au-C<math>\gamma</math></b>	135°C; 2 h	-	$\gamma$
<b>Au-C<math>\epsilon</math></b>	170°C; 5 h	H <sub>2</sub> O/ CHCl <sub>3</sub>	$\epsilon$

[a] The Greek symbol indicates the crystalline form of the syndiotactic polystyrene domains.

Finally, the formation of nanochannels within the polymeric support, namely the formation of the **Au-C $\epsilon$**  sample was achieved treating the **Au-C $\beta$**  catalyst with a solvent mixture of water and chloroform. In this case chloroform was used in mixture with water to prevent the polymeric matrix dissolutions.

### 3.3: Morphological Characterization of the **Au-C $\delta$** , **Au-C $\beta$** , **Au-C $\gamma$** , **Au-C $\epsilon$** catalysts

The characterization of the four catalysts sample was effectuated by means of WAXD analysis, TEM and SEM images, and N<sub>2</sub> sorption measurements.

The WAXD spectra are reported in **Figure 3.2**. From the inspection of **Au-C $\delta$**  WAXD spectrum (**a**, **Figure 3.2**), the presence of syndiotactic polystyrene blocks in the  $\delta$  form with THF molecules still clathrate inside the polymeric matrix was confirmed; in this sample, the AuNPs had an average size of 4.9 nm (**Figure 3.2**).

Considering the different thermal annealing used to obtain the compact **Au-C $\beta$**  and **Au-C $\gamma$**  samples, in addition to the change of the morphology of syndiotactic polystyrene blocks, also the AuNPs changed in size, reaching the values of 8.0 nm and 6.9 nm respectively for **Au-C $\beta$**  and **Au-C $\gamma$** : this result can be explained considering that the temperature used in both cases was higher than the  $T_g$  of syndiotactic polystyrene, thus causing the softening of the polymeric support and reducing the stabilization of the AuNPs, which are allowed to move within the sPSB support.

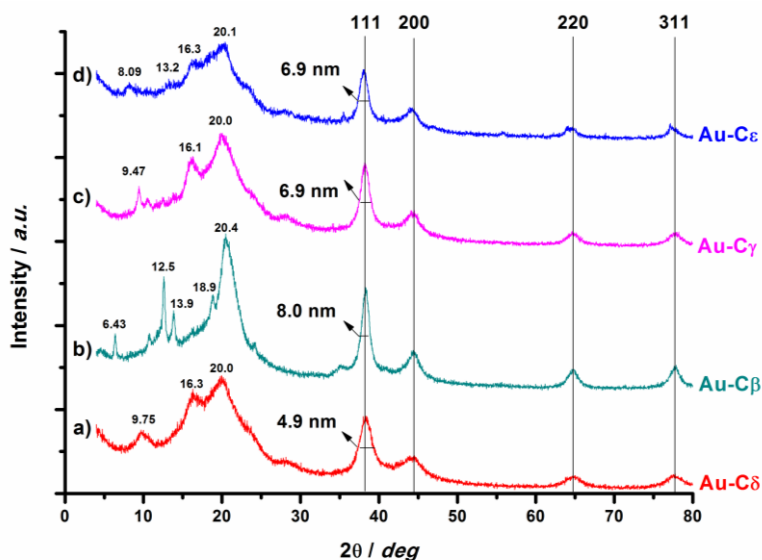
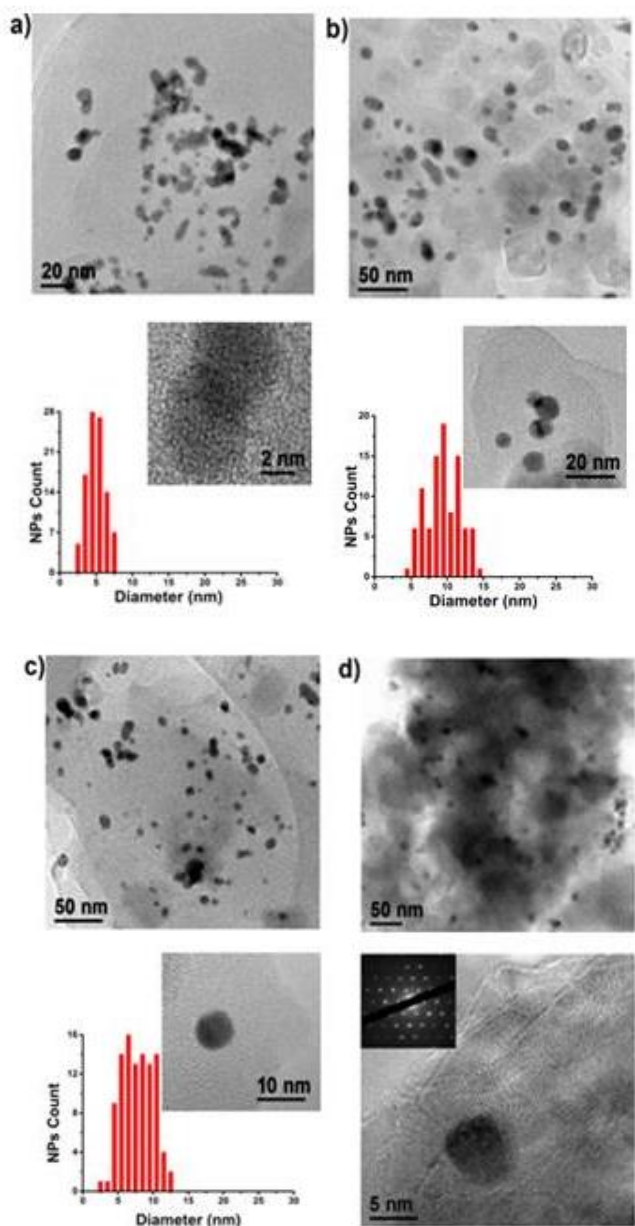


Figure 3.2: WAXD pattern for the samples: a) **Au-C $\delta$** ; b) **Au-C $\beta$** ; c) **Au-C $\gamma$**  and d) **Au-C $\epsilon$** .

Surprisingly, from the analysis of **Au-C $\epsilon$**  WAXD spectrum a decrease in the AuNPs size to 6.9 nm was observed. Recently Hardacre *et al.* reported that halohydrocarbons are able to reduce the AuNPs size by means of fragmentation of larger nanoparticles with halogen atoms until the atomic



**Figure 3.3:** TEM images and AuNPs size distribution for the samples: **a) Au-C $\delta$** ; **b) Au-C $\beta$** ; **c) Au-C $\gamma$**  and **d) Au-C $\epsilon$** . The inset in figure **d)** reports the SAED pattern of the crystalline region of the polymeric matrix.

scale or through the progressive removal of gold-X species (where X stands for halogen atom) from the surface of the nanoparticle.<sup>73</sup> Hence, the decrease in the AuNPs size from **Au-C $\beta$**  to **Au-C $\epsilon$**  could be interpreted in light of that.

The four catalyst samples have been analysed with TEM and SEM analysis in order to achieve informations, respectively, on the AuNPs size and on the morphology of the support.

In **Figure 3.3** the TEM images of the **Au-C $\delta$** , **Au-C $\beta$** , **Au-C $\gamma$**  and **Au-C $\epsilon$**  are reported.

The first thing to be noticed is that a good dispersion of the AuNPs within the polymeric support was achieved, and this was not affected neither by thermal annealing nor by solvent treatment.

TEM images were used to calculate a distribution of the AuNPs size. A quite sharp distribution was obtained for the **Au-C $\delta$**  catalyst (**a**, **Figure 3.3**), centered at around 5 nm, thus confirming the data earlier obtained with WAXD spectrum (4.9 nm, **Figure 3.2**). Broader distributions were achieved for both **Au-C $\beta$**  and **Au-C $\gamma$**  as consequence of the different thermal annealing (**b** and **c**, **Figure 3.3**); however, quite a good agreement with the WAXD data can be recognized (**Figure 3.2**). TEM analysis of **Au-C $\epsilon$**  catalyst confirmed the decrease in the AuNPs size after the treatment with water and chloroform; the AuNPs are still homogeneously dispersed in the support, and surrounded by a highly crystalline polymeric matrix (SAED pattern, inset in **d**, **Figure 3.3**).

SEM images of the four catalyst samples are reported in **Figure 3.4**.

**Au-C $\delta$**  shows a globular morphology, with polymer particles dimension which relays in the micrometric scale (**a**, **Figure 3.4**). Thermal annealing to obtain **Au-C $\beta$**  and **Au-C $\gamma$**  affects their morphology, since from the **Au-C $\delta$**  porous catalyst a compact morphology is generated, where the poly-

---

<sup>73</sup> **a)** K. Morgan, A. Goguet, C. Hardacre, *ACS Catal.* **2015**, *5*, 3430–3445; **b)** J. Sá, A. Goguet, S. F. R. Taylor, R. Tiruvalam, C. J. Kiely, M. Nachttegaal, G. J. Hutchings, C. Hardacre, *Angew. Chem. Int. Ed.* **2011**, *50*, 8912–8916.

mer presents a corrugated surface (b and c, Figure 3.4). **Au-C $\epsilon$**  catalyst clearly shows a porous morphology similarly to **Au-C $\delta$**  (d, Figure 3.4). From the inspection of SEM images of the **Au-C $\delta$**  and **Au-C $\epsilon$**  samples it can be said that, apart from the presence of microporosity (nanocavities and nanochannels), also macropores are present.

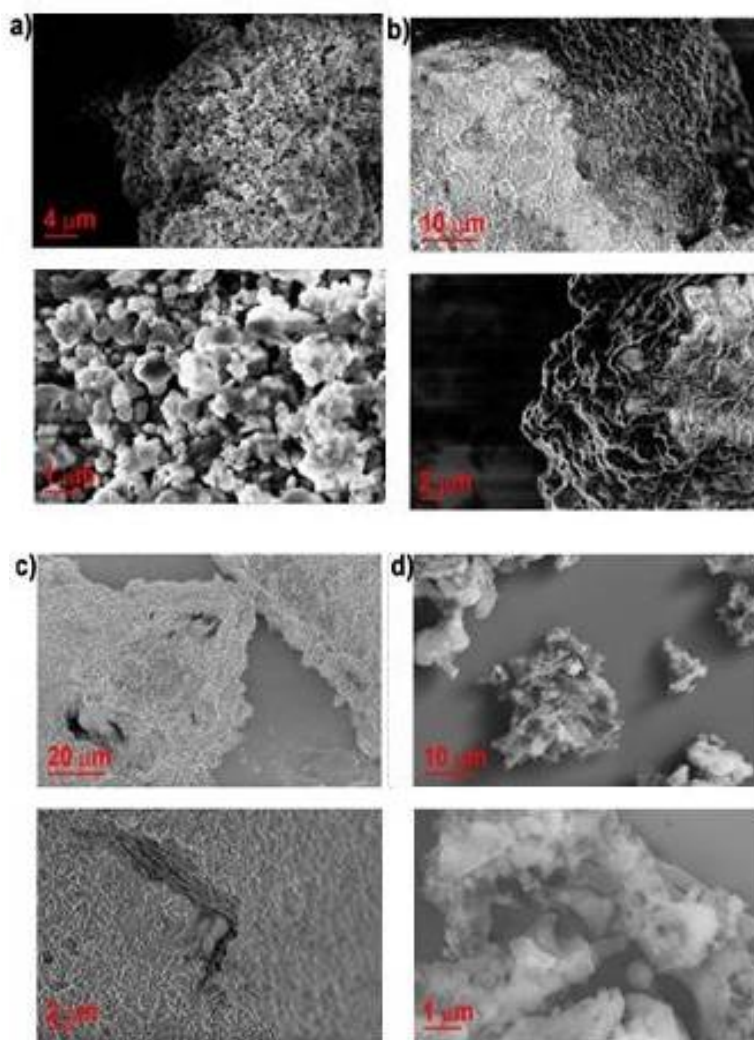


Figure 3.4: SEM images of the samples: a) **Au-C $\delta$**  b) **Au-C $\beta$** ; c) **Au-C $\gamma$**  and d) **Au-C $\epsilon$** .

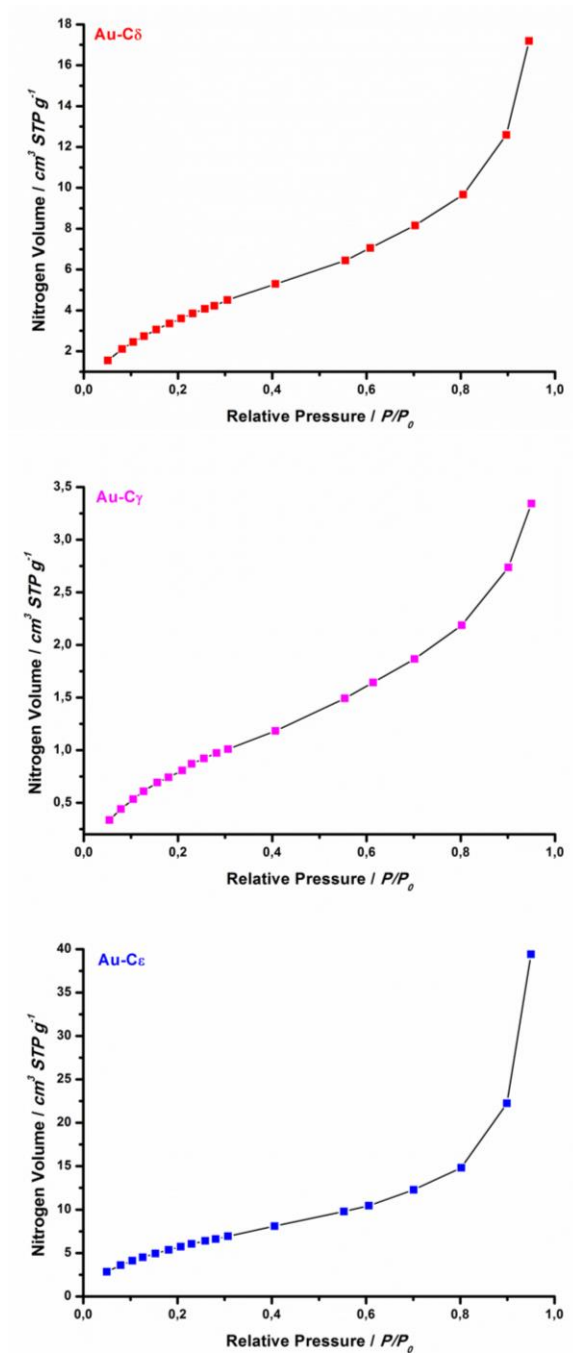


Figure 3.5.  $\text{N}_2$  sorption isotherms for the samples Au-C $\delta$ , Au-C $\gamma$  and Au-C $\epsilon$ .

To confirm the presence of above-mentioned morphologies with polymeric support having high surface area, measurements of N<sub>2</sub> uptake by the different catalyst sample were considered; the obtained isotherms are reported in **Figure 3.5**, and these were interpreted according to the BET theory.

The resulting surface area for each catalyst confirmed the morphology that resulted from SEM images, furnishing the following values: 16 m<sup>2</sup>/g for **Au-C $\delta$** , of 3.9 m<sup>2</sup>/g for **Au-C $\gamma$**  and of 24 m<sup>2</sup>/g for **Au-C $\epsilon$** . Previous measurements of surface area of syndiotactic polystyrene powders in  $\delta$  and  $\gamma$  forms gave as result respectively 43 and 4 m<sup>2</sup>/g.

### **3.4: Concluding remarks**

The AuNPs-sPSB catalyst was synthesized according to the procedure already reported in literature, which involves the sPSB dissolution in THF, addition of the gold precursor and reduction with NaBHET<sub>3</sub>.<sup>53</sup>

The native catalyst **Au-C $\delta$**  was thermally annealed in order to form **Au-C $\beta$**  and **Au-C $\gamma$** ; **Au-C $\epsilon$**  was formed from **Au-C $\beta$**  with treatment in the solvent mixture H<sub>2</sub>O/CHCl<sub>3</sub>.

WAXD spectra confirmed the presence of the desired polymorphous form of syndiotactic polystyrene in the sPSB support and revealed the AuNPs dimensional range was 4.9-8.0 nm. These data were confirmed by the inspection of TEM images, which revealed a homogeneous dispersion of the AuNPs within the support even after thermal annealing or solvent treatment. Particularly, for the **Au-C $\epsilon$**  catalyst sample SAED pattern showed the presence of a highly crystalline phase surrounding the AuNPs. SEM images revealed the presence of macroporous support in the **Au-C $\delta$**  and **Au-C $\epsilon$**  catalysts, in contrast with the morphology of the support in **Au-C $\beta$**  and **Au-C $\gamma$**  catalyst samples.



# CHAPTER 4



## OXIDATION REACTIONS CATALYZED BY AUNPs-SPSB



### 4.1: Introduction

AuNPs are generally accepted as green catalysts since they are able to operate under mild reaction conditions, *e.g.*: *i*) low pressure of O<sub>2</sub>; *ii*) low reaction temperatures; *iii*) low catalyst loading; *iv*) avoidance of costly or/and toxic additives.<sup>19b, 74</sup> A further positive feature to be considered is that they are reusable when supported on solids and can show high selectivity.

AuNPs catalyse a large number of reactions, such as oxidation of CO, toluene, methane, sugars, amine and alcohols.<sup>19a</sup> Moreover reduction of nitrogroups can be successfully obtained (**Figure 4.1**).<sup>75, 76</sup> Compared to other noble metals, gold allows the achievement of the desired products with high selectivities.<sup>76</sup>

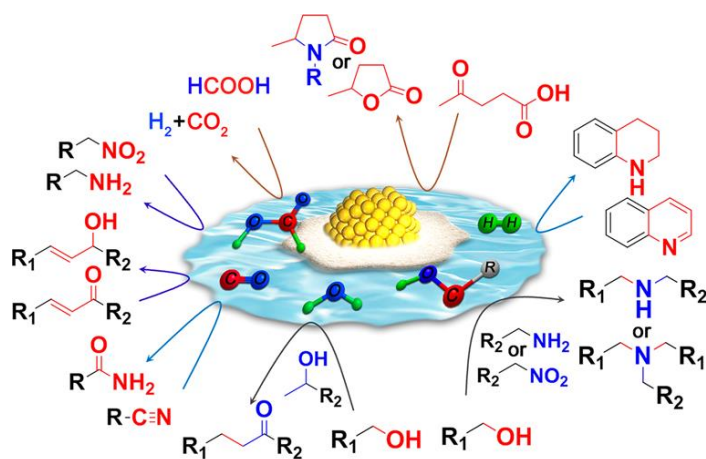


**Figure 4.1:** An overview over the reactions catalyzed by AuNPs.<sup>76</sup>

<sup>74</sup> J. K. Edwards, B. N Solsona, A. F. Carley, A. A. Herzing, C. J. Kiely, G. J. Hutchings, *Science* **2009**, 323, 1037–1041.

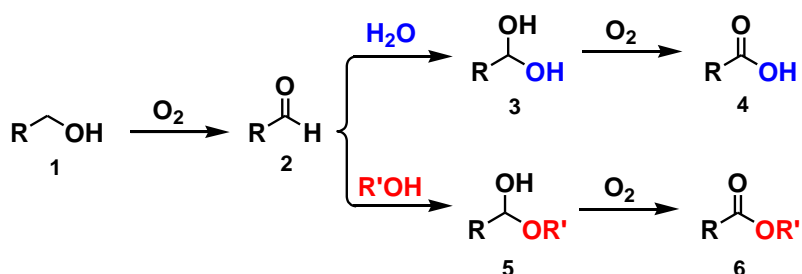
<sup>75</sup> S. K. Hasmi, G. Hutchings, *Angew. Chem. Int. Ed.* **2006**, 45, 7896–7936.

<sup>76</sup> X. Liu, L. He, Y.-M. Liu, Y. Cao, *Acc. Chem. Res.* **2014**, 47, 793–804.

Oxidation reactions are usually performed with strong oxidizing agents such as Jones and Collins reagents, pyridinium chlorochromate (PCC) (all based on the cancerogenic  $\text{Cr}^{+6}$ ),<sup>77</sup>  $\text{KMnO}_4$ ,  $\text{MnO}_2$  and dimethyl sulfoxide (DMSO), Dess-Martin reagents, (2,2,6,6-Tetramethylpiperidin-1-yl)oxyl, TEMPO).<sup>78</sup>

To avoid the use of toxic reagent or  $\text{H}_2\text{O}_2$  solutions, as well as harsh reaction conditions, alcohol oxidations can be readily achieved with catalytic systems based on AuNPs.

In oxidation reactions, considering a generic  $\text{RCH}_2\text{OH}$  alcohol different oxidation products can be obtained (**Scheme 4.1**).



**Scheme 4.1:** Generic reaction pathways for the oxidation of a generic primary alcohol.

Primary alcohols (1, **Scheme 4.1**) like benzyl alcohol are oxidized to the corresponding aldehyde (2), that can further react according to two different pathways: *i*) in water the geminal diol (3) can be oxidized to furnish the final carboxylic acid (4); *ii*) in the presence of a generic  $\text{R}'\text{OH}$  alcohol the hemiacetal (5) can be oxidized to furnish the ester (6).<sup>19b, 79</sup> Therefore, the oxidation to carboxylic acid and ester are examples of two-

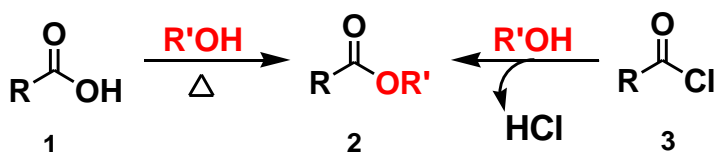
<sup>77</sup> Chromium (VI) compounds, IARC Monographs– 100C.

<sup>78</sup> F. A. Carey, R. J. Sundberg; *Advanced Organic Chemistry*, 5<sup>th</sup> Edition, Springer, 2007.

<sup>79</sup> M. Besson, P. Gallezot, *Catal. Today* **2000**, 57, 127–141.

steps reaction, and the AuNPs can show high selectivity in this reaction pathway.

According to the number of alcohols, different esterification products can be obtained: *i)* *self-coupling* ester if only one alcohol ROH is considered; *ii)* *cross-coupling* products are achieved when more than one alcohol is introduced in the reaction medium.<sup>80</sup>



**Scheme 4.2:** Conventional synthetic strategies to achieve esters starting from carboxylic acids or acyl chlorides.

In the acid catalyzed condensation of a carboxylic acid (**1**) with an alcohol water is formed as by-product and this is an equilibrium reaction (**Scheme 4.2**).<sup>81</sup> To achieve high yields it is necessary to separate water from the reaction medium using high temperatures and distillation devices. On the contrary, the use of acyl chlorides in an irreversible reaction with the alcohols leads to toxic by-products (**Scheme 4.2**).<sup>81</sup> This is undesirable from the point of view of *green* and *sustainable* chemistry.

The synthetic route shown in **Scheme 5.1** can be performed using milder reaction conditions and the AuNPs catalysts; the two-steps of reaction occur in the same batch, without any further purification, thus preventing formation of by-products.

<sup>80</sup> **a)** B. Xu, J. Haubrich, C. G. Freyschlag, R. J. Madix, C. M. Friend, *Chem. Sci.* **2010**, *1*, 310–314; **b)** B. Xu, R. J. Madix, C. M. Fan, *J. Am. Chem. Soc.* **2010**, *132*, 16571–16580.

<sup>81</sup> *Organic Chemistry*, J. Mc Murry, Thomson Brooks/Cole, Seventh Edition, 2008.

### 4.1.1: Oxidation reactions catalyzed by Gold Nanoparticles

Benzyl alcohol oxidation has been widely used as benchmark reaction to assess the activity and selectivity of supported AuNPs. The oxidation of this alcohol in liquid phase generally proceeds smoothly and the relative yields of benzaldehyde, benzoic acid and benzyl benzoate can be used to test the selectivity of a gold catalyst that is also affected by the solvent.<sup>74</sup> In fact, carboxylic acid is generally obtained in water, while esters and aldehydes are formed in organic solvents.<sup>82</sup>

An interesting study has been conducted by Repo *et al.*,<sup>83</sup> who reported on benzyl alcohol oxidation catalyzed by the AuNPs-Al<sub>2</sub>O<sub>3</sub> in water and methanol, using NaOH as base, at 100°C and 10 bar of O<sub>2</sub>. In water benzoic acid is obtained with a selectivity of 100% in only 1 h (*yield*=100 mol%), while in methanol, methyl benzoate (*cross-coupling* product) was obtained in the same reaction time with a selectivity of 96mol% (*yield*=100 mol%). The esterification reaction with other alcohols such as ethanol, isopropanol and cyclohexanol led to lower conversions and selectivities.

Different supports for the AuNPs have been employed, such as carbon based materials,<sup>84</sup> TiO<sub>2</sub>, CeO<sub>2</sub>, Al<sub>2</sub>O<sub>3</sub>, SiO<sub>2</sub>,<sup>85</sup> zeolites,<sup>86</sup> and metal-organic framework.<sup>19a</sup> Wang *et al.* studied the synthesis of methyl benzoate with the AuNPs on different oxide-based supports.<sup>87</sup> The main results are reported in **Table 4.1**. Good results were obtained with all of the catalysts; however, the highest conversions and selectivities in methyl benzoate were achieved with Au-CeO<sub>2</sub> and Au-ZrO<sub>2</sub> (entries **1** and **2**, **Table 4.1**).

<sup>82</sup> A. Corma, H. García, *Chem. Soc. Rev.* **2008**, *37*, 2096-2126.

<sup>83</sup> A. Rautiainen, O. Simakova, H. Guoa, A.-R. Leino, K. Kordás, D. Murzin, M. Leskelä, T. Repo, *App. Catal. A: General* **2014**, *485*, 202-206.

<sup>84</sup> **a)** P. Mondal, N. Salam, A. Mondal, K. Ghosh, K. Tuhina, Sk. M. Islam, *J. Coll. Interf. Sci.* **2015**, *459*, 97-106; **b)** J. Wang, S. A. Kondrat, Y. Wang, G. L. Brett, C. Giles, J. K. Bartley, L. Lu, Q. Liu, C. J. Kiely, G. J. Hutchings, *ACS Catal.* **2015**, *5*, 3575-3587.

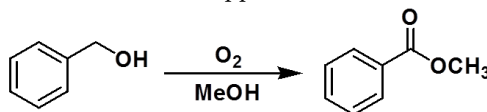
<sup>85</sup> R. L. Oliveira, P. K. Kiyohara, L. M. Rossi, *Green Chem.* **2009**, *11*, 1366-1370.

<sup>86</sup> D. Esken, S. Turner, O. I. Lebedev, G. Van Tendeloo, R. A. Fischer, *Chem. Mater.* **2010**, *22*, 6393-6401.

<sup>87</sup> H. Wei, J. Li, J. Yu, J. Zheng, H. Su, X. Wang, *Inorg. Chim. Acta* **2015**, *427*, 33-40.

The poor catalytic activity of Au-Al<sub>2</sub>O<sub>3</sub> can be attributed to the amphoteric nature of the support, which is damaged in basic mediums of reaction.

**Table 4.1:** Aerobic esterification of benzyl alcohol with AuNPs on different oxide-based supports.



Entry	Catalyst	AuNPs size range [nm]	Conversion [mol%]	Selectivity [mol%]
1	Au-CeO <sub>2</sub>	3-6	99.7	99.4
2	Au-ZrO <sub>2</sub>	4-7	100	99.0
3	Au-TiO <sub>2</sub>	5-7	88.9	85.8
4	Au-HT	10-13	82.2	84.1
5	Au-Al <sub>2</sub> O <sub>3</sub>	5-7	39.3	79.3

Reaction Conditions: benzyl alcohol (2.0 mmol), 25°C, Cs<sub>2</sub>CO<sub>3</sub> (10 mol%), CH<sub>3</sub>OH (5 mL), O<sub>2</sub> (1 atm), 25 mg catalyst (3 wt% of Au), 6h.

Polymers have been used to support AuNPs for aerobic esterification of benzyl alcohol.

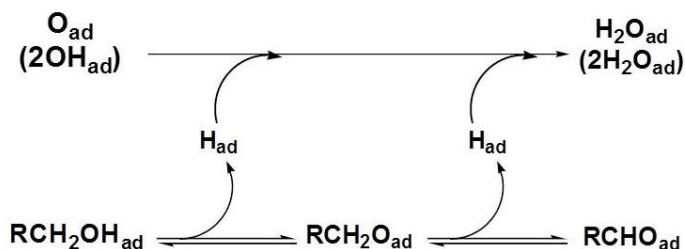
Kobayashi used the AuNPs-PI<sup>43</sup> (Polystyrene Incarcerated) for both alcohol oxidation<sup>71b</sup> and benzyl alcohol aerobic esterification to methyl benzoate;<sup>88</sup> in the latter case, methyl-4-methylbenzoate was obtained with 99 mol% in selectivity, using 1 mol% of Au, K<sub>2</sub>CO<sub>3</sub> as base, methanol and water as solvent mixture, at room temperature and atmospheric pressure of oxygen. It is important to underline that even if water was used as co-solvent, the selectivity towards the ester was high, since the polymeric support is hydrophobic. This synthetic procedure was successfully applied also to aerobic esterification of different *p*-substituted benzyl alcohols, with yields in the range 60-99 mol%.

<sup>88</sup> H. Miyamura, T. Yasukawa, S. Kobayashi, *Green Chem.* **2010**, *12*, 776-778.

### 4.1.2: Mechanistic hypothesis on alcohol oxidation and oxidative esterification of alcohols catalyzed by Gold Nanoparticles

Three main hypothesis have been currently reported in the literature to explain the mechanism of alcohols oxidation.<sup>19e</sup> The oxidation of both geminal diol or hemiacetal intermediates can occur *via* the same oxidation pathway hypothesized for the alcohol.

According to the **Scheme 4.3** (model A), generally accepted for platinum and palladium, the alcohol is adsorbed on gold surface producing an alcoholate and a hydrogen atom. Since the C-H bond in  $\beta$  position become weaker after the adsorption, it is cleaved forming the desired aldehyde (or ketone) and this is also the rate-determining step of the overall reaction. The catalytic activity is restored by reaction of oxygen or hydroxyl with the hydrogen atom on the gold surface. An indirect evidence of the presence of hydrogen atom adsorbed on gold surface is the reduction of the double bond of cinnamyl alcohol when this is used as reagent in oxidation reactions.



**Scheme 4.3:** Dehydrogenation pathway (model A) for alcohol oxidation over Pd and Pt.

A second mechanistic proposal (model B) hypothesizes that the rate-determining step is the reaction between the adsorbed oxidizing reagent and alcohol: this model can be thus described according the Langmuir-Hinshelwood mechanism.

The third and last mechanistic proposal (model C) is similar to the model A, but differs from this since a different mechanism of action is attributed to oxygen. In fact, the value of dissociation energy of oxygen on gold calculated by DFT suggests that the formation of two oxygen atoms adsorbed on gold surface can be really difficult (**Figure 4.2**). Hence, all the mechanistic proposals which involve the dissociation of the oxygen molecule bond have low probability to occur.<sup>89</sup>

<b>Cr</b>	<b>Mn</b>	<b>Fe</b>	<b>Co</b>	<b>Ni</b>	<b>Cu</b>
		-6,30	-5,07	-3,90	-2,51
<b>Mo</b>	<b>Tc</b>	<b>Ru</b>	<b>Rh</b>	<b>Pd</b>	<b>Ag</b>
-7,48		-4,62	-4,03	-1,20	-0,65
<b>W</b>	<b>Re</b>	<b>Os</b>	<b>Ir</b>	<b>Pt</b>	<b>Au</b>
-8,62			-4,65	-2,17	+0,54

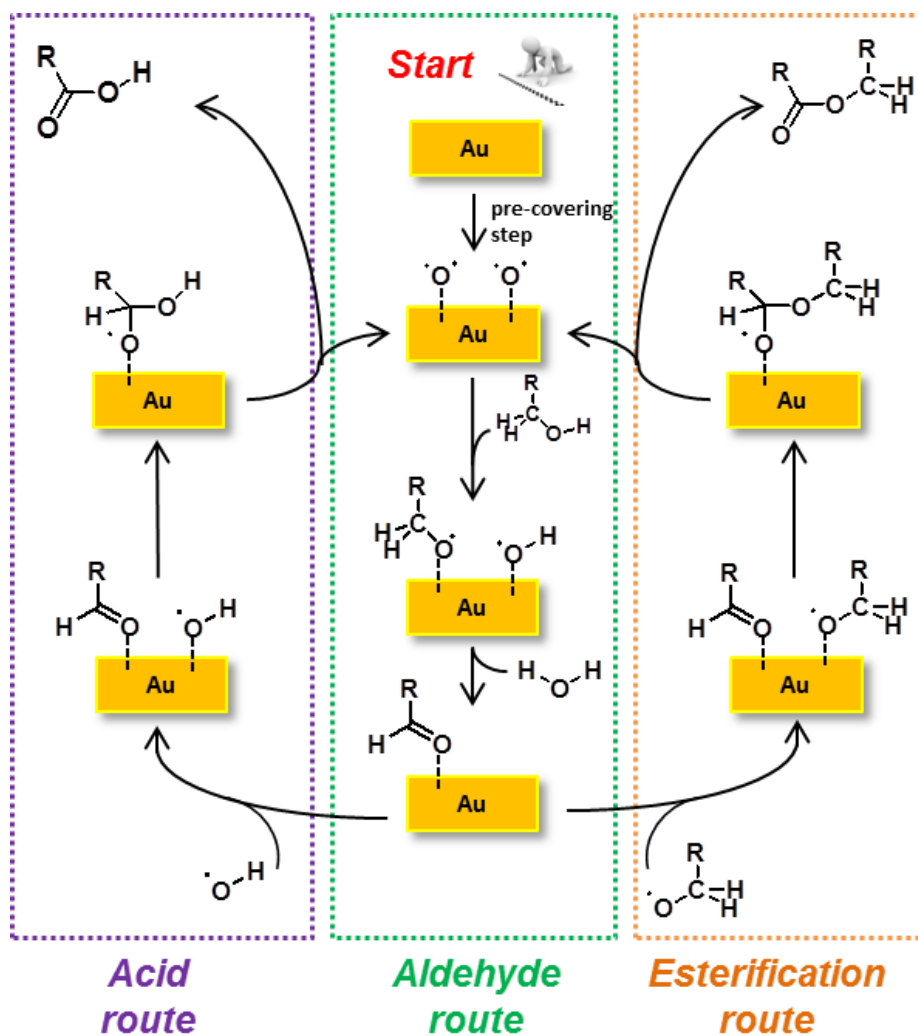
**Figure 4.2:** Dissociation energies for the chemisorption of oxygen over different transition metals.

Friend *et al.*<sup>90</sup> studied methanol oxidation to methyl formate with nanoporous gold structures pre-covered with oxygen atoms by plasma activation where these act as Brønsted base to form methoxy adsorbed species. The general reaction pathway for alcohol oxidation to aldehyde, acid or ester has been depicted in **Scheme 4.4**.

After the pre-covering step the adsorbed oxygen atom reacts with the hydroxyl proton of the alcohol, which is in turn adsorbed on gold surface.

<sup>89</sup> B. Hvolbæk, T. V. W. Janssens, B. S. Clausen, H. Falsig, C. H. Christensen, J. K. Nørskov, *NanoToday* **2007**, 2, 14–18.

<sup>90</sup> A. Wittstock, V. Zielasek, J. Biener, C. M. Friend, M. Bäumer, *Science* **2010**, 327, 319–322.



**Scheme 4.4:** Reaction pathway for alcohol oxidation to aldehyde, ester or acid hypothesized by Friend.<sup>90</sup>

The hydroxyl group is then allowed to take the  $\beta$ -hydrogen from the alcoholate, thus eliminating water and furnishing the desired aldehyde (*aldehyde route*, **Scheme 4.4**). At this point, the reaction can continue accord-

ing to the two conventional pathways (carboxylic acid or ester formation). If the extent of oxygen pre-covering is large the formation of the ester is disfavoured, since the gold surface will be covered by a high number of hydroxyl groups. DFT calculation showed that the  $\beta$ -H elimination is the rate-determining step of the reaction.<sup>91</sup>

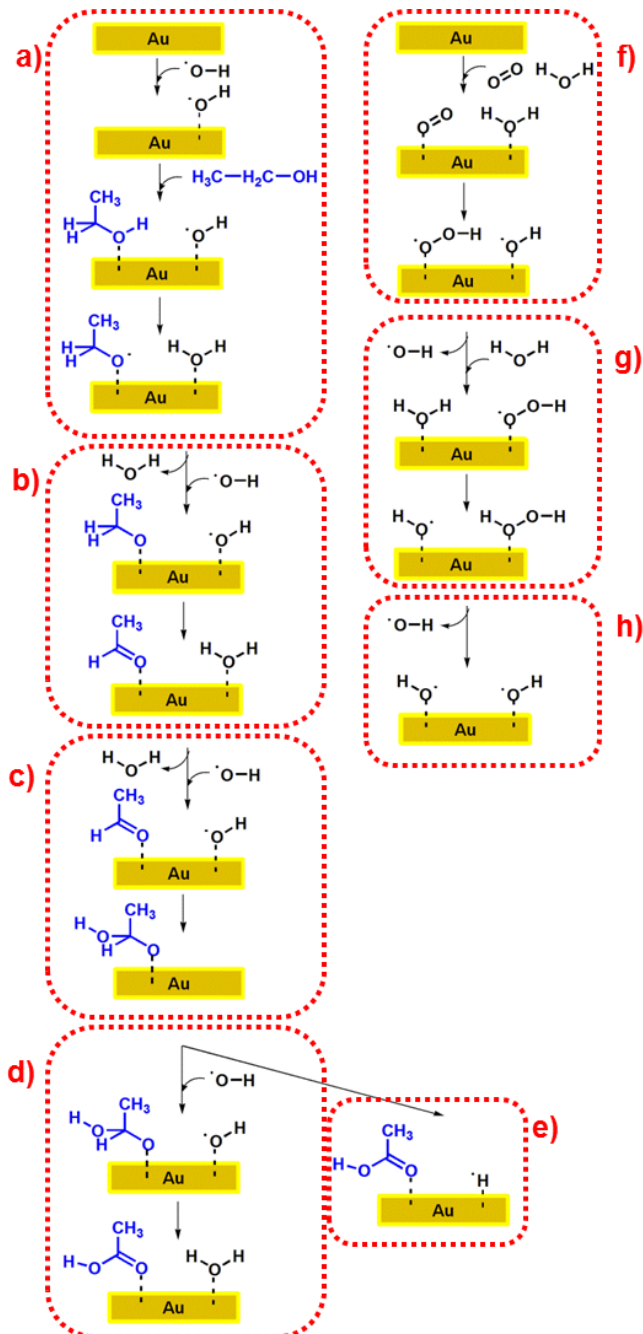
A different reaction pathway has been proposed by Davis *et al.*,<sup>92</sup> who focused the attention on ethanol oxidation, in aqueous basic reaction medium, using labelled  $^{18}\text{O}_2$  and  $\text{H}_2^{18}\text{O}$  experiments. The main steps of this mechanism are briefly reported in **Scheme 4.5**.

The hydroxyl species and one ethanol molecule are both adsorbed on gold surface; then the deprotonation of the alcohol occurs (**Scheme 4.5**). The  $\beta$ -hydrogen elimination from the adsorbed ethoxy species by an adsorbed hydroxyl group produces a geminal diol ( $52 \text{ kJ mol}^{-1}$ , **c**, **Scheme 4.5**). In the final step of reaction acetic acid is formed by a second  $\beta$ -hydrogen elimination (respectively **d** and **e**, **Scheme 4.5**); the energies for these two steps are, in order, 29 and  $21 \text{ kJ mol}^{-1}$  (this last value has been experimentally evaluated). The reaction of one oxygen and one water molecules forms two different radicals, one hydroxyl and one hydroperoxyl ( $16 \text{ kJ mol}^{-1}$ , **Scheme 4.5**) According to this mechanism, ethyl acetate could occur also result from two alcoholate species which give the intermediate hemiacetal.

---

<sup>91</sup> B. Xu, R. J. Madix, C. M. Friend, *Acc. Chem. Res.* **2014**, *47*, 761-772.

<sup>92</sup> B. N. Zope, D. D. Hibbitts, M. Neurock, R. J. Davis, *Science* **2010**, *330*, 74-78.



Scheme 4.5: Mechanism of ethanol oxidation according to Davis.92

A different reaction pathway has been proposed by Corma<sup>93</sup> and later confirmed by Chechik,<sup>71a</sup> reported in **Scheme 4.6**. According to their hypothesis, the adsorption of one alcohol molecule onto gold surface can be facilitated by the presence of a base, leading to an alcoholate species. The rate determining step is the  $\beta$ -hydride elimination from the adsorbed alcoholate which produces the Au-H species and aldehyde. Oxygen doesn't take part directly to alcohol oxidation but regenerates gold surface by reacting with the adsorbed hydrogen atom to form water.<sup>71a, 92<sup>92</sup>, 93</sup>

According to this proposal, the formation of carboxylic acid and ester can be explained by involving the formation of geminal diol or hemiacetal molecule respectively adsorbed on gold surface.<sup>34, 94</sup> Further oxidation of geminal diol or hemiacetal intermediates can occur with the same mechanism of alcohol oxidation to aldehyde.

The presence of Au-H involved in the mechanism of alcohol oxidations has been widely reported in literature. For example, Baiker *et al.* studied the oxidation of cinnamyl alcohol to cinnamaldehyde,<sup>95</sup> and found, among the other by-products, 3-phenyl-1propanol and dihydrocinnamaldehyde: their formation is an indirect evidence of the formation of Au-H.<sup>96</sup> Some years later Baiker studies on cinnamyl alcohol oxidation, some experimental evidences for the formation of Au-H species in oxidation reactions were provided.<sup>71a</sup> The formation of Au-H during oxidation processes was definitively assessed by EPR studies on 3-octanol oxidation in toluene at 70°C. The use of spin traps like *N*-tert-butyl- $\alpha$ -phenylnitron (PBN) in 1-phenylethanol oxidation allowed the formation of PBN-H species, detected in the EPR spectra.

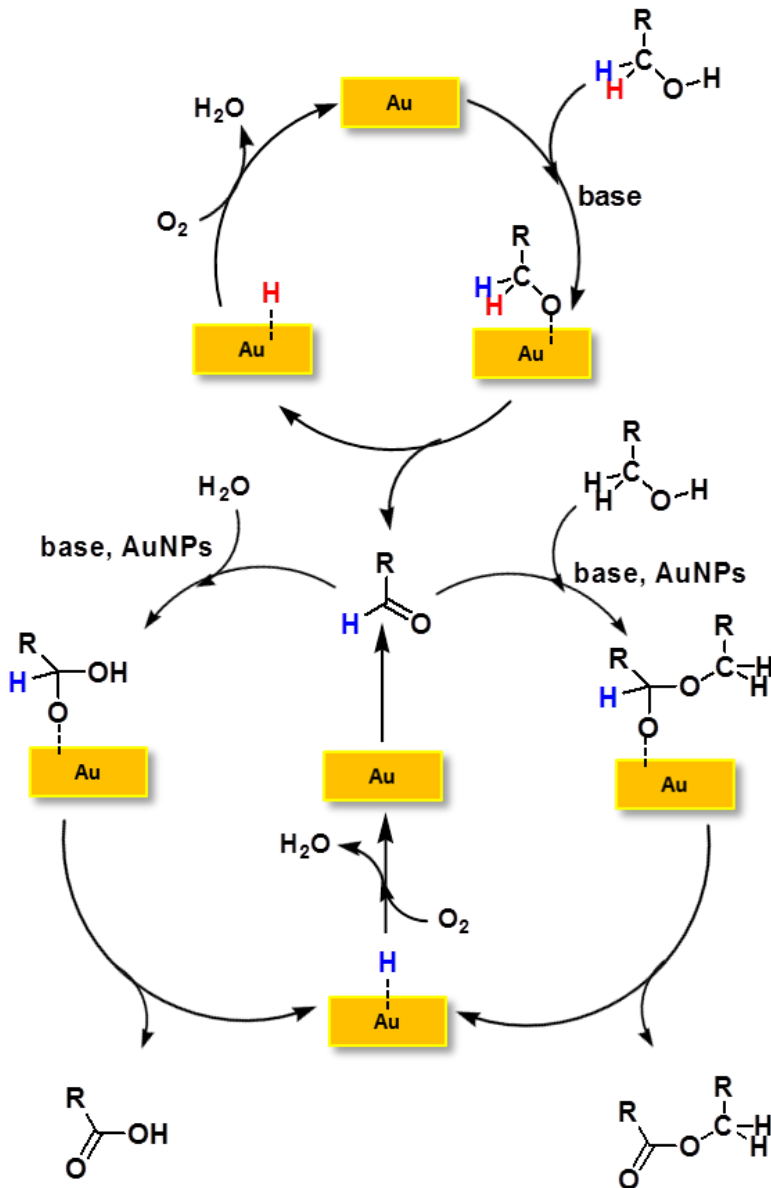
---

<sup>93</sup> A. Abad, A. Corma, H. García, H.; *Chem. Eur. J.* **2008**, *14*, 212–222.

<sup>94</sup> L. Kesavan, R. Tiruvalam, M. Hasbi Ab Rahim, M- Izham bin Saiman, D. I. Enache, R. L. Jenkins, N. Dimitratos, J. A. Lopez-Sanchez, S. H. Taylor, D. W. Knight, C.J. Kiely, G. J. Hutchings, *Science* **2011**, *331*, 195-199.

<sup>95</sup> C. Keresszegi, T. Bürgi, T. Mallat, A. Baiker, *J. Catal.* **2002**, *211*, 244-251.

<sup>96</sup> X. Ge, A. Sumboja, D. Wu, T. An, B. Li, F. W. T. Goh, T. S. A. Hor, Y. Zong, Z. Liu, *ACS Catal.* **2015**, *5*, 4643-4667.



Scheme 4.6: Mechanism proposed by Corma for alcohol oxidation.<sup>93</sup>

## 4.2: Cinnamyl alcohol oxidative esterification catalyzed by AuNPs-sPSB

Cinnamyl alcohol (CA), cinnamic acid, or cinnamates are compounds which can be extracted from natural sources and find applications in both pharmaceutical and cosmetic industries. For example, cinnamic acid shows an antioxidant, hepatoprotective, anxiolytic, insect repellent, anti-diabetic and anticholesterolemic activity.<sup>97</sup>

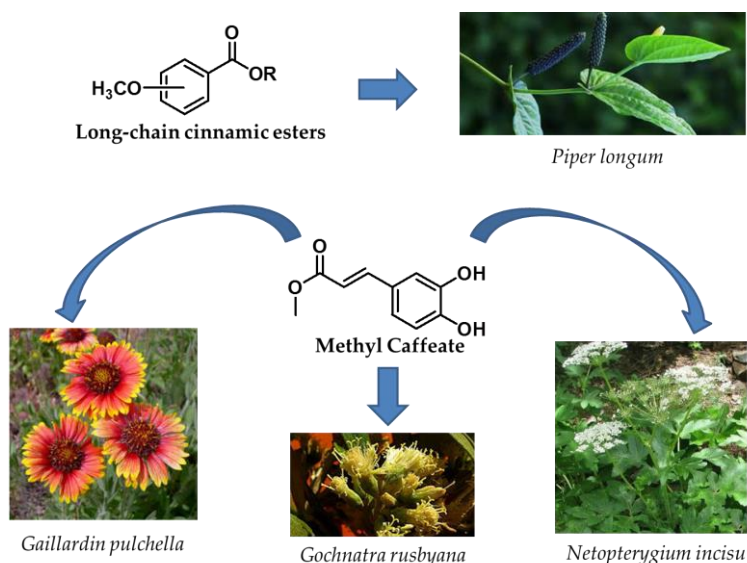


**Figure 4.3:** Some natural sources of cinnammic esters.

Methyl caffeate is one example of cinnamyl ester with interesting pharmaceutical properties. It can be found in *Gaillardin pulchella*, *Gochnatra rusbyana*, *Netopterygium incisum* (**Figure 4.3**) and has been reported to possess antitumor activity against Sarcoma 180 as well as antimicrobial activ-

<sup>97</sup> P. Sharma, *J. Chem. Pharm. Res.* **2011**, 3, 403–423.

ity.<sup>98</sup> Long-chain cinnamic esters are actually used as sunscreen agents and in cosmetic products since they do not irritate skin and prevent the drying effect of the wind.<sup>99</sup> Methoxy substituted long-chain cinnamic esters can be found, for example, in *Piper longum*, and they are active in controlling inflammatory diseases (**Figure 4.3**).<sup>100</sup>

The AuNPs, being active in oxidation reaction, have been reported as catalysts in cinnamate esters formation.

Hydrotalcite has been used as support for the AuNPs in the aerobic esterification of CA.<sup>101</sup> Using methanol as solvent at 60°C and oxygen at atmospheric pressure, methyl cinnamates were obtained with 100 mol% in selectivity in 5 h.

Quite the same results were previously obtained by Cao *et al.*<sup>102</sup>, who synthesised methyl cinnamates with a selectivity of 94 mol% in 4.5 h, at 90°C and 5 atm of O<sub>2</sub> using as support β-Ga<sub>2</sub>O<sub>3</sub>. This support contains acid site that could favour the hemiacetal formation from cinnamaldehyde and methanol. Cacchi and Vallribera<sup>103</sup> immobilized AuNPs on a fluorosilica gel and used this catalyst in both oxidation and esterification of primary and secondary alcohols. Methyl cinnamate was obtained by *cross-coupling* of CA with methanol with a selectivity of 89 mol% in 24 h at 100°C.

Considering CA oxidation, eight different subproducts can be obtained in addition to cinnamaldehyde (**Scheme 4.7**). Moreover, considering the aerobic esterification of CA with 1-butanol, oxidation products coming

---

<sup>98</sup> N.H. Nam, Y.J. You, Y.D. Kim, H. Hong, H.M. Kim, Y.Z. Ann, *Bioorg. Med. Chem. Lett.*, **2001**, *11*, 1173.

<sup>99</sup> A. Alexander, R.K. Choudhary, US Patent No. 5527947, **1996**.

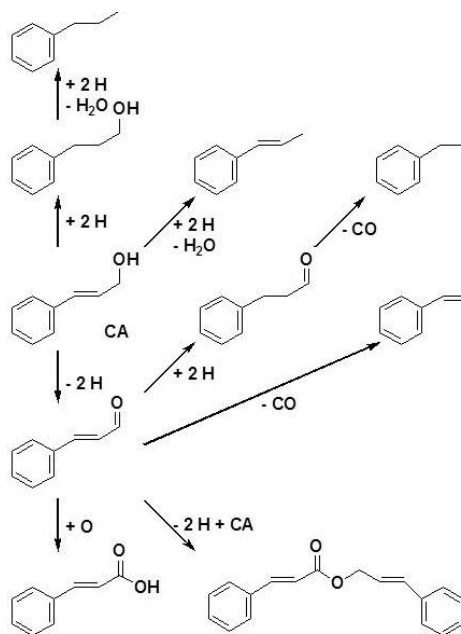
<sup>100</sup> S. Kumar, P. Arya, C. Mukherjee, B.K. Singh, N. Singh, V.S. Prasad, A.K. Ghose, *Biochemistry*, **2005**, *44*, 15944.

<sup>101</sup> P. Liu, C. Li, E. J. M. Hensen, *Chem. Eur. J.* **2012**, *18*, 12122-12129.

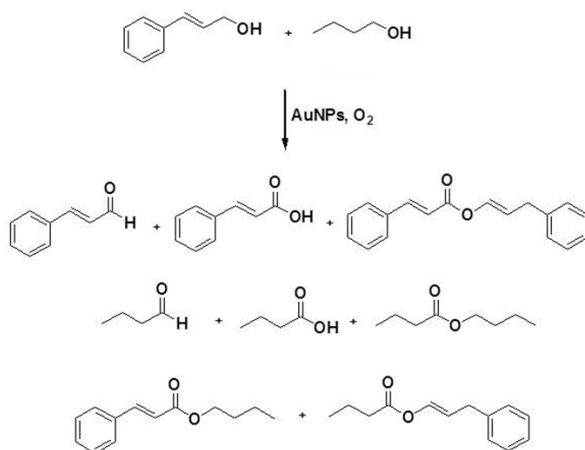
<sup>102</sup> F.-Z. Su, J. Ni, H. Sun, Y. Cao, H.-Y. He, K.-N. Fan, *Chem. Eur. J.* **2008**, *14*, 7131-7135.

<sup>103</sup> R. Bernini, S. Cacchi, G. Fabrizi, S. Niembro, A. Pastaro, A. Shafir, A. Vallribera, *ChemSusChem* **2009**, *9*, 1036-1040.

from the alkyl alcohol can be obtained at least in theory, together with the formation of *self-coupling* esters (**Scheme 4.8**).



**Scheme 4.7:** Different reaction pathways for oxidation of cinnamyl alcohol.



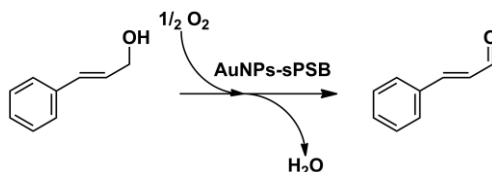
**Scheme 4.8:** Different reaction product for esterification of CA with 1-

Considering that the activity of AuNPs-sPSB catalyst has been already reported in literature,<sup>53</sup> the aerobic oxidative esterification of CA was studied in order to gain informations about the selectivity of the catalyst and to investigate the role of the polymeric matrix.

#### 4.2.1: Cinnamyl alcohol oxidation

CA oxidation was initially studied using the reaction conditions already reported in literature for the AuNPs-sPSB catalyst (35°C, water/chloroform 1:1 *v/v*,  $P_{O_2}$  = 1 bar, 1 equiv. of KOH).<sup>53</sup> The formation of the nanoporous  $\epsilon$  form of syndiotactic polystyrene was achieved *in situ*.

**Table 4.2:** Aerobic oxidation of CA with the AuNPs-sPSB catalyst.



Entry <sup>[a]</sup>	T [°C]	KOH/CA [molar ratio]	t [h]	Conv. <sup>[b]</sup> [mol%]	Selec. <sup>[b]</sup> [mol%]
1	35	1	2	97	97
2	35	6	1.5	>99	99
3	35	20	4	>99	92
4	10	6	8	>99	95
5	25	6	5	98	96
6	45	6	0.75	97	99

[a] Reaction conditions: CA (0.51 mmol), **Au-C $\beta$**  (200 mg, 2 *wt%* in Au), O<sub>2</sub> (1 atm), water/chloroform *v/v* = 1:1, total volume 6 mL. [b] Conversions and yields evaluated using GC-MS analysis with anisole as internal standard.

Cinnamaldehyde was always obtained as the main reaction product, and the only by-product formed in small quantities was 3-phenyl-1-propanol from reduction of the olefinic double bond of CA.<sup>71a</sup> Without KOH the conversion of CA was only 21 *mol%* in 24 h. One equivalent of KOH led

to a conversion of 97 mol% and cinnamaldehyde with a selectivity of 97 mol% (entry 1, Table 4.2). With 6 equivalent of KOH, the reaction is quantitative after 1.5 h with a selectivity of 99 mol% (entry 2, Table 4.2 and Figure 4.4). A further increase in KOH to 20 equivalent, slightly slows down the oxidation rate with a total conversion of CA in 4 h (entry 3, table 4.2).<sup>104</sup> The kinetic plot of entry 2, Table 4.2 is reported in Figure 4.4.

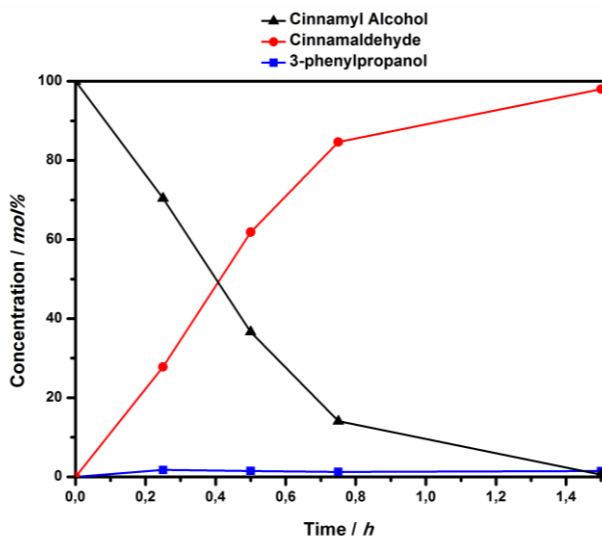


Figure 4.4: Kinetic plot of CA oxidation carried out with 6 equivalent of KOH (entry 2, Table 4.2).

The reaction is *pseudo* first order in CA, and the kinetic constants found at variance of KOH concentration are:  $(5.9 \cdot 10^{-4} \pm 7.9 \cdot 10^{-5}) \text{ s}^{-1}$  for  $0.09 \text{ mol L}^{-1}$  of KOH,  $(1.0 \cdot 10^{-3} \pm 9.8 \cdot 10^{-5}) \text{ s}^{-1}$  for  $0.5 \text{ mol L}^{-1}$  of KOH and finally  $(4.1 \cdot 10^{-4} \pm 3.0 \cdot 10^{-5}) \text{ s}^{-1}$  for  $1.7 \text{ mol L}^{-1}$  of KOH.

Thus the plot of  $k$  vs KOH concentration shows a volcano profile that can be explained according to the Langmuir-Hinshelwood mechanism, in

<sup>104</sup> A. Buonerba, A. Noschese, A. Grassi, *Chem. Eur. J.* **2014**, *20*, 5478 – 5486.

which both the reagents need to be adsorbed on catalyst surface (**Figure 4.5**).

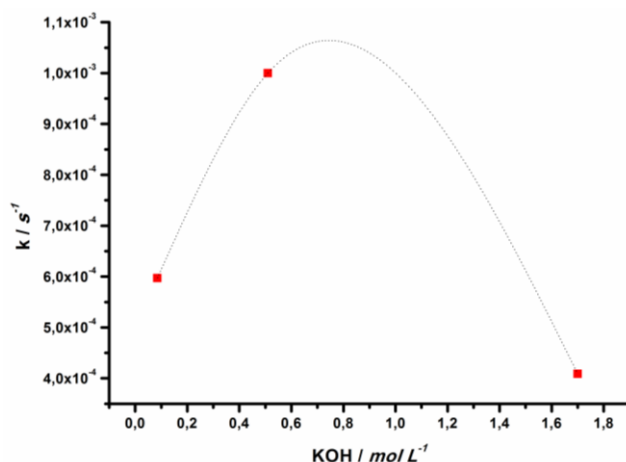


**Figure 4.5:** Dependence of the conversion constant of CA  $k$  on the concentration of KOH (0.09, 0.51 and 1.7 mol L<sup>-1</sup>) at a constant concentration of CA (0.09 mol L<sup>-1</sup>) at 35°C. Langmuir Hinshelwood fitting is represented by the dot line.

Thus CA and KOH compete for the same catalytic sites, and the presence of an excess of one of the reagents slows down the rate of reaction.<sup>105</sup> This finding supports the oxidation mechanism proposed by Davis<sup>9292</sup>, in which both ethanol and hydroxyl specie need to be both adsorbed on the AuNPs surface.

When the reaction temperature was decreased, high conversions and selectivities were achieved at longer reaction times (entries **4** and **5**, **Table 4.2**). On the contrary the increase of temperature to 45°C shortens the reaction time, leaving totally unaffected both conversion and selectivity (entry **6**, **Table 4.2**).

<sup>105</sup> *Physical Chemistry*, Keith J. Laidler, John H. Meiser, Benjamin/Cummings, 1982.

To clarify the effect of temperature on the cinnamaldehyde formation, CA oxidation was performed in the temperature range of 10-45°C (**Figure 4.6**).

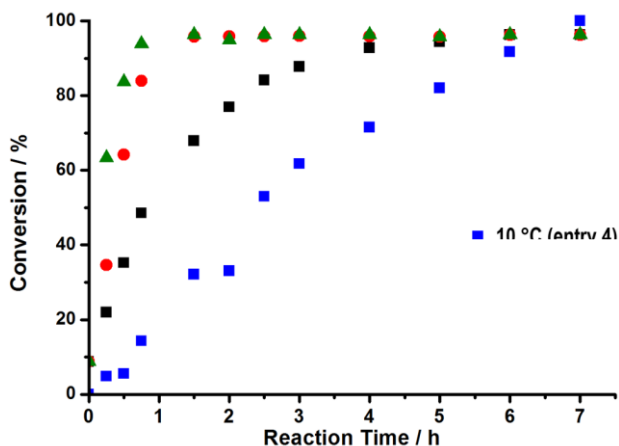


**Figure 4.6:** CA oxidation to cinnamaldehyde in the temperature range of 10-45°C.

The CA conversion considerably increases passing from 10°C to 25°C, while the increase of temperature from 35°C to 45°C doesn't produce significant increases of CA conversion. The oxidation of CA to cinnamaldehyde was found to be a *pseudo* first order reaction respect to the alcohol. The calculated kinetic constants for the four reactions reported in **Figure 4.6** are  $(1.1 \cdot 10^{-4} \pm 7.0 \cdot 10^{-6}) \text{s}^{-1}$  at 10°C,  $(2.2 \cdot 10^{-4} \pm 2.6 \cdot 10^{-6}) \text{s}^{-1}$  at 25°C,  $(1.0 \cdot 10^{-3} \pm 9.8 \cdot 10^{-5}) \text{s}^{-1}$  at 35°C and finally  $(1.3 \cdot 10^{-3} \pm 1.3 \cdot 10^{-4}) \text{s}^{-1}$  at 45°C (**a, Figure 4.7**). The corresponding Arrhenius plot gives an activation energy ( $E_a$ ) value of  $57.8 \pm 11.5 \text{ kJ mol}^{-1}$  (**b, figure 4.7**), in agreement with the  $E_a$  found for *p*-methyl benzyl alcohol oxidation with the AuNPs-CeO<sub>2</sub><sup>993</sup> and higher than the one found for oxidation of *p*-hydroxybenzyl alcohol catalyzed by the AuNPs incarcerated in PVP.<sup>40</sup>

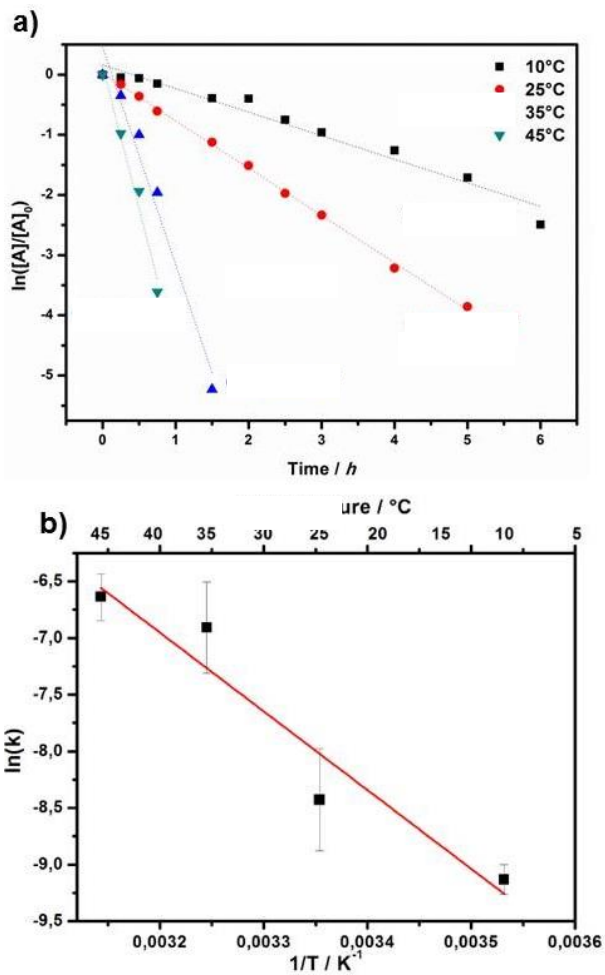


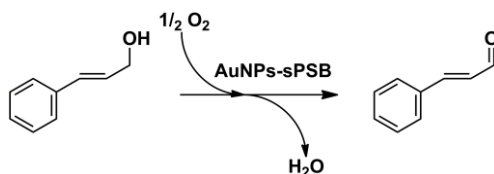
**Figure 4.7:** a) *pseudo* first order plots for the reactions in the range 10-45°C, and b) Arrhenius plot.

**4.2.2: The reaction solvent**

CA oxidation was also screened in different solvents to find more sustainable conditions for this reaction.<sup>104</sup>

The solvent mixture H<sub>2</sub>O/Ethyl acetate (*v/v*=1:1) causes a strong decrease in CA conversion which drops to 20 mol%, probably for the reduced swelling of the polymeric matrix and for the poor diffusion of reagents towards active sites; however cinnamaldehyde is still the main reaction product with a selectivity of 91 mol% (entry 1, Table 4.3). In H<sub>2</sub>O/2-butanone (*v/v*=1:1) the conversion of CA was 44 mol% (entry 2, Table 4.3).

**Table 4.3:** Oxidation of CA performed with different solvents.



Entry <sup>[a]</sup>	Solvent	t [h]	Conv. <sup>[b]</sup> [mol%]	Product	Selec. <sup>[b]</sup> [mol%]
1	H <sub>2</sub> O/ Ethyl Acetate	24	20	Cinnamaldehyde	91
				3-Phenyl-1-propanol	9.0
2	H <sub>2</sub> O/ 2-Butanone	8	44	7-phenylhepta-4,6-dien-3-one	69
				Cinnamaldehyde	8.7
				3-Phenyl-1-propanol	8.3
3	H <sub>2</sub> O/ Cyclohexanone	6	56	Cinnamaldehyde	93
				3-Phenyl-1-propanol	7.0
6	H <sub>2</sub> O/Toluene	3	90	Cinnamaldehyde	93
				3-Phenyl-1-propanol	1.4

[a] Reaction conditions: CA (0.51 mmol), 35°C, KOH/CA=6 (molar ratio), **Au-Cβ** (200 mg, 2 wt% of Au), O<sub>2</sub> (1 atm), solvent *v/v* = 1:1, total volume 6 mL. [b] Conversions and yields evaluated using GC-MS analysis with anisole as internal standard.

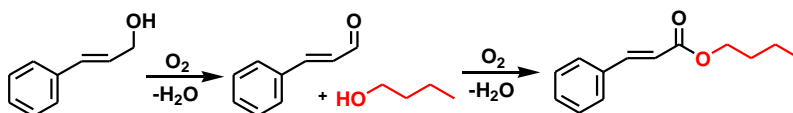
The solvent mixture H<sub>2</sub>O/Cyclohexanone (*v/v*=1:1) allows the conversion of CA up to 56 mol%, with cinnamaldehyde selectivity of 93 mol% (entry 3, **Table 4.3**), whereas toluene produced a CA conversion of 90 mol% and a cinnamaldehyde selectivity of 93 mol%: hence this aromatic solvent guarantees a good swelling of the polymeric support and a good accessibility of the substrates to the AuNPs incarcerated within the copolymer, but unfortunately it is not a green solvent.

#### **4.2.3: Cinnamyl alcohol oxidative esterification**

The direct oxidative esterification of CA with 1-butanol was preliminary investigated. The results are reported in **Table 4.4**.<sup>104</sup> Butyl cinnamate was the only ester to be formed, and no oxidation products coming from the alkyl alcohol were detected.

When 3 equivalents of 1-butanol were initially used, butyl cinnamate was obtained in moderate yield (22 mol%, entry 1, **Table 4.4**); the increase in 1-butanol concentration slightly increases the conversion into butyl cinnamate (entry 2, **Table 4.4**). On varying the KOH concentration from 1 to 12 equivalents, the best result was obtained with 6 equivalents of base, achieving a total conversion of CA and butyl cinnamate and cinnamaldehyde in 48 mol% and 46 mol% in yield respectively (entry 4, **Table 4.4** and **Figure 4.7**). A further increase in the concentration of the base resulted in a slightly decrease in catalytic activity.

A complete formation of butyl cinnamate was obtained for long reaction time (24 h, not included in the plot of **Figure 4.7**) using 6 or 12 equivalents of base. The kinetic plot of the entry 4 **Table 4.4** is reported in **Figure 4.7**. From the inspection of this figure it is clear that the aerobic oxidative esterification of CA is a two-step reaction, where the alkyl ester, namely butyl cinnamate is formed only after that CA oxidation into cinnamaldehyde is complete.

**Table 4.4:** Synthesis of butyl cinnamates by aerobic oxidative esterification of CA.

Entry <sup>[a]</sup>	KOH/CA	1-butanol /CA	Products	Yield <sup>[b]</sup> [mol%]
1	1	3	butyl cinnamate	22
			cinnamaldehyde	69
			2-phenyl-1-propanol	8.0
2	1	10	butyl cinnamate	29
			cinnamaldehyde	69
			2-phenyl-1-propanol	2.0
3	3	10	butyl cinnamate	28
			cinnamaldehyde	69
			2-phenyl-1-propanol	3.0
4	6	10	butyl cinnamate	48
			cinnamaldehyde	46
			2-phenyl-1-propanol	6.0
5	12	10	butyl cinnamate	44
			cinnamaldehyde	48
			2-phenyl-1-propanol	8.0

[a] Reaction conditions: CA (0.51 mmol), **Au-C $\beta$**  (200 mg, Au=2%w/w), 1-butanol (5.1 mmol), 35°C, O<sub>2</sub> (1 atm), H<sub>2</sub>O/CHCl<sub>3</sub> (*v/v*=1:1, total volume=6 mL), 3h, conversion of CA >99%. [b] Conversions and yields evaluated using GC-MS analysis with anisole as internal standard.

To gain informations on the activation energy for the formation of butyl cinnamate, esterification of cinnamaldehyde with 1-butanol in the temperature range of 10-45°C was performed (**Table 4.5**).

The conversion plots of the reactions reported **Table 4.5** is reported in **a**, **Figure 4.8**. The  $E_a$  found through the Arrhenius plot (**b**, **figure 4.8**) is equal to (62.7±16.7) kJ mol<sup>-1</sup>. It is important to note that in this second reaction step no traces of 3-phenyl-1-propanol were found, suggesting that this compound is formed as by-product only in the first step of the reaction by CA reduction.

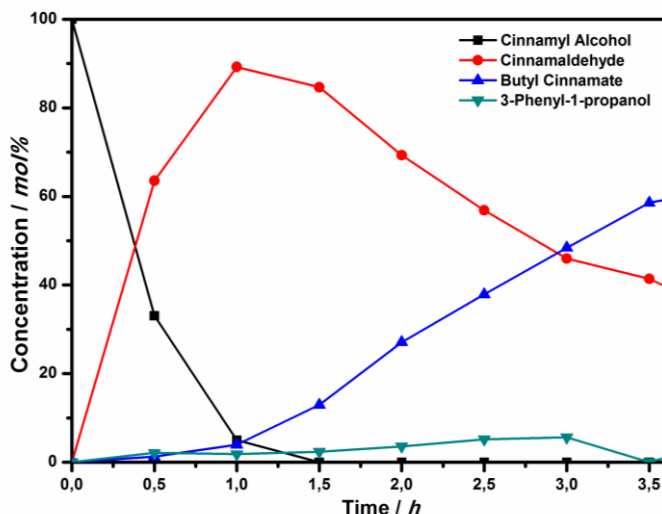
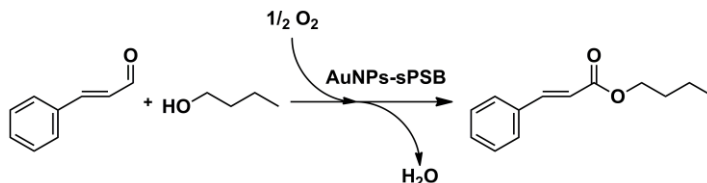


**Figure 4.7:** Kinetic profile of aerobic oxidative esterification of the reaction reported in entry 4, Table 4.4.

**Table 4.5:** Esterification of cinnamaldehyde with 1-butanol



Entry <sup>[a]</sup>	T [°C]	t [h]	Yield <sup>[b]</sup> [mol%]	Selectivity <sup>[b]</sup> [mol%]
1	10	6	6.7	>99
2	25	7	12	>99
3	35	6	>99	>99
4	45	6	89	>99

[a] Reaction conditions: cinnamaldehyde (0.51 mmol), 1-butanol (5.1 mmol), **Au-C $\beta$**  (200 mg, Au=2%w/w), O<sub>2</sub> (1 atm), H<sub>2</sub>O/CHCl<sub>3</sub> (*v/v*=1:1, total volume=6 mL), KOH (3.06 mmol, 6 equiv.). [b] Yields and selectivities evaluated with GC-MS analysis using anisole as internal standard.

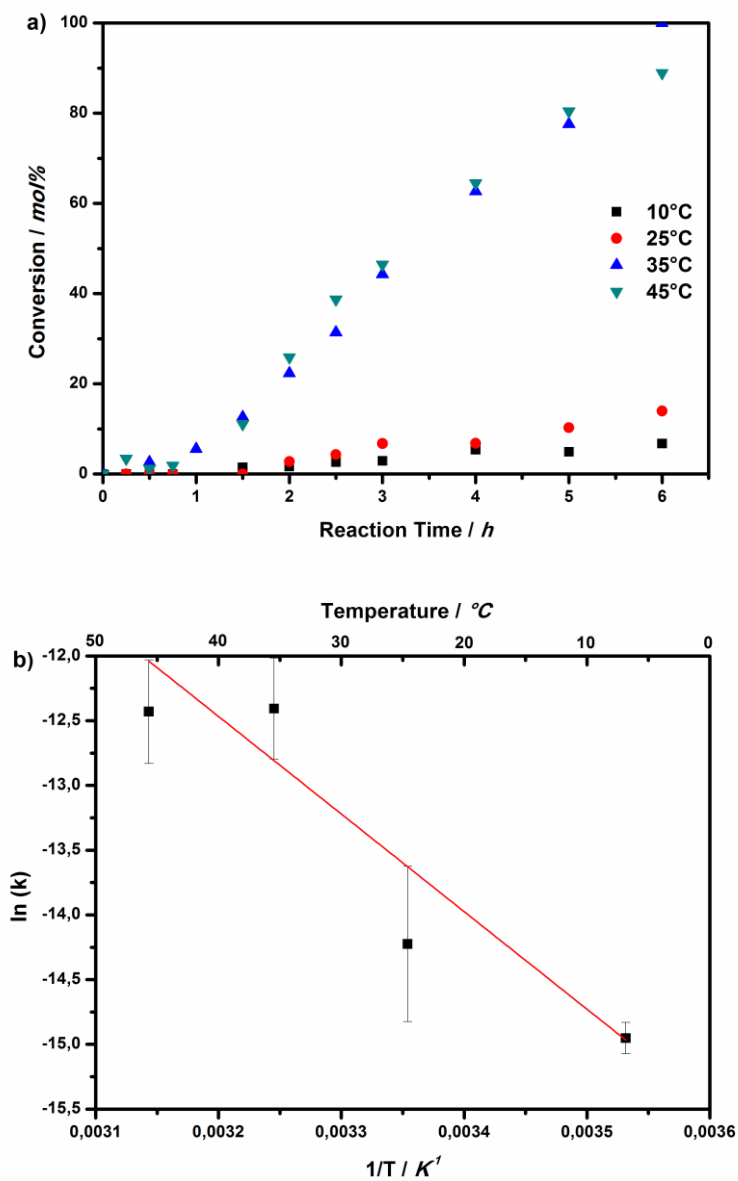
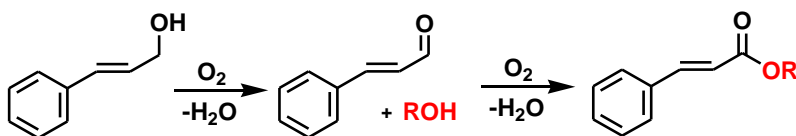


**Figure 4.8:** Cinnamaldehyde esterification with 1-butanol: **a)** conversion in the rate 10-45°C and **b)** Arrhenius plot.

**4.2.4: Esterification with different alkyl alcohols**

Different alkyl alcohols such as methanol, ethanol, 2-propanol, 1-hexanol, 1-octanol and 2-phenylpropanol were tested at 35°C with 6 equivalents of KOH; the results are reported in **Table 4.6**.<sup>104</sup>

**Table 4.6:** Synthesis of alkyl cinnamates by aerobic oxidative esterification of CA.



Entry	Alkyl Alcohol	t [h]	Products	Yield <sup>[b]</sup> [mol%]
1	methanol	4	methyl cinnamate	90
			cinnamaldehyde	8.1
			2-phenyl-1-propanol	1.9
2	ethanol	5	ethyl cinnamate	94
			2-phenyl-1-propanol	6.0
3	2-propanol	5	isopropyl cinnamate	9.2
			cinnamaldehyde	86
			2-phenyl-1-propanol	4.8
4	1-hexanol	5	hexyl cinnamate	12
			cinnamaldehyde	85
			2-phenyl-1-propanol	3.0
5	1-octanol	5	octyl cinnamate	11
			cinnamaldehyde	86
			2-phenyl-1-propanol	3.0
6	2-phenylethanol	5	2-phenylethyl cinnamate	44
			cinnamaldehyde	50
			2-phenyl-1-propanol	2.0

[a] Reaction conditions: CA (0.51 mmol), **Au-C $\beta$**  (200 mg, Au=2%w/w), alkyl alcohol (5.1 mmol), KOH/CA=6 (molar ratio), 35°C, O<sub>2</sub> (1 atm), H<sub>2</sub>O/CHCl<sub>3</sub> (v/v=1:1, total volume=6 mL), conversion of CA >99%. [b] Yields evaluated using GC-MS analysis with anisole as internal standard.

## Oxidation Reactions catalyzed by AuNPs-sPSB

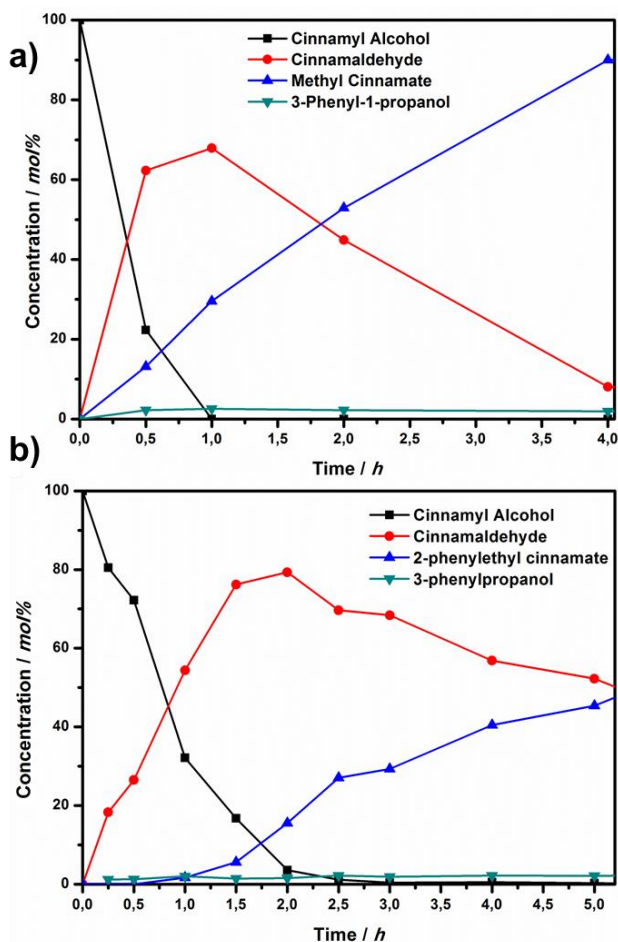


**Figure 4.9:** Kinetic plots of CA esterification with: **a)** methanol and **b)** 2-phenylethanol (Table 4.6).

Methanol and ethanol yielded respectively methyl and ethyl cinnamate in high yields (90 mol%, 4h, entry 1; 94 mol%, 5h, entry 2, Table 4.6), and a total conversion was achieved in both cases after 24 h. The reaction slows down when bulkier alkyl alcohol were used (entries 3-6, Table 4.6), since the diffusion toward the AuNPs through the polymeric matrix is hampered by their bulkiness. However, 2-phenylpropanol furnished excellent

results since 2-phenylethyl cinnamate was obtained with a yield of 44 mol% in 5 h, probably for the affinity of the aromatic moiety with polystyrene host matrix.<sup>54, 57, 106</sup>

The kinetic profiles of esterification of CA with methanol and 2-phenylethanol (entries 1 and 6, Table 4.6) are compared in Figure 4.9. In the first case CA is completely converted to the aldehyde in only 1 h and the highest yield in methyl cinnamate were reached after 4h (90 mol%, entry 1, Table 4.6). In the second case the oxidation of CA is complete only after 2.5 h, and 44 mol% yield of the ester was achieved after 5 h: this result can be explained considering that CA as well as 2-phenylethanol shows a fast diffusion into the polymeric matrix. The kinetic constants were calculated considering the second step of the overall reaction, since the ester is formed only when CA is completely oxidized.

**Table 4.7.** Rate constants for the oxidative esterification of cinnamaldehyde with alkyl alcohols evaluated from the second reaction step of the CA oxidation.

Entry <sup>[a]</sup>	Alkyl Alcohol <sup>[b,c]</sup>	$k_{\text{obs}}$ [mol L <sup>-1</sup> s <sup>-1</sup> ]	Evaluated from table 4.6, entry x
1	methanol	$4.63 \cdot 10^{-6}$	1
2	ethanol	$4.65 \cdot 10^{-6}$	2
3	1-butanol	$4.93 \cdot 10^{-6}$	3
4	2-propanol	$5.38 \cdot 10^{-7}$	4
5	1-hexanol	$6.12 \cdot 10^{-7}$	5
6	1-octanol	$1.14 \cdot 10^{-6}$	6
7	2-phenylethanol <sup>[d]</sup>	$4.35 \cdot 10^{-5} \text{ s}^{-1}$	7

[a] Reaction conditions: cinnamyl alcohol (0.51 mmol), Au-C $\beta$  (200 mg, gold=2 wt%), alkyl alcohol (5.1 mmol), KOH (3.06 mmol), 35°C, O<sub>2</sub> (1 atm), H<sub>2</sub>O/CHCl<sub>3</sub> (v/v=1:1, total volume=6 mL), anisole as an internal standard (0.51 mmol). [c] Pseudo-zero-order reaction. [d] Pseudo first-order reaction.

<sup>106</sup> R.-M. Ho, C.-P. Lin, H.-Y. Tsai, E.-M. Woo, *Macromolecules* **2000**, 33, 6517-6526.

From the inspection of **Table 4.7** it is clear that the esterification of cinnamaldehyde proceeds faster with short chain alkyl alcohols (methanol, ethanol, butanol), while alcohols showing higher steric hindrance (2-propanol, 1-hexanol, 1-octanol) react slower. The different mechanism of access inside the polymeric matrix was confirmed by the different kinetic order found: the reaction is *pseudo* zero order for all the alkyl alcohols whereas is *pseudo* first order just for 2-phenylethanol (**Figure 4.9**). However, the oxidation of CA to cinnamaldehyde proceeds always faster than the oxidative coupling of this with the alkyl alcohols.

The AuNPs-sPSB catalyst thus exhibits a high activity in the one pot synthesis of alkyl cinnamates under mild conditions.<sup>80, 85, 88, 102, 103, 107</sup> The TOF calculated for the first step of reaction at 35°C is 21.2 h<sup>-1</sup>, whereas a TOF=5.6 h<sup>-1</sup> was found for the esterification of CA to methyl cinnamate (entry **1**, **Table 4.7**); it is noteworthy this is one of the highest values of TOF already reported in literature for oxidative esterification of CA to methyl cinnamate is 7.4 h<sup>-1</sup> at 100°C.<sup>103</sup>

#### **4.2.5: Esterification of p-substituted cinnamyl alcohols**

Different *p*-substituted cinnamyl alcohols have been tested to assess the general validity of the synthetic protocol here described. As previously described, these compounds are important chemicals in the pharmaceutical and cosmetic industries.<sup>97</sup> The results are reported in **Table 4.8**.<sup>104</sup>

From **Table 4.8** it can be observed that *p*-substituted CA produced the corresponding methyl cinnamates in high yields. Two examples of kinetic plots are reported in **Figure 4.10**.

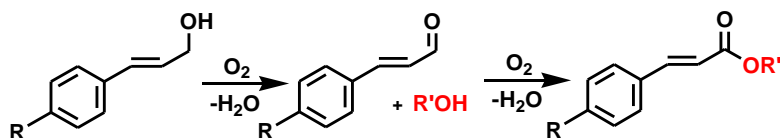
*p*-methoxy cinnamyl alcohol is oxidized faster to aldehyde than *p*-chloro cinnamyl alcohol, as result of an activating effect of Electron Donating

---

<sup>107</sup> **a)** T. Ishida, M. Nagaoka, T. Akita, M. Haruta, *Chem. Eur. J.* **2008**, *14*, 8456–8460; **b)** C. Marsden, E. Taarning, D. Hansen, L. Johansen, S. K. Klitgaard, K. Egeblad, C. H. Christensen, *Green Chem.* **2008**, *10*, 168–170; **c)** B. Xu, X. Liu, J. Haubrich, C. M. Friend, *Nat. Chem.* **2010**, *2*, 61–65.

Group (EDG): this supports the idea of the formation of ionic intermediate specie bearing a positive charge on the carbinol carbon atom to be oxidized.<sup>93</sup> Considering **b**, **Figure 4.10**, an activating effect of Electron Withdrawing Group (EWG) can be observed for the ester formation, since in this case *p*-chloro atom subtracts electronic density favouring the formation of the hemiacetal intermediate after the reaction between the *p*-chlorocinnamaldehyde and the alkyl alcohol.

**Table 4.8:** Oxidative esterification of CA with methanol and 1-butanol.



Entry <sup>[a]</sup>	R	Alkyl Alcohol	Products	Yield <sup>[b]</sup> [mol%]
1	-OMe	methanol	methyl <i>p</i> -methoxycinnamate	21
			<i>p</i> -methoxycinnamaldehyde	76
2	-OMe	1-butanol	butyl <i>p</i> -methoxycinnamate	6.2
			<i>p</i> -methoxycinnamaldehyde	91
3	-Cl	methanol	methyl <i>p</i> -chlorocinnamate	52
			<i>p</i> -chlorocinnamaldehyde	48
4	-Cl	1-butanol	butyl <i>p</i> -chlorocinnamate	26
			<i>p</i> -chlorocinnamaldehyde	74

[a] Reaction conditions: *p*-substituted CA (0.51 mmol), alkyl alcohol (5.1 mmol), **Au-Cβ** (200 mg, Au=2%w/w), O<sub>2</sub> (1 atm), H<sub>2</sub>O/CHCl<sub>3</sub>, (*v/v*=1:1, total volume= 6 mL); 35°C, KOH (3.06 mmol), 6 h, conversion >99%. [b] Conversions and yields calculated with GC-MS analysis, using anisole as internal standard.

The analysis of EDG and EWG effect on the overall conversion of *p*-substituted CA into methyl cinnamates supports the presence of a two steps mechanism and gives informations on the electronic effects which

affect the reaction kinetic of both CA oxidation into cinnamaldehyde and ester formation from the aldehyde.

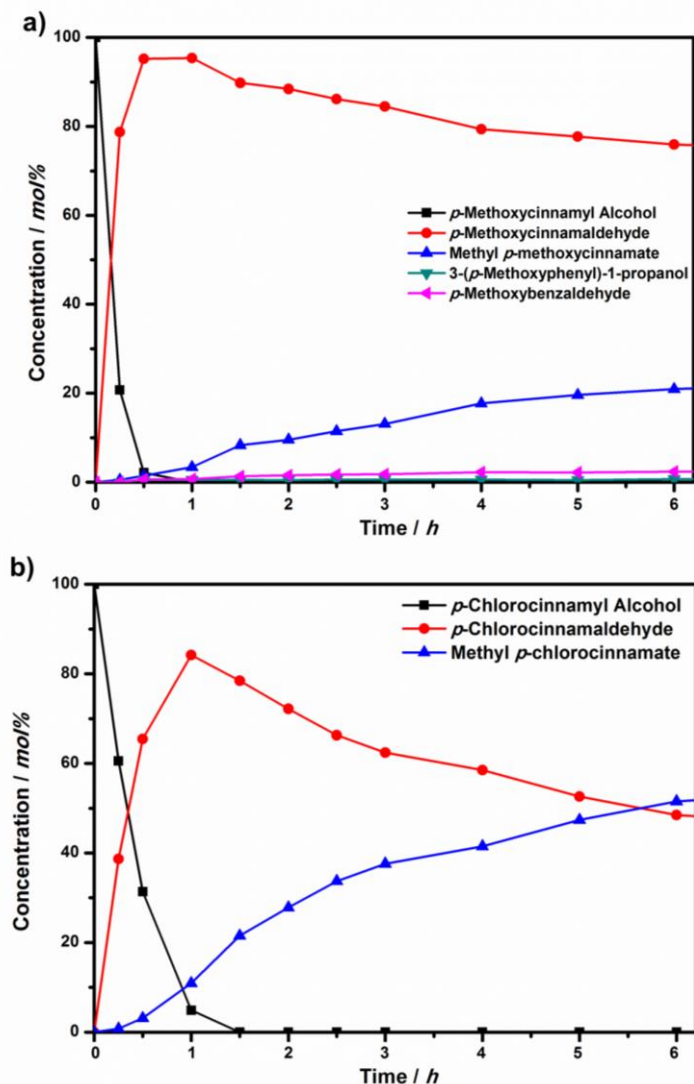
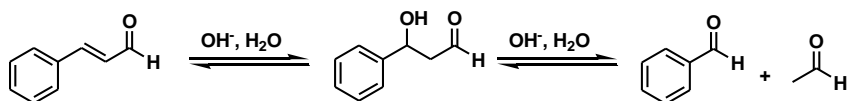


**Figure 4.10:** Methyl cinnamates synthesis with a) *p*-methoxy and b) *p*-chloro cinnamyl alcohols.

#### 4.2.6: Side reactions

In the course of our studies on CA oxidation, benzaldehyde was found in traces, and this could come from the retro-aldol reaction in basic medium (**Scheme 4.9**).<sup>81, 108</sup>



**Scheme 4.9:** Retro-aldol reaction of cinnamaldehyde in basic medium which furnishes benzaldehyde and acetaldehyde.

We decided to further investigate this reaction at high oxygen pressure to understand if other parallel and secondary reaction pathways could occur. Cinnamaldehyde was oxidized at 25°C and 55°C with high pressures of O<sub>2</sub> (25 bar), using a KOH/cinnamaldehyde molar ratio of 12 in D<sub>2</sub>O:CD<sub>3</sub>CN (*v/v* = 6:1) as solvent mixture to allow NMR characterization of the reaction products.

The product distribution achieved is reported in **Table 4.9**.

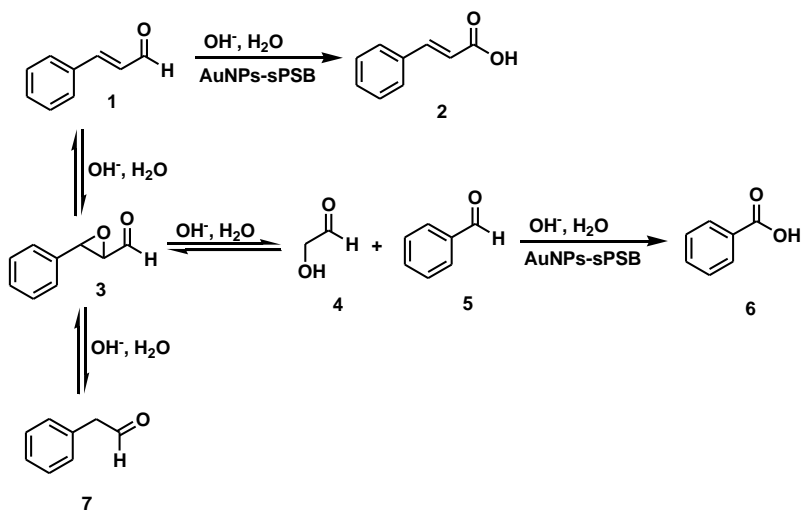
The wide range of products detected can be explained according to the reaction mechanism reported in **Scheme 4.10**. The epoxide intermediate (3-phenyloxirane-2-carbaldehyde, **3**) can be formed in basic medium leading to the formation of acetaldehyde, phenylacetaldehyde (**7**) or benzaldehyde (**5**), which analogously to cinnamaldehyde (**1**), can react to give benzoic acid (**6**). Formic acid could come from a further cleavage of 2-hydroxyacetaldehyde or as by-product in the achievement of phenylacetaldehyde.

<sup>108</sup> a) W. Zhou, J. Ye, *International Patent*, 1911891, 2007; b) G. D. Yadav, G. P. Fernandes, *Catal. Today* **2013**, 207, 162–169.

**Table 4.9:** Side reactions with of cinnamaldehyde at high oxygen pressure.

Entry <sup>[a]</sup>	T [°C]	t [h]	Product	Yield <sup>[b]</sup> [mol%]
1	25	24	Benzoic Acid	42
			Benzoate	6.4
			Cinnamic Acid	12
			Cinnamate	21
			Formic Acid	13
			3-phenyloxirane-2-carbaldehyde	1.4
			Phenylacetaldehyde	4.5
2	55	3	Benzoic Acid	17
			Benzoate	10
			Cinnamic Acid	28
			Cinnamate	2.8
			Formic Acid	10
			3-phenyloxirane-2-carbaldehyde	11
			Phenylacetaldehyde	12

[a] Reaction conditions: Cinnamaldehyde (2.03 mmol), KOH/Cinnamaldehyde=1.51 (molar ratio), D<sub>2</sub>O:CD<sub>3</sub>CN (*v/v*=6:1, 7 mL), O<sub>2</sub> (25 bar), **Au-Cε** (200 mg, 1mol% of Au), conversion >99%.

**Scheme 4.10:** Side reaction pathway starting from cinnamaldehyde in basic medium.

The epoxidation of double bonds catalyzed by the AuNPs has been already reported in literature.<sup>109</sup> Metal oxides have been used to support the AuNPs; H<sub>2</sub>O<sub>2</sub> is generally used as oxidant agent, and it can be generated in situ by reaction of H<sub>2</sub> and O<sub>2</sub>.

The data here reported show that the AuNPs-sPSB catalyst could be able to form epoxide starting from cinnamaldehyde,<sup>110</sup> using low reaction temperature. However, in the case here reported, the use of basic medium doesn't allow the formation of the epoxide **3** in high yields, thus further studies are therefore required.

### **4.3: Aerobic oxidation of amino-alcohols**

Aminoalcohols are a very interesting class of organic compounds used as intermediates in several chemical transformations. However the co-presence of the amino substituent requires the use of protective groups<sup>111</sup> since these can be easily oxidized or eliminated,<sup>112</sup> thus introducing two extra synthetic steps (protection and deprotection).

Since the AuNPs-sPSB catalyst have been successfully used for oxidation of *p*-substituted benzyl<sup>53</sup> and cinnamyl alcohol,<sup>104</sup> this catalyst was preliminarily tested in the aerobic oxidation and esterification of *p*-

---

<sup>109</sup> **a)** A. K. Sinha, S. Seelan, S. Tsubota, M. Haruta, *Angew. Chem. Int. Ed.* **2004**, *43*, 1545-1548; **b)** A. K. Sinha, S. Seelan, S. Tsubota, M. Haruta, *Top. Catal.* **2004**, *29*, 95-102; **c)** D. K. Dumbre, V. R. Choudhary, N. S. Patil, B. S. Uphade, S. K. Chavgava *J. Coll. Inter. Sci.* **2014**, *415*, 111-116; **d)** C.-O. L. Crites, G. L. Hallet-Tapley, M. Gonzalez-Bejar, J. C. Netto-Ferreira, J. C. Scaiano, *Chem. Comm.* **2014**, *50*, 2289-2291;

<sup>110</sup> **a)** S. N. Juliá, J. Masana, J. C. Vega, *Angew. Chem Int Ed.* **1980**, *19*, 920; **b)** S. Juliá, J. Góizer, J. Masana, J. Rocas, S. Colonna, R. Annunziata, H. Molinari, *J. Chem. Soc. Perkin Trans. 1* **1998**, *1*, 3171.

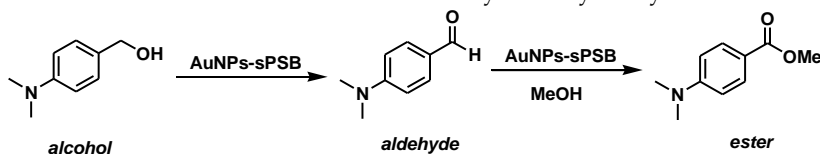
<sup>111</sup> *Greene's Protective Groups in Organic Synthesis*, P. G. M. Wuts, T. W. Greene, 4th ed., Wiley, Hoboken, **2006**.

<sup>112</sup> **a)** K. Geoghegan, P. Evans, *J. Org. Chem.* **2013**, *78*, 3410 – 3415; **b)** H. Y. Lin, R. Causey, G. E. Garcia, B. B. Snider, *J. Org. Chem.* **2012**, *77*, 7143 – 7156; **c)** M. H. Becker, P. Chua, R. Downham, C. J. Douglas, N. K. Garg, S. Hiebert, S. Jaroch, R. T. Matsuoka, J. A. Middleton, F.W. Ng, L. E. Overman, *J. Am. Chem. Soc.* **2007**, *129*, 11987 – 12002.

dimethylamino benzyl alcohol (DMABA), where the use of a tertiary amine should minimize side reactions.

DMABA oxidation was carried out at different gold loading from 4 mol% to 0.2 mol% respect to the alcohol. In the latter case a complete conversion was achieved in 30 min where *p*-dimethylamino benzaldehyde is the only product, obtained in high selectivities (entry 3, Table 4.10).<sup>53, 82, 104</sup>

Table 4.10: Aerobic DMABA oxidation to aldehyde catalyzed by the AuNPs-sPSB.



Entry <sup>[a]</sup>	Au [mol%]	Methanol [mmol]	t [h]	Conv. <sup>[b]</sup> [mol%]	Product	Selec. <sup>[b]</sup> [mol%]
1	4.0	-	1	>99	Aldehyde	>99
2	0.2	-	0.5	>99	Aldehyde	>99
3	4.0	25	24	>99	Aldehyde Ester	50 50
4 <sup>[c]</sup>	4.0	25	24	83	Ester	>99

[a] Reaction Conditions: DMABA (0.51 mmol), 35°C, KOH/DMABA=6 (molar ratio), H<sub>2</sub>O:CHCl<sub>3</sub> (*v/v*=1:1, total volume=6 mL), O<sub>2</sub> (1 bar), **Au-Cβ** used as catalyst. [b] Conversions and selectivities evaluated with GC-MS analysis using anisole as internal standard. [c] Aldehyde as initial reagent (0.51 mmol).

In order to evaluate the selectivity of the AuNPs-sPSB in amino-alcohol oxidation, a secondary amine having a higher molecular weight compared to DMABA (1-(4-((S)-1-(benzylamino)ethyl)phenyl)ethanol, **1**, Scheme 4.11), was successfully oxidized under the reaction conditions reported in entry 1, Table 4.10. 1-(4-((S)-1-(benzylamino)ethyl)phenyl)ethanone (**2**, Scheme 4.11) was obtained in high selectivity (>99 mol%) after 24 h, thus confirming the high selective behaviour of the catalyst.



**Scheme 4.11:** Oxidation of a high molecular weight aminoalcohol.

Methyl 4-(dimethylamino)benzoate was obtained with a selectivity of 50mol% using DMABA as reagent (entry 4, **Table 4.10**). This same is obtained in higher yield and selectivity if 4-(dimethylamino)benzaldehyde is considered as initial reagent (entry 5, **Table 4.10**).

#### **4.4: Concluding remarks**

The **Au-C $\epsilon$**  catalyst is highly active and selective in the aerobic oxidation and esterification of CA. The nanoporous  $\epsilon$  form is generated in situ using the solvent mixture water/chloroform.

The esterification of CA is a two-step reaction. In the first reaction CA is oxidized to cinnamaldehyde; in the second step cinnamaldehyde reacts with an alkyl alcohol to form a hemiacetal, which is in turn oxidized to the ester.

*Benzyl-like* alcohols are rapidly oxidized to aldehyde for their rapid diffusion into the nanochannels of the polymeric matrix, since they establish strong interactions with the aromatic moieties of the syndiotactic polystyrene blocks in the *co*-polymer. On the contrary, alkyl alcohols are not oxidized by the **Au-C $\epsilon$**  catalyst. The different reaction order found for the oxidation and esterification of CA with 2-phenylethanol (*pseudo*-first reaction order respect to CA,) and with different alkyl alcohols (*e.g.* methanol, 1-butanol, 1-octanol, *pseudo*-zero reaction order respect to CA) support the idea that these alcohols diffuse within the polymeric matrix according two different mechanisms. The activation energies for the two reaction steps were calculated in the esterification of CA with 1-butanol, and were respectively equal to (57.8 $\pm$ 11.5) kJ mol<sup>-1</sup> and (62.7 $\pm$ 16.7) kJ mol<sup>-1</sup>.

The use of *p*-substituted CA furnished some informations about the reaction mechanism. The aldehyde formation is favoured with EDG, thus demonstrating the development of a positive charge on the carbinol atom to be oxidized, while the second step is favoured by the presence of EWG making the hemiacetal formation easier.

The synthetic protocol here described was extended to the chemoselective oxidation of aminoalcohols or more complex systems.

The importance of the choice of the solvent is a critical reaction parameter for the reagents/products vehiculation in/out the polymeric matrix and to guarantee a good swelling of the support. A complete change in solvent polarity leads to secondary reaction pathway, which could not require the direct participation of the AuNPs based catalysts.



# CHAPTER 5



## NITROARENES REDUCTION CATALYZED BY AuNPs-sPSB



## 5.1: Introduction

Nitrobenzene (NB) and its derivatives are precursors for a very important class of organic molecules, the aromatic amines: their use is fundamental for nitrogen based compounds, such as dyes, polymers. They are also intermediate molecules in many synthetic processes to achieve, for example, amides, imines, azocompounds and diazonium salts.<sup>113</sup>

The use of nitroarene derivatives in pharmaceutical industries is well documented: for example, the well-known paracetamol, having analgesic and antipyretic properties, is generally obtained by acetylation of *p*-aminophenol. Some other drugs which contain nitroaromatic derivatives are biclutamide, nitulamime and erlotinib, all used as anticancer (**Figure 5.1**).<sup>113</sup>

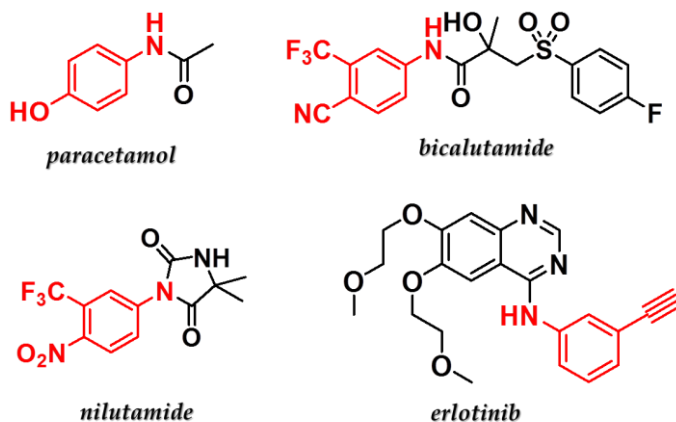


**Figure 5.1:** Some pharmaceutical compounds where the skeleton of nitroaromatic origin is represented in red.

Aromatic amines are generally obtained by reduction of the corresponding nitroarenes (**Scheme 5.1**). One of the first examples dates back to 1854,

<sup>113</sup> H. K. Kadam, S. G. Tilve, *RSC Adv.* **2015**, *5*, 83391-83407.

when Bechamp reduced both nitronaphtalene and NB using Fe in acidic medium;<sup>114</sup> alternatively, chlorides based on Zn and Sn can be used, always in acidic medium.



**Scheme 5.1:** Generic nitroarenes reduction scheme.

Some procedures consider cobalt and ruthenium sulphides as catalysts, which are very selective in reducing nitro compounds in the presence of carbon-carbon double bonds, but the yields are low and many sulphur-based by-products are obtained.<sup>115</sup>

Therefore many attempts have been made to find new greener methodologies employing heterogeneous catalysts showing higher activity and selectivity.

### **5.1.1: Nitrobenzene reduction catalyzed by Gold Nanoparticles**

Gold nanoparticles have been successfully tested in NB reduction under mild reaction conditions. The main reducing agents already reported in the literature for these reactions are H<sub>2</sub>,<sup>116</sup> ammonia-borane complex,<sup>117</sup> sodium borohydride,<sup>118</sup> isopropanol,<sup>119</sup> silanes<sup>120</sup> and CO/H<sub>2</sub>O<sup>121</sup> (Water

<sup>114</sup> V. Vojir, *Chem. Prum.* **1981**, *31*, 74-5

<sup>115</sup> R. Braden, H. Knupfer, S. Hartung, *U.S. Patents* 4,002,673 and 4,051,177 (1977).

<sup>116</sup> A. Corma, P. Serna, *Science* **2006**, *313*, 332-334.

<sup>117</sup> E. Vasilikogiannaki, C. Gryparis, V. Katzabasaki, I. N. Lykakis, M. Stratakis, *Adv. Synth. Catal.* **2013**, *355*, 907-911.

<sup>118</sup> **a)** I. Tamiolakis, S. Fountoulaki, N. Vordos, I. N. Lykakis, S. G. Armatas, *J. Mater. Chem. A* **2013**, *1*, 14311-14319; **b)** K. Layek, M. L. Kantam, M. Shirai, D. Nishio-Hamane, T. Sasaki, H. Maheswaran, *Green Chem.* **2012**, *14*, 3164-3174; **c)** Q. Ge, J. Ran, L. Wu, T. Xu, *J. Appl. Polym. Sci.* **2015**, *132*, 41268; **d)** Q. An, M. Yu, Y. Zhang, W. Ma, J. Guo, C. Wang, *J. Phys. Chem. C* **2012**, *116*, 22432-22440; **e)** D. Shah, H. Kaur, *J. Mol. Catal. A: Chem.* **2014**,

Gas Shift reaction as hydrogen source). The search for new alternative reducing agents is caused by the concerns in transporting and storage of H<sub>2</sub>. NaBH<sub>4</sub> has been often employed as clean hydrogen source in fuel cells; in reduction reactions it generally produces non-toxic sodium borate as by-products. An additional advantage in using NaBH<sub>4</sub> relays in the ease of handling.<sup>113</sup> One interesting example of its use in NB reduction is reported by Lykakis *et al.*<sup>118f</sup> 4-nitrotoluene was successfully reduced to 4-toluidine using 1 mol% of gold and MTA (mesoporous titania) as support, ethanol and NaBH<sub>4</sub> (reductant/reagent=6 molar ratio) respectively as solvent and reducing agent, at room temperature. Successful results were achieved also using 1,1,3,3-tetramethyldisiloxane (TMDS) in 4-nitroanisole reduction. The catalyst was found selective towards nitro-group even in the presence of halogen atoms, carboxylic, ester or ciano functionalities. However, starting from 4-nitrobenzaldehyde, 4-aminobenzyl alcohol was achieved. The same authors explored NB reduction with ammonia-borane complexes.<sup>117</sup> Again 4-toluidine was achieved in 100 mol% in yield in only 30 min, using Au-TiO<sub>2</sub>, ethanol as solvent at room temperature; also in this case, the nitrogroup reduction was achieved in a very selective manner.

Intriguingly, NB reduction was accomplished with gold based catalysts, but using CO and H<sub>2</sub>O as source of hydrogen<sup>121</sup> through the well-known water-gas shift reaction.<sup>122</sup> <sup>117</sup>NB reduction to aniline was accomplished in 1h with a yield >99 mol% using 5 bars of CO at room temperature, with Au/TiO<sub>2</sub> (1 mol% gold) and EtOH/H<sub>2</sub>O (15 mL, 2:1 *v/v*) as solvent mixture.

---

381, 70-76; **f**) S. Fountoulaki, V. Daikopoulou, P. L. Gkizis, I. Tamiolakis, G. S. Armatas, I. N. Lykakis, *ACS Catal.* **2014**, *4*, 3504-3511.

<sup>119</sup> X. Liu, S. Ye, H. Li, Y. Liu, Y. Cao, K. Fan, *Catal. Sci. Technol.* **2013**, *3*, 3200-3206.

<sup>120</sup> **a**) J. Tormo, D. S. Hays, G. C. Fu, *J. Org. Chem.* **1998**, *63*, 5296-5297; **b**) R. G. de Noronha, C. C. Romão, A. C. Fernandes, *J. Org. Chem.* **2009**, *74*, 6960-6964.

<sup>121</sup> L. He, L. Wang, H. Sun, J. Ni, Y. Cao, H. He, K. Fan, *Angew. Chem. Int. Ed.* **2009**, *48*, 9538-9541.

<sup>122</sup> S. R. J. Byron, M. Loganathan, M. S. Shantha, *Int. Chem. React. Eng.* **2010**, *8*, 1-32.

The methodology was applied also on a larger scale (NB=250 mmol), and using 15 bars of CO at 100°C; the total conversion in aniline was achieved in 2.5 thus showing a chance to be applied also on larger scale compared to the laboratory ones .

### 5.1.2: Mechanistic hypothesis on the NB reduction catalyzed by Gold Nanoparticles and other noble metals

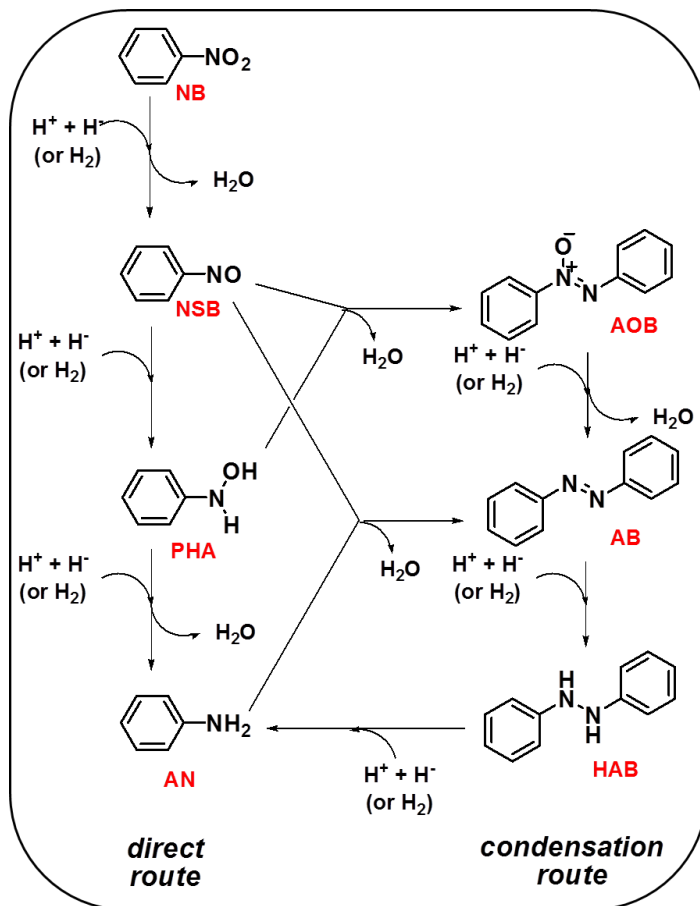
The first reaction mechanism for NB reduction was proposed by Haber in 1898<sup>123</sup> (**Scheme 5.2**), who hypothesized two different multistep mechanisms.

According to the *direct route*, the first intermediates are, in the order, nitrosobenzene (NSB) and *N*-phenylhydroxylamine (PHA); the rate determining step is the final reduction of PHA to aniline (AN). Alternatively, NSB and PHA could condensate (see *condensation route*, **Scheme 5.2**) without the participation of the gold catalyst to furnish azoxybenzene (AOB), that is reduced to azobenzene (AB). Notably AB could be also obtained by condensation of NSB and AN. Moreover AB reduction leads to the formation of hydrazobenzene (HAB), which is finally reduced to AN. The choice of the reaction pathway or the other one could depend on the experimental conditions, namely nitroaromatic/reductant molar ratio, temperature, metal catalyst and prevalingly the nature of the reductant. All noble metals allow nitro groups reduction using H<sub>2</sub> as reductant. Among AuNPs-TiO<sub>2</sub>, Pd-C and Pt-C the highest selectivities in the reduction of 3-nitrostyrene, 4-nitrobenzaldehyde, 4-nitrobenzotrile, 4-nitrobenzamide and 1-nitro-1-cyclohexene are achieved with AuNPs-TiO<sub>2</sub>.<sup>116</sup>

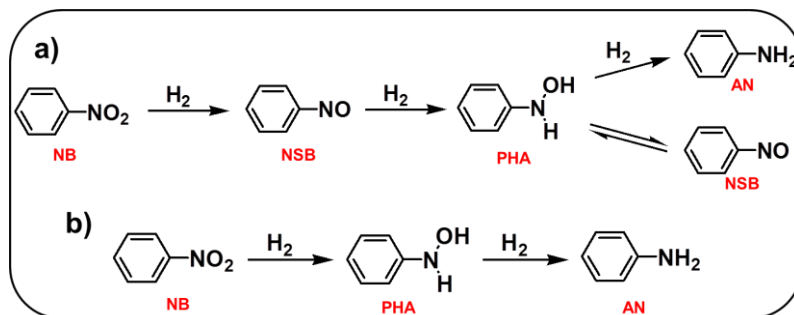
When Ir, Pt and Pt were supported on carbon, a direct pathway was claimed, where PHA produces AN through a disproportion reaction (**a**, **Scheme 5.3**).<sup>124</sup>

<sup>123</sup> F. Harber, *Z. Elektrochem.* **1898**, *4*, 506.

<sup>124</sup> I. A. Makaryan, V.I. Savchenko, *Stud. Surf. Sci. Catal.* **1993**, *75*, 2439.



Scheme 5.2: Mechanism for nitrobenzene reduction proposed by Haber in 1898.<sup>116</sup>



Scheme 5.3: Nitrobenzene reduction: **a)** via disproportionation of PHA or **b)** via direct reaction with PHA as the only intermediate.

A deeper investigation on the mechanism with the Pd-C catalyst by using calorimetric analysis, FTIR-ATR and gas-uptake figured out the presence of a direct mechanism where PHA is the only intermediate that is accumulated in the progress of the reaction (**b**, **Scheme 5.3**).<sup>125</sup> The absence of NSB intermediate is often explained because of its high reactivity, and consequently this compound is difficult to be detected in catalytic conditions.

The first report about NB reduction with gold based catalysts has been reported by Corma *et al.*:<sup>116</sup> using TiO<sub>2</sub> and Fe<sub>2</sub>O<sub>3</sub> as support; different substituted nitroarenes were reduced using harsh conditions (10-25 bars of H<sub>2</sub> and temperatures in the range 100-130°C).

These authors gave a great contribution in understanding the NB reduction mechanism with the AuNPs supported onto TiO<sub>2</sub> and CeO<sub>2</sub>.<sup>126</sup> They found that the *direct route* (**Scheme 5.2**) is present when the AuNPs/TiO<sub>2</sub> catalyst is used, whereas using the AuNPs/CeO<sub>2</sub> catalyst the *condensation route* is preferred (**Scheme 5.2**).

To shed light on the real reaction pathway, three experiments were considered: *i*) reduction at different NSB concentration with AuNPs-TiO<sub>2</sub>; *ii*) FT-IR analysis of NB adsorption on both AuNPs-TiO<sub>2</sub> and AuNPs-CeO<sub>2</sub>; *iii*) FT-IR analysis of NSB adsorption on both AuNPs-TiO<sub>2</sub> and AuNPs-CeO<sub>2</sub>.<sup>126</sup>

NSB reduction was studied over the AuNPs-TiO<sub>2</sub> through FT-IR monitoring of the reaction. NSB was considered as starting reagent since it is the first reaction intermediate in both *direct* and *condensation route*, and it can form both PHA and AOB. At low NSB concentration, a *direct route* was found, while the *condensation route* was present at high NSB concentration. These findings suggest that the transformation of NSB into PHA is a

<sup>125</sup> F. Visentin, G. Puxty, O. M. Kut, K. Hungerbuehler, *Ind. Eng. Chem. Res.* **2006**, *45*, 4544.

<sup>126</sup> **a**) Corma, A.; Concepción, P.; Serna, P., *Angew. Chem. Int. Ed.* **2007**, *46*, 7266-7269; **b**) D. Combata, P. Concepción, A. Corma, *J. Catal.* **2014**, *311*, 339-349.

slow step reaction. As soon as PHA is formed this reacts rapidly with NSB when this is in high concentration.

NB adsorption on the AuNPs-TiO<sub>2</sub> and AuNPs-CeO<sub>2</sub> catalysts was investigated with FT-IR analysis. NB adsorbs in the same way on both catalysts, giving two intense IR bands located at 1523 cm<sup>-1</sup>, 1351 cm<sup>-1</sup> (AuNPs-TiO<sub>2</sub>), and 1509 cm<sup>-1</sup>, 1343 cm<sup>-1</sup> (AuNPs-CeO<sub>2</sub>), associated with the asymmetric and symmetric stretching vibrations of the nitro group. The band shift detected in the second catalyst was explained with the higher basicity of ceria compared to titania.

Different results were achieved studying NSB adsorption onto the AuNPs-TiO<sub>2</sub> and AuNPs-CeO<sub>2</sub> catalysts. Since different IR bands were detected for the adsorbed NSB, it can be supposed that this compound adsorbs in different ways; in particular NSB adsorbs stronger on AuNPs-CeO<sub>2</sub> compared to AuNPs-TiO<sub>2</sub>.

Hence, the *condensation route* is prevalent when the AuNPs-CeO<sub>2</sub> catalyst is used since high NSB concentrations are achieved for its stronger interaction with the catalyst. In this case PHA and NSB are not detected since they react in a very fast manner to furnish AOB.

On the contrary, since NSB is weakly adsorbed on AuNPs/TiO<sub>2</sub> in this case the *direct route* is preferred.

### **5.1.3: Nitrobenzene reduction with nitroreductases**

A family of enzymes called nitroreductases are known to catalyse different nitroarenes reduction using flavin mononucleotide (FMN) or flavin adenine dinucleotide (FAD) as prosthetic groups and nicotinamide adenine dinucleotide (NADH) or nicotinamide adenine dinucleotide phosphate (NADPH) as hydride donors.<sup>127</sup> Therefore studying NB reduction by nitroreductases, it is possible a comparison between the reaction mechanisms which occur with these nitroreductases and classical

---

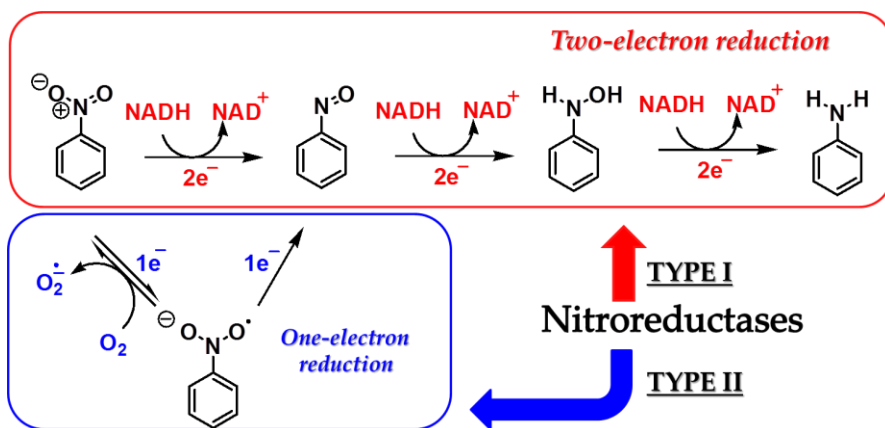
<sup>127</sup> **a)** W. Pitsawong, J. P. Hoben, A.-F. Miller, *J. Biolog. Chem.* **2014**, 289, 15203-15214; **b)** P. R. Race, A. L. Lovering, R. M. Green, A. Ossor, S. A. White, P. F. Searle, C. J. Wrighton, E. I. Hyde, *J. Biolog. Chem.* **2005**, 280, 13256-13264.

chemical reducing agents.

Nitroreductases can be divided in two different families according to the reduction mechanism; in both cases the aniline formation is achieved with the Haber *direct route*.

Type I nitroreductases act with a sequential two-electrons mechanism, where NSB and PHA are produced as intermediates (**Scheme 5.4**). Type II nitroreductases reduce NB with a single electron transfer to the nitro group, generating the superoxide anion in the presence of oxygen; this one-electron transfer is repeated to achieve NSB (**Scheme 5.4**).<sup>128</sup>

In this cascade reaction, the NSB intermediate is really reactive, thus it is difficult to isolate, since its transformation into PHA is faster than the first two-electrons transfer. Nevertheless, the biological mechanism is similar to the one hypothesized into the direct route by Haber (**Scheme 5.2**)<sup>123</sup> and to Corma proposal in NB reduction with H<sub>2</sub> over AuNPs-TiO<sub>2</sub>.<sup>126a</sup>



**Scheme 5.4:** Nitroreductases reduction mechanism with a two-electrons route (type I) where NSB and PHA are obtained as intermediates and the one-electron mechanism (type II) where one single electron is transferred to NB forming a nitro anion radical, which in the presence of oxygen forms the superoxide anion.

<sup>128</sup> Current Research, Technology and Education Topics in Applied Microbiology and Microbial Biotechnology -Microbiology Book Series - Number 2, A. Méndez-Villa, Badajoz, Spain, 2010, pp.1008-1019.

## 5.2: Co-crystals formed by nitroarenes and nanoporous forms of syndiotactic polystyrene

The nanoporous  $\delta$  and  $\epsilon$  crystalline forms of syndiotactic polystyrene are able to form *co*-crystals with guests having low molecular weight, as evidenced in the previous chapters. The volume of these molecules should be in a defined range. Thus, *clathrates* are obtained with guest molecules having a volume lower than  $0.26 \text{ nm}^3$ ,<sup>62</sup> whereas *intercalates* are obtained with molecules having a volume included in the range  $0.15\text{-}0.36 \text{ nm}^3$ .<sup>62</sup>

The *co*-crystals can be easily formed with chlorinated and/or aromatic hydrocarbons;<sup>54a</sup> when voluminous molecules are considered, they can modify the packing of the polymeric chains, and about half of the cavities initially present can be lost and the other half increases their size, thus being able to host bigger molecules.<sup>62, 129</sup>

Many nitroarenes derivatives involved in the reduction mechanism from NB into AN form *co*-crystals with the nanoporous forms of syndiotactic polystyrene. For example, both *p*-nitroaniline ( $V \approx 0.12 \text{ nm}^3$ ) and 1,4-dinitrobenzene ( $V \approx 0.134 \text{ nm}^3$ ) form crystalline clathrates with the crystalline  $\delta$  form of syndiotactic polystyrene,<sup>130, 131</sup> while AB forms intercalate compounds.<sup>132</sup> The  $\epsilon$  form of syndiotactic polystyrene forms clathrates with *p*-nitroaniline.<sup>130, 132</sup> Stable *co*-crystals with bulky and polar guest molecules are formed using  $\delta$  form of syndiotactic polystyrene.<sup>62</sup> The guest molecules used were NB, *p*-nitroanisole, *p*-dimethylaminobenzaldehyde, *trans*- $\beta$ -nitrostyrene, *p*-nitroaniline, *trans*-*p*-methoxy- $\beta$ -nitrostyrene and *p*-dimethylaminocinnamaldehyde, having a molecular volume comprised in the range  $0.161\text{-}0.275 \text{ nm}^3$ .

---

<sup>129</sup> P. Rizzo, G. Ianniello, A. R. Albuñia, M. R. Acocella, G. Guerra, *J. Solution Chem.* **2014**, *43*, 158-171.

<sup>130</sup> O. Tarallo, V. Petraccone, *Macromolecules* **2010**, *43*, 8549-8558.

<sup>131</sup> O. Tarallo, M. M. Schiavone, V. Petraccone, *Macromolecules* **2010**, *43*, 1455-1466.

<sup>132</sup> A. R. Albuñia, P. Rizzo, M. Coppola, M. De Pascale, G. Guerra, *Polymer* **2012**, *53*, 2727-2735.

### 5.3: Nitroarenes reduction by AuNPs-sPSB

The AuNPs-sPSB catalyst has been successfully tested in aerobic oxidation and esterification of CA, as described in the previous chapter;<sup>104</sup> particularly it was shown that the presence of nanoporous polymeric support can influence the access of reagents towards the AuNPs.

Considering that NB reduction is a multistep reaction with different intermediates which have a strong affinity for the nanoporous polymer matrix, the AuNPs-sPSB catalyst was tested in this reaction in order: *i*) to assess its activity and selectivity under conditions different from the ones already reported for CA oxidation; *ii*) to gain informations about the influence of the polymeric support on the reaction pathway.

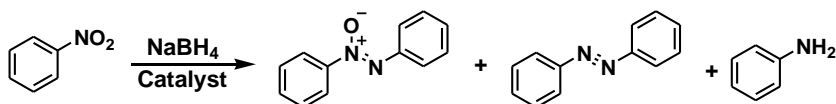
#### 5.3.1: NB reduction catalyzed by Au-C $\delta$ , Au-C $\beta$ , Au-C $\gamma$ and Au-C $\epsilon$

To investigate the role of the polymeric matrix, NB reduction was initially studied using four different catalysts samples, containing the polymeric support in one of the crystalline forms of syndiotactic polystyrene: Au-C $\delta$  and Au-C $\epsilon$  present the  $\delta$  and  $\epsilon$  nanoporous forms, whereas Au-C $\beta$  and Au-C $\gamma$  present the compact  $\beta$  and  $\gamma$  forms of syndiotactic polystyrene. The reactions were carried out in methanol since this solvent doesn't change the morphology of the polymeric support during the run.

The preliminary tests were carried out at 35°C with a high concentration of both NB and NaBH<sub>4</sub>, respectively equal to 0.42 and 2.53 M (NaBH<sub>4</sub>/NB=6, molar ratio), and using 0.2 mol% of Au.<sup>133</sup> Inert atmosphere was used, since the presence of oxygen could favour aniline oxidation to azobenzene.<sup>134</sup> The results are reported in **Table 5.1**.

<sup>133</sup> A. Noschese, A. Buonerba, P. Canton, S. Milione, C. Capacchione, A. Grassi, *Efficient and Selective Reduction of Nitroarenes into Anilines Catalyzed by Gold Nanoparticles Incarcerated in a Nanoporous Polymer Matrix: Role of the Polymeric Support and Insight into the Reaction Mechanism* (manuscript in preparation)

<sup>134</sup> a) A. Gorrane, A. Corma, H. García, *Science* **2008**, 322, 1661-1664; b) A. Gorrane, A. Corma, H. García, *Nature* **2010**, 5, 429-438.

Table 5.1: NB reduction using **Au-Cδ**, **Au-Cβ**, **Au-Cε** and **Au-Cγ** at 35°C.

Entry <sup>[a]</sup>	Catalyst	t [min]	Conv. <sup>[b]</sup> [mol%]	Selectivity <sup>[b]</sup> [mol%]			TOF <sup>[c]</sup> [h <sup>-1</sup> ]
				AOB	AB	AN	
1	<b>Au-Cδ</b>	60	>99	-	-	>99	500
2	<b>Au-Cβ</b>	60	85	66	16	2.9	-
3	<b>Au-Cγ</b>	60	66	55	6.9	2.5	-
4	<b>Au-Cε</b>	45	>99	-	-	>99	667
5	-	30	87	66	14	5.3	-

[a] Reactions conditions: NB (2.54 mmol; 0.42 M), catalyst (50 mg, 0.2 mol% in Au), NaBH<sub>4</sub> (15.2 mmol, 2.53 M), 35°C, methanol (6 mL), N<sub>2</sub> protective atmosphere (P<sub>N<sub>2</sub></sub>=1 bar). [b] Conversions and selectivities evaluated by GC-MS analysis using anisole as internal standard. [c] Turnover Frequency ( $mol_{AN} mol^{-1}_{Au} h^{-1}$ ).

The “as synthesized” **Au-Cδ** allowed the total NB conversion in AN in 60 min (entry 1, Table 5.1), corresponding to a TOF value of 500 h<sup>-1</sup>. Using **Au-Cε** the conversion of NB into AN was complete in 45 min (entry 4, Table 5.1), corresponding to a TOF value of 667 h<sup>-1</sup>: the latter value is one of the highest TOF already reported in literature for NB reduction catalyzed by the AuNPs in presence of NaBH<sub>4</sub> as reducing agent.<sup>113, 119, 121</sup>

The kinetic plots of these two reactions are compared in Figure 5.2.

NB is consumed within the first reaction minutes with AOB as first reaction intermediate in both cases; then the cascade of reactions seems to follow the *condensation route* by Haber. However, the kinetic plots showed in Figure 5.2 are slightly different. Using **Au-Cδ**, the reaction intermediates AOB and AB are partially accumulated, whereas they are quickly consumed with the catalyst **Au-Cε**.

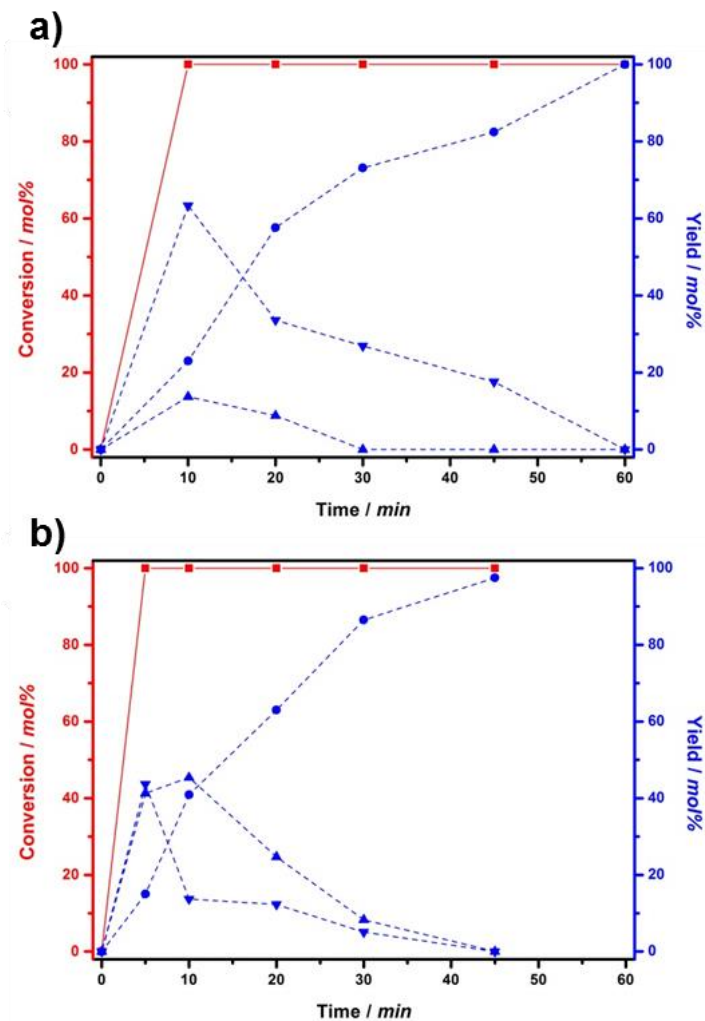


**Figure 5.2:** Kinetic plots of reaction described in **table 5.1** and catalyzed by: **a) Au-C $\delta$** , entry 1, and **b) Au-C $\epsilon$** , entry 2. (■ = NB conversion; ▼ = AOB yield; ▲ = AB yield; ● = AN yield).

The kinetic plots of the reactions reported in the entries 2 and 3, **Table 5.1** catalyzed by **Au-C $\beta$**  and **Au-C $\gamma$**  are shown in **Figure 5.3**. The two plots share the same evolution: NB is always rapidly reduced to AOB, but the

reaction ends at this level. The situation appears clearer if the kinetic plot of the blank reaction run is considered (entry 5, Table 5.1 and Figure 5.4).

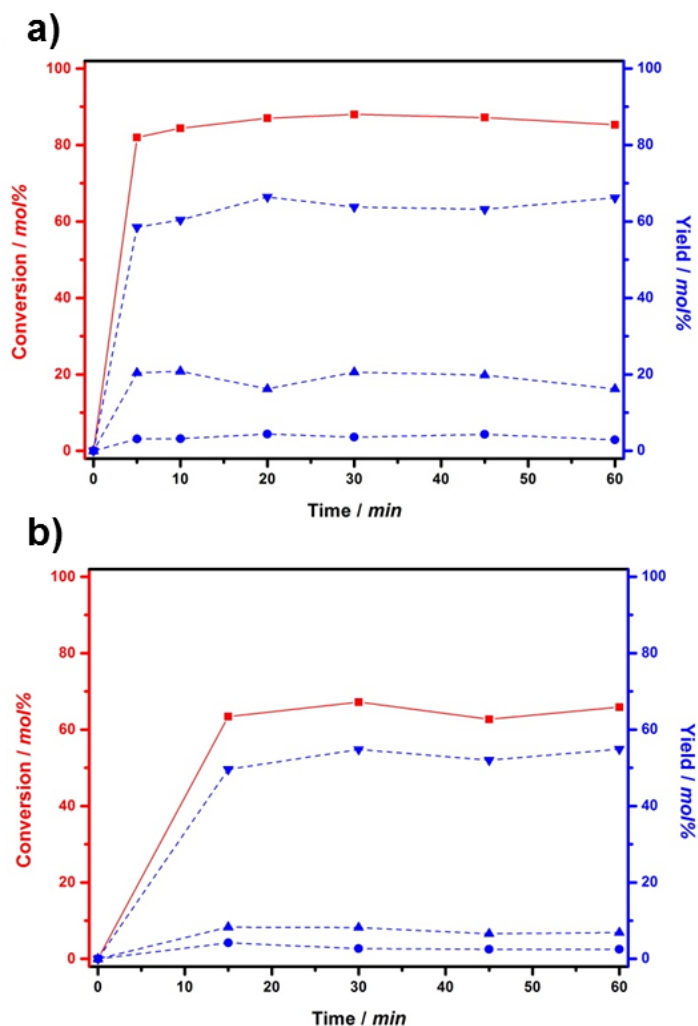


**Figure 5.3:** Kinetic plots of reaction described in table 5.1 and catalyzed by: a) Au-C $\beta$ , entry 2, and b) Au-C $\gamma$ , entry 3. (■ = NB conversion; ▼ = AOB yield; ▲ = AB yield; ● = AN yield).

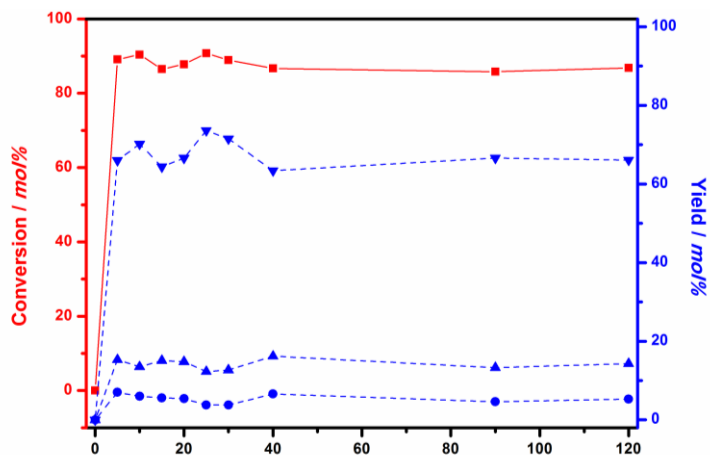


**Figure 5.4:** Kinetic plot of the blank reaction run without catalyst and described in entry 5, **table 5.1**. (■ = NB conversion; ▼ = AOB yield; ▲ = AB yield; ● = AN yield).

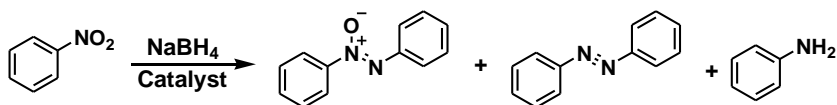
Surprisingly, in this reaction a fast reduction of NB is observed and AOB is the main reaction product: this demonstrates that the first step of the overall reduction can be achieved also outside the polymer matrix. The AuNPs are catalytically active in the most challenging reduction of AOB into AN. The high TOF values found for the **Au-C $\delta$**  and **Au-C $\epsilon$**  demonstrate that AOB and NB can have an easy access to the AuNPs, forming AN in high activity and selectivity.

### **5.3.2: NB reduction with Au-C $\epsilon$ on varying the reaction conditions**

Further investigations on NB reduction were carried out using **Au-C $\epsilon$**  as catalyst.

The reaction temperature was changed in order to understand the evolution of all the reaction intermediates over the reaction time. The results are reported in **Table 5.2**.

Table 5.2: NB reduction explored at different temperatures.



Entry <sup>[a]</sup>	T [°C]	t [min]	Conv. <sup>[b]</sup> [mol%]	Selectivity <sup>[b]</sup> [mol%]		
				AOB	AB	AN
1	25	5	>99	66	20	14
		45	>99	13	4.0	83
		60	>99	-	-	>99
2	45	5	97	30	12	55
		20	97	22	-	75
		60	>99	-	-	99
3	55	30	>99	-	-	96

[a] Reactions conditions: NB (2.54 mmol; 0.42 M), **Au-Ce** (50 mg, 2 mol% in gold), NaBH<sub>4</sub>/NB= 6 (molar ratio), methanol (6 mL), N<sub>2</sub> protective atmosphere (P<sub>N<sub>2</sub></sub>=1 bar). [b] Conversions and selectivities evaluated by GC-MS analysis using anisole as internal standard.

At 25°C, AN formation was complete in 60 min (entry 1, Table 5.2). An increase of the reaction temperature up to 45°C caused a complete NB conversion into AN in 45 min (entry 2, Table 5.2); a fast conversion into AN was achieved also at 55°C, where the AN was obtained in 96 mol% in yield after 30 min (entry 3, Table 5.2).

The kinetic plots of entries 1 and 3, Table 5.2, are reported in Figure 5.5. After 20 min, at 25°C NB conversion was 99 mol%, and AN as the main product (53 mol%); AOB and AB were obtained in 33 and 13 mol% in yield, respectively. At the same reaction time at 55°C, AN was obtained in

92 mol% yield; in this case, the TOF reached the impressive value of 1000 h<sup>-1</sup>.

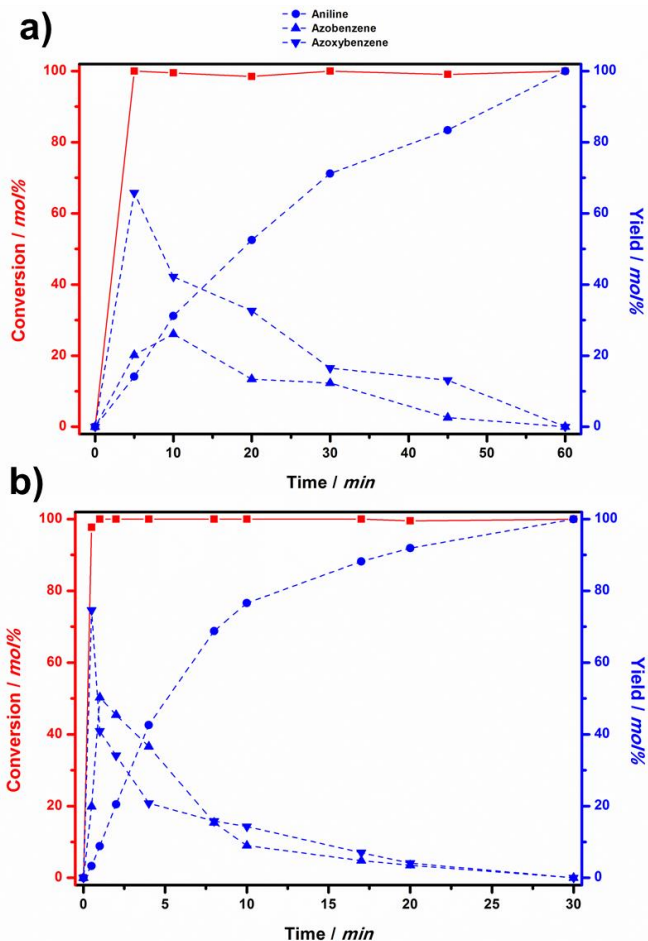


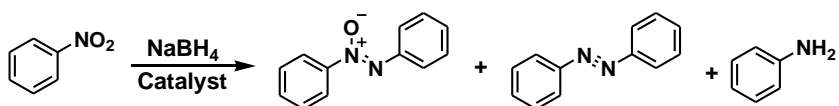
**Figure 5.5:** Kinetic plot of reaction described in table 5.2 a) 25°C (entry 1) and b) 55°C (entry 3). (■ = NB conversion; ▼ = AOB yield; ▲ = AB yield; ● = AN yield)

Considering that AOB and AB are formed prevalently outside of the polymeric support, a rough evaluation of kinetic order and  $E_a$  can be done considering the last steps of the overall transformation of NB into AN in the range of temperature 25-55°C. In this case, the mole concentration of

AN increases linearly with the reaction time, and the calculated apparent rate constant are  $1.21 \cdot 10^{-4} \pm 1.6 \cdot 10^{-5} \text{ mol L}^{-1} \text{ s}^{-1}$  at  $25^\circ\text{C}$ ,  $1.92 \cdot 10^{-4} \pm 2.4 \cdot 10^{-5} \text{ mol L}^{-1} \text{ s}^{-1}$  at  $35^\circ\text{C}$ , and  $5.55 \cdot 10^{-4} \pm 4.0 \cdot 10^{-5} \text{ mol L}^{-1} \text{ s}^{-1}$  at  $55^\circ\text{C}$ . The activation energy found was  $42 \pm 3 \text{ kJ mol}^{-1}$ ; this value well compares with the ones already reported for 4-nitrophenol reduction ( $21\text{--}55 \text{ kJ mol}^{-1}$ ).<sup>118,118f, 135</sup>

The reaction was then studied by varying the amount of gold catalyst; the results are reported in **Table 5.3**.

**Table 5.3:** NB reduction using different amount of gold.



Entry <sup>[a]</sup>	Au [mol%]	t [min]	Conv. <sup>[b]</sup> [mol%]	Selectivity <sup>[b]</sup> [mol%]		
				AOB	AB	AN
1	0.1	5	97	80	14	2.0
		30	>99	24	59	17
		105	>99	-	-	>99
2 <sup>[c]</sup>	0.05	10	94	75	16	2.1
		120	>99	51	38	11

[a] Reactions conditions: NB (2.54 mmol; 0.42 M), **Au-Cε** (2 wt% in gold),  $25^\circ\text{C}$ , NaBH<sub>4</sub>/NB= 6 (molar ratio), methanol (6 mL), N<sub>2</sub> protective atmosphere (P<sub>N<sub>2</sub></sub>=1 bar). [b] Conversions and selectivities evaluated by GC-MS analysis using anisole as internal standard. [c] NB = 5.08 mmol.

Lowering the amount of Au down to 0.1 mol% (respect to NB), NB reduction to aniline was complete in 105 min (entry **1**, **Table 5.3**). Using 0.05 mol% of gold resulted NB, AOB was achieved as the main reaction prod-

<sup>135</sup> **a)** T. Aditya, A. Pal, T. Pal, *Chem. Commun.* **2015**, 51, 9410-9431; **b)** S. Wunder, Y. Lu, M. Albrecht, M. Ballauff, *ACS Catal.*, **2011**, 1, 908-916; **c)** S. Wunder, F. Polzer, Y. Lu, Y. Mei and M. Ballauff, *J. Phys. Chem. C*, **2010**, 114, 8814-8820.

uct (entry 2, Table 5.3). In Figure 5.6 the kinetic plots of reactions described in Table 5.3 are reported.

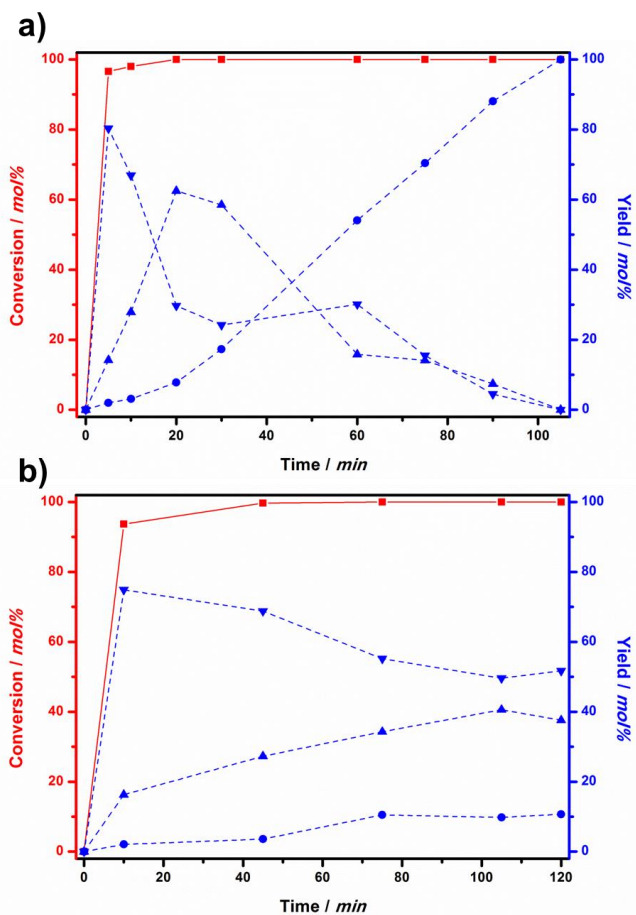


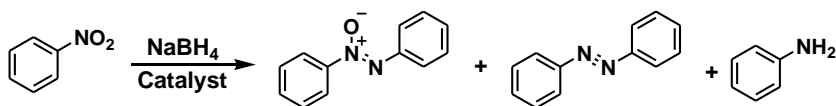
**Figure 5.6:** Kinetic plot of reaction described in table 5.3, catalyzed by different gold amount: **a)** 0.1 mol% (entry 1) and **b)** 0.05 mol% (entry 2). (■ = NB conversion; ▼ = AOB yield; ▲ = AB yield; ● = AN yield)

The use of 0.1 mol% of gold slowed down the reaction rate (**a**, Figure 5.6) allowing a partial accumulation of the intermediates AOB and AB. The

TOF value calculated at 105 min was  $571 \text{ h}^{-1}$ . A short induction period can be observed in the first reaction minutes for the formation of AN, corresponding to the formation of AB.

A further decrease in the amount of gold caused a substantial decrease in the rate of reaction (**b**, **Figure 5.6**). The first step of the reaction always occurs prevalently out of the polymeric matrix. After 75 min, considering kinetic plot **a**, **Figure 5.6** the yields of AN, AOB and AB were respectively 70 mol%, 15 and 14 mol%. Considering **b**, **Figure 5.6** at the same reaction time, the main reaction product is AOB (55 mol%), whereas the yields of AB and AN are, respectively, 34 and 11 mol%.

**Table 5.4:** NB reduction using different amounts of  $\text{NaBH}_4$ .



Entry <sup>[a]</sup>	$\text{NaBH}_4/\text{NB}$ [molar ratio]	t [min]	Conv. <sup>[b]</sup> [mol%]	Selectivity <sup>[b]</sup> [mol%]		
				AOB	AB	AN
1	1	20	93	87	5.1	0.7
		120	93	89	3.5	0.4
2	3	5	92	74	14	3.7
		60	>99	44	29	27
		120	>99	50	15	35
3	12	30	>99	80	16	2.4
		120	>99	29	60	11
		24 h	>99	-	-	>99

[a] Reactions conditions: NB (2.54 mmol; 0.42 M), **Au-Ce** (25 mg, 0.1 mol% in gold), 25°C, methanol (6 mL),  $\text{N}_2$  protective atmosphere ( $P_{\text{N}_2}=1$  bar). [b] Conversions and selectivities evaluated by GC-MS analysis using anisole as internal standard.

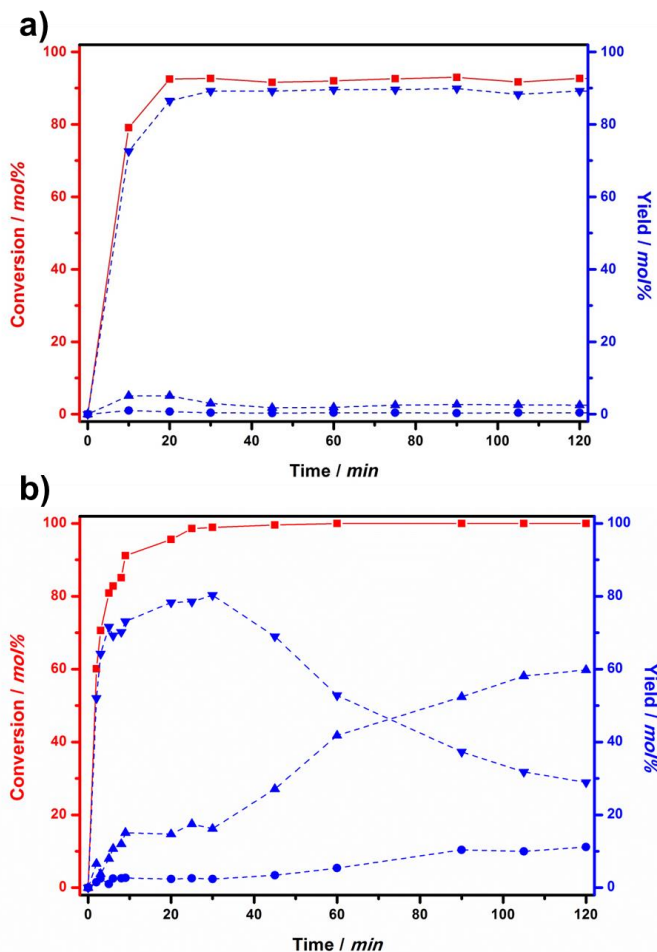


**Figure 5.7:** Kinetic plot of reaction described in Table 5.4, where different amounts of  $\text{NaBH}_4/\text{NB}$  (molar ratio) were used: **a)**  $\text{NaBH}_4/\text{NB}=1$  (entry 1) and **b)**  $\text{NaBH}_4/\text{NB}=12$  (entry 3). (■ = NB conversion; ▼ = AOB yield; ▲ = AB yield; ● = AN yield)

The amount of  $\text{NaBH}_4$  strongly influences both reaction rate and selectivity of the **Au-C $\epsilon$**  catalyst. Lowering the molar ratio between  $\text{NaBH}_4/\text{NB}$  to 3 or 1, even for long reaction time (120 min) the complete conversion of NB into AN was not achieved. In fact, using a  $\text{NaBH}_4/\text{NB}$  molar ratio of 3, the yields of AOB, AB and AN were, respectively, 50 mol%, 15 mol%

and 35 mol% after 120 min (entry 2, **Table 5.4**). When a molar ratio of  $\text{NaBH}_4/\text{NB}$  equal to 1 was used, after 120 min the yields of AOB, AB and AN were, respectively, 89 mol%, 3.5 mol% and 0.4 mol% (entry 1, **Table 5.4**). At  $\text{NaBH}_4/\text{NB}$  molar ratio of 12, AN complete conversion of NB and intermediates into AN was achieved only after 24 h (entry 3, **Table 5.4**). The kinetic plots of entries 1 and 3, **Table 5.4**, are reported in **Figure 5.7**. Considering plot **Figure 5.7 a**, namely at a  $\text{NaBH}_4/\text{NB}$  molar ratio of 1, the amount of reducing agent is not sufficient for the complete NB reduction and AOB is produced outside of the polymeric matrix. The decrease of the reaction rate at the  $\text{NaBH}_4/\text{NB}$  molar ratio equal to 12 (**b**, **Figure 5.7**) can be easily understood if a Langmuir-Hinshelwood mechanism is considered.

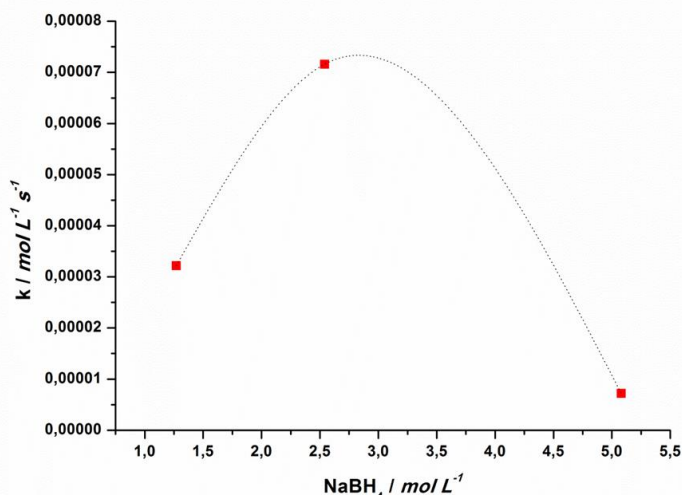


**Figure 5.8:** Dependence of the formation constant of aniline  $k$  at 25°C on the concentration of  $\text{NaBH}_4$  (1.3, 2.5 and 5.1  $\text{mol L}^{-1}$ ) at a concentration of NB of 0.42  $\text{mol L}^{-1}$  with the Langmuir-Hinshelwood fitting represented by the dotted curve.

The reaction rates calculated for NB reduction performed with a  $\text{NaBH}_4/\text{NB}$  molar ratio of 3, 6 and 12 and at constant amount of NB moles were plotted *vs.*  $\text{NaBH}_4$  molar concentration. The inspection of **Figure 5.8** confirmed the presence of a Langmuir-Hinshelwood mechanism.<sup>118b, 135</sup> The kinetic constants of **Figure 5.8** are:  $3.2 \cdot 10^{-5} \pm 1.0 \cdot 10^{-6} \text{ mol L}^{-1} \text{ s}^{-1}$  at  $\text{NaBH}_4/\text{NB}=3$ ,  $\text{NaBH}_4=1.3 \text{ M}$  (entry 2, **Table 5.4**),  $7.2 \cdot 10^{-5} \pm 3.3 \cdot 10^{-6} \text{ mol L}^{-1} \text{ s}^{-1}$  at  $\text{NaBH}_4/\text{NB}=6$ ,  $\text{NaBH}_4=2.54 \text{ M}$  (entry 1, **Table 5.4**) and  $7.2 \cdot 10^{-6} \pm 3.3 \cdot 10^{-7} \text{ mol L}^{-1} \text{ s}^{-1}$  at  $\text{NaBH}_4/\text{NB}=12$ ,  $\text{NaBH}_4=5.08 \text{ M}$  (entry 3, **Table 5.4**).

If the reaction is performed in air, the yield of AN was 87 *mol%* at 105 min, with AB as minor product (**Figure 5.9**). This finding rules out that the oxidation of AN, under our experimental conditions, could lead to high yields in AB.<sup>134</sup>

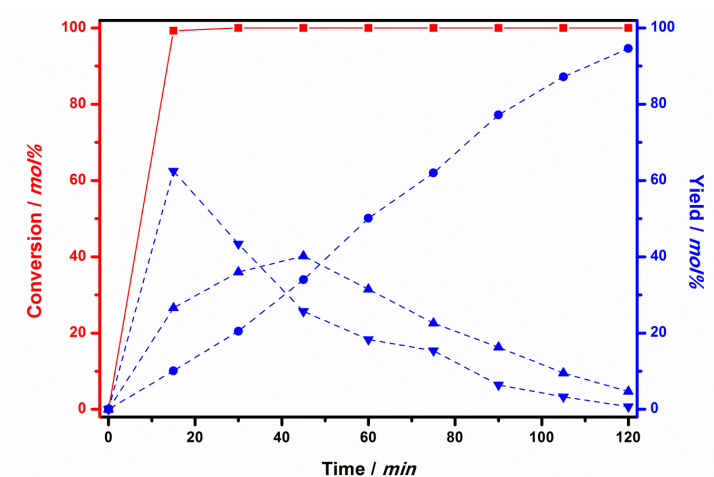


**Figure 5.9:** Kinetic plot of reaction carried under air. Reaction conditions: NB (2.54 mmol, 0.42M), **Au-Ce** (25 mg, 0.1 *mol%* of gold),  $\text{NaBH}_4$  (15.2 mmol), 25°C, methanol (6 mL), under air. (■ = NB conversion; ▼ = AOB yield; ▲ = AB yield; ● = AN yield)

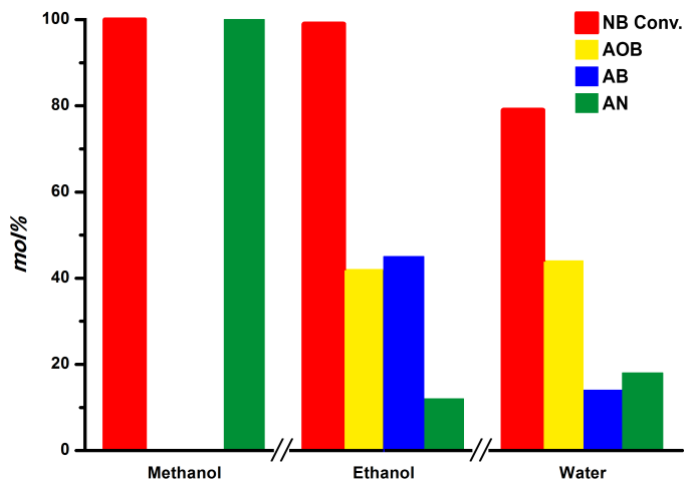


**Figure 5.10:** Different products distribution achieved in different solvents, using  $C\epsilon$  as catalyst. NB (2.54 mmol, 0.42M),  $Au-C\epsilon$  (25 mg, 0.1 mol% of Gold),  $NaBH_4$  (15.2 mmol), 25°C, solvent (6 mL),  $N_2$  protective atmosphere (1 bar), reaction time of 105 min.

Methanol was initially selected as solvent for the NB reduction.

When the reaction is performed in ethanol, the product distribution is completely different (**Figure 5.10**): in fact, even if NB conversion was completely achieved, the yields of AOB and AB were, respectively, 42 and 45 mol%, and the AN yield was just 13 mol%.

In water the NB conversion was 78 mol%, while the yields in AOB, AB and AN were respectively 45, 15 and 18 mol%. This result can be ascribed to the hydrophobic polymeric matrix, that doesn't allow a good diffusion of reagents into the polymeric matrix for the poor swelling of the polymer in water.

In 1-propanol or 1-butanol, AOB is the main reaction product since these bulky solvents slowly diffuse through the channels of the nanoporous support.<sup>104</sup>

These catalytic tests underline the importance in selecting the right solvent for NB reduction with the AuNPs-sPSB catalyst. Methanol is the solvent of election for NB reduction using the **Au-C $\epsilon$**  catalyst. The inspection of the WAXD spectrum of the recovered catalyst is confirmed that methanol doesn't affect the morphology of the support (**Figure 5.11**) and no significant change in the AuNPs size was detected.

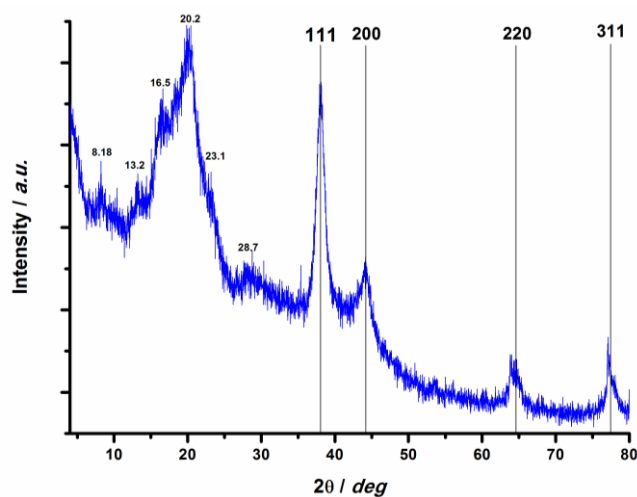


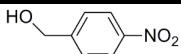
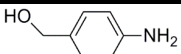
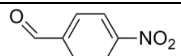
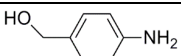
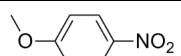
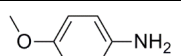
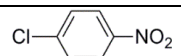
**Figure 5.11:** WAXD spectra of **Au-C $\epsilon$**  recovered after the catalytic run of entry 4, **table 5.1**.

The catalyst is very stable under the reaction conditions (entry **1**, **Table 5.3**), and can be used at least three times without any loss of activity or selectivity.

### **5.3.3: Reduction of *p*-substituted nitroarenes**

To test the general validity of the synthetic protocol, different *p*-substituted nitroarenes were used (**Table 5.5**).

**Table 5.5:** Reduction of different *p*-substituted nitroarenes catalyzed by **Au-Ce**.

Entry <sup>[a]</sup>	Substrate	t [h]	Products	Selec. <sup>[b]</sup> [mol%]
1 <sup>[c]</sup>	 4-nitrobenzyl alcohol	1.5	 4-aminobenzyl alcohol	>99
2 <sup>[c]</sup>	 4-nitrobenzaldehyde	2	 4-amino benzylalcohol	>99
3	 4-nitroaniline	6	 1,4-diaminobenzene	>99
4	 4-nitrotoluene	6	 4-toluidine	98
5	 4-nitroanisole	6	 4-anisidine	91
6	 4-chloro nitrobenzene	24	 4-chloroaniline	93

[a] Reaction conditions: nitroarene (2.54 mmol), **Au-Ce** (0.1 mol% of gold), 35°C, NaBH<sub>4</sub>/NB=6 (molar ratio), methanol (6 mL), N<sub>2</sub> protective atmosphere (1 bar), conversion > 99 mol%; [b] Conversions and yield evaluated by <sup>1</sup>H-NMR analysis. [c] Reaction carried out at 25°C.

4-aminobenzyl alcohol results from both 4-nitrobenzyl alcohol and 4-nitrobenzaldehyde<sup>118e, 118f</sup> after, respectively, 1.5 and 2 h (entries 1 and 2, **Table 5.5**). The <sup>1</sup>H-NMR spectrum of entry 2, **Table 5.5** evidenced that aldehyde is reduced before the nitro group.

*p*-EDG, e.g. amino, methyl or methoxy, allow the complete conversion of nitroarenes within 6 h, and the selectivities of the related *p*-substituted

anilines were >99, 98 and 91 mol% respectively (entries 3, 4 and 5, Table 5.5). *p*-nitroanisole (entry 5, Table 5.5) produced AOB as minor product with a selectivity of 6.8 mol%. AOB was obtained as by-product also in the reduction of *p*-chloronitrobenzene, in 6 h it was obtained with a selectivity of 7 mol%. Longer reaction time (24 h) was required for the complete conversion of 4-chloronitrobenzene in 4-chloroaniline (entry 6, Table 5.5).

A clear dependence of the course of the reaction from the nature of the substituents could not be depicted for the higher complexity of *condensation route* compared to *direct route*.<sup>126b</sup> In addition to that, the polarity and the steric bulkiness of the molecules which have to diffuse within the polymeric matrix should be taken into account.<sup>63</sup>

#### **5.3.4: Mechanism of NB reduction with the Au-C $\epsilon$ catalyst**

As evidenced in the previous sections, many proposals about the mechanism of nitroarenes reduction have been reported in the literature. The presence of a *direct* or *condensation route* depends on the reaction conditions used. The *direct route* has been mainly reported with the AuNPs and H<sub>2</sub> as reducing agent; however a clear mechanistic hypothesis of the NB reduction with NaBH<sub>4</sub> has not been reported yet.

Under the reaction conditions here described and using the AuNPs-sPSB catalyst, the *condensation route* is preferred, since the AOB formation occurs rapidly in the first reaction minutes outside of the polymeric matrix, thus without the participation of the AuNPs, as evidenced from the blank experiment (Figure 5.4). The possibility that the reducing agent can react with NB event without the catalyst is completely ignored by many authors.<sup>118</sup> The AOB formation is an indirect proof of the presence of NSB and PHA in the reaction medium, which rapidly condense to furnish AOB. The final reductions of AOB and AB could not occur easily only with NaBH<sub>4</sub>, thus requiring the participation of the AuNPs.

### **5.4: Concluding remarks**

In addition to oxidation reactions, the AuNPs-sPSB catalyst is active also in the reduction of nitroarenes. The nanoporous **Au-C $\delta$**  and **Au-C $\epsilon$**  catalysts showed higher activity and selectivity compared to the AuNPs supported on metal oxides already reported in literature. The possibility of forming *co*-crystals of NB derivatives and nanoporous forms of the catalyst could be responsible of the high activity found. However the achievement of these *co*-crystals could be hampered by the polarity and the steric bulkiness of the guest molecules.

The data here reported support the presence of a *condensation route* rather than a *direct route* since the first stage of the reaction, namely AOB formation, can occur also outside the polymeric matrix. The  $E_a$  value found for AN formation (considering that AOB and AB formation occur without the participation of the catalyst) is in the range of the values already reported in literature for *p*-nitrophenol<sup>118, 135</sup>



# **CHAPTER 6**



## **GOLD COLLOIDS IMMOBILIZED ON POLYMERIC SUPPORT**



### **6.1: Catalytic activity of immobilized Gold Colloids**

The sol immobilization technique is based on a different approach consisting of two steps: *i*) synthesis of the AuNPs in the presence of stabilizers (liquid phase); *ii*) immobilization on a support.<sup>136</sup>

Immobilization is generally achieved by dipping the support in the sol, and this essentially depends on the stabilizer used for the sol formation and from the morphology of the support.

This synthetic procedure offers the advantage of synthesizing nanoparticles having very low size. The main limitation is the presence of the stabilizer and the AuNPs are consequently not accessible to the reagents. Thus, after the immobilization, thermal decomposition of the stabilizer is necessary to obtaining its removal from the catalyst.<sup>137</sup>

Actually many literature examples deal with the use of the sol immobilization technique for the achievement of supported metal catalysts.<sup>138</sup>

Some reaction parameters were found to be critical for the synthesis of colloidal AuNPs. The influence of temperature and solvent was deeply investigated by Sakai and Alexandris<sup>139</sup> in relation to AuNPs formation with P123 (poly(ethylene glycol)-*block*-poly(propylene glycol)-*block*-poly(ethylene glycol)). In fact, these authors found that an increase in temperature caused an increase in the AuNPs size.

---

<sup>136</sup> S. Coluccia, G. Martra, F. Porta, L. Prati, M. Rossi, *Catal.Today* **2000**, *61*, 165.

<sup>137</sup> A. Villa, D. Wang, G. M. Veith, F. Vindigni, L. Prati, *Catal. Sci. Technol.* **2013**, *3*, 3036-3041

<sup>138</sup> **a)** I. Sevonkaev, V. Privman, D. Goia, *J. Solid State Electrochem* **2013**, *17*, 279-297; **b)** H. Atae-Esfahani, M. Imura, Y. Yamauchi, *Angew. Chem. Int. Ed.* **2013**, *52*, 13611–13615; **c)** J. A. Lopez-Sanchez, N. Dimitratos, P. Miedziak, E. Ntainjua, J. K. Edwards, D. Morgan, A. F. Carley, R. Tiruvalam, C.J. Kiely, G.J. Hutchings, *Phys. Chem. Chem. Phys.* **2008**, *10*, 1921–1930; **d)** L. B. Okhlopkova, M. A. Kerzhentsev, F. V. Tuzikov, Y. V. Larichev, I. P. Prosvirin, Z. R. Ismagilov, *J Nanopart Res* **2012**, *14*,1089; **e)** S. O. Blavo, E. Qayyum, L. M. Baldyga, V. A. Castillo, M. D. Sanchez, K. Warrington, M. A. Barakat, J. N. Kuhn, *Top. Catal.* **2013**, *56*, 1835-1842; **f)** K. Gude, R. Narayanan, *J. Phys. Chem. C* **2011**, *115*, 12716–12725; **g)** Y. Zhao, L. Jia, J. A. Medrano, J. R. H. Ross, L. Lefferts, *ACS Catal.* **2013**, *3*, 2341–2352.

<sup>139</sup> T. Sakai, P. Alexandridis, *J. Phys. Chem. B* **2005**, *16*, 7766–7777.

Colloidal Pt nanoparticles stabilized with P123 and then immobilized on mesoporous silica were investigated by Somorjai *et al.*<sup>140</sup> The removal of the stabilizer was achieved by thermal annealing under air or oxygen atmosphere. The final catalyst, having AuNPs size in the range 1.8-7.9 nm, was found active in the ethane hydrogenation and the related TOF values were in the range 10-620 s<sup>-1</sup>.

Benzyl alcohol oxidation is often used as benchmark test to assess the activity of new catalysts. For example, the Au/Pd-TiO<sub>2</sub> catalyst obtained with the sol immobilization method (colloidal nanoparticles stabilized with PVA) is active in the benzyl alcohol oxidation at 120°C and 10 bar of O<sub>2</sub>:<sup>141</sup> in 6 h, the conversion of benzyl alcohol was 61 mol%, and the two main products were benzaldehyde and toluene, obtained with a selectivity of 72 mol% and 19 mol% respectively. In this case, the bimetallic nanoparticles were deprotected by solvent treatment previously the catalytic tests.

Monometallic gold based catalyst was used in the aerobic oxidation of benzyl alcohol. Hutchings *at al.* reported the use of PVA as stabilizer for the colloidal solution, and TiO<sub>2</sub> was employed as solid support.<sup>142</sup> The AuNPs size in the colloidal solution was ≈2.2 nm, whereas after the immobilization on titania the size of the AuNPs was 3.9 nm. The “as synthesized” catalyst was tested in the aerobic oxidation of benzyl alcohol at high oxygen pressure. After the PVA removal by thermal annealing at 250°C in air, a benzyl alcohol conversion of 68 mol% was achieved.

---

<sup>140</sup>H. Song, R. M. Rioux, J. D. Hoefelmeyer, R. Komor, K. Niesz, M. Grass, P. Yang, G. A. Somorjai, *J. Am. Chem. Soc.* **2006**, *128*, 3027-3037.

<sup>141</sup>J. A. Lopez-Sanchez, N. Dimitratos, C. Hammond, G. L. Brett, L. Kesavan, S. White, P. Miedziak, R. Tiruvalam, R.L. Jenkins, A. F. Carley, D. Knight, C. J. Kiely, G. J. Hutchings, *Nature Chem.* **2011**, *3*, 551-556.

<sup>142</sup>N. Dimitratos, J. A. Lopez-Sanchez, D. Morgan, A. Carley, L. Prati, G. J. Hutchings, *Catal. Tod.* **2007**, *122*, 317-324.

It should be noted that thermal treatments can influence dramatically both the size and shape of metal nanoparticles.<sup>143</sup> Therefore Hutchings *et al.*<sup>141</sup> investigated the possibility of removing the stabilizer by different methods. A colloidal gold solution stabilized with PVA was immobilized on titania. The catalyst was treated in water at 90°C to remove the stabilizer: no significant changes in the AuNPs morphology and size were detected (3.0 nm *vs* 4.4 nm). Treating the catalyst at 400°C to remove PVA caused a large increase in the AuNPs size to 10.4 nm. The catalyst was tested in the CO oxidation, and a total conversion of the initial reagent was detected for the catalyst treated for 30 min in water at 90°C. Hence, if the support used for the colloid is not thermally stable, treatment with solvents can be useful to remove the stabilizer.

## 6.2: Sol-immobilization technique: preliminary results

Since few examples deal with the use of polymeric supports for gold colloids, the sol immobilization technique was thus explored.

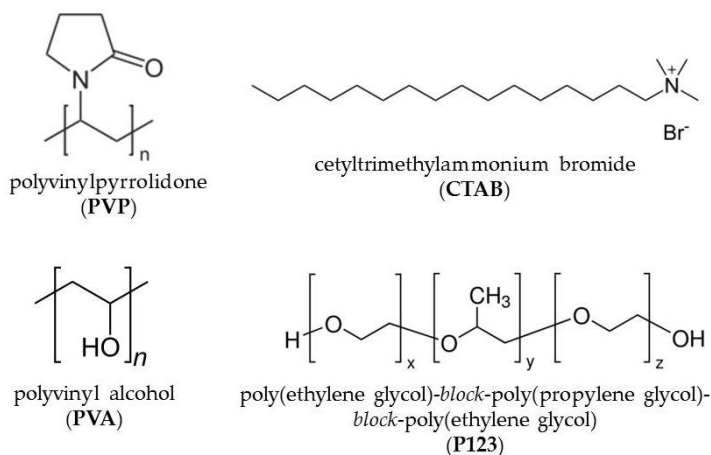


**Figure 6.1:** Structure of the some stabilizers used in the synthesis of the colloidal AuNPs solutions.

<sup>143</sup> **a)** J. D. Grunwaldt, C. Kiener, C. Wögerbauer, A. Baiker, *J. Catal.* **1999** *181*, 223–232; **b)** M. Comotti, W.-C. Li, B. Spliethoff, F. Schüth, *J. Am. Chem. Soc.* **2006**, *128*, 917–924.

For the synthesis of gold colloids, PVP, CTAB, PVA and P123 were considered as stabilizer (**Figure 6.1**) and polyphenylene oxide (PPO) was considered for the immobilization of the gold colloids. PPO is a commercially available polymer showing characteristics of high thermal stability and elevated porosity similar to syndiotactic polystyrene.<sup>144</sup>

### 6.2.1: Synthesis and characterization of gold colloids before and after immobilization on PPO

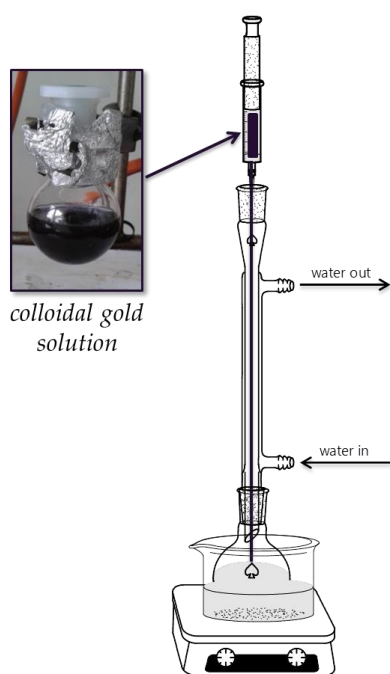


**Figure 6.2:** Gold colloids sol-immobilization under reflux

The general procedure adopted for the synthesis of gold colloids is based on three steps: *i*) dissolution of gold the precursor ( $\text{HAuCl}_4$ ); *ii*) addition of the stabilizer solution; *iii*) addition of the reducing agent solution ( $\text{NaBH}_4$ ).<sup>145</sup>

The dropwise addition of the reductant favors the formation of small AuNPs, and the colour of the solutions changed from yellow to dark brown, thus confirming the formation of the protected AuNPs.

The as-synthesized colloidal solutions were then supported on PPO by using the same procedure. PPO was dissolved in THF and the colloidal solution was added drop to drop under reflux (**Figure 6.2**). Finally the solution

<sup>144</sup> a) C. Daniel, S. Longo, M. Galizia, *Macromol. Symp.* **2014**, 335, 70-77; b) C. Daniel, S. Longo, G. Fasano, J. G. Vitillo, G. Guerra, *Chem. Mater.* **2011**, 23, 3195–3200; c) M. Galizia, C. Daniel, G. Fasano, G. Guerra, G. Mensitieri, *Macromolecules* **2012**, 45, 3604–3615.

<sup>145</sup> J. Pritchard, L. Kesavan, M. Piccinini, Q. He, R. Tiruvalam, N. Dimitratos, J. A. Lopez-Sanchez, A. F. Carley, J. K. Edwards, C. J. Kiely, G. J. Hutchings, *Langmuir* **2010**, 26, 16568–16577.

was allowed to cool down to room temperature, and the hybrid polymeric material was coagulated in methanol, deeply washed with both methanol and water, filtrated and dried under vacuum. The entrapment of the colloidal gold solution is quantitative and corresponds to a final gold content in the solid catalyst of 2 wt%.

The colloidal solutions were characterized by means of UV-Vis spectroscopy, while the colloidal AuNPs supported on PPO by WAXD analysis (Table 6.1).

Au-CTAB and Au-PVP samples show a spherical morphology of the AuNPs. For the Au-P123 and Au-PVA solutions the low intensity UV-band peak at  $\approx 370$  nm in both cases indicates the presence of  $(\text{Au})_n^{\delta+}$  small clusters<sup>146</sup>, while the signal at  $\approx 700$  nm suggests the presence of nanorods: therefore a more complex morphology for the AuNPs was achieved.

**Table 6.1:** Characterization of preliminary colloidal AuNPs samples both in solutions and supported on PPO.

Entry	Gold Colloid <sup>[a]</sup>	Immobilized Gold Colloid	$d_{\text{AuNPs}}$ (UV-Vis) [nm]	$d_{\text{AuNPs}}$ (WAXD) [nm]
1	Au-PVA	Au-PVA-PPO	6.7	10
2	Au-P123	Au-P123-PPO	11	20
3	Au-PVP	Au-PVP-PPO	4.6	-
4	Au-CTAB	Au-CTAB-PPO	8.3	5.9

In Figure 6.3 the UV-Vis spectra of the colloidal Au-PVP, Au-CTAB, Au-PVA and Au-P123 solutions are reported.

From the inspection of UV-Vis spectra of Figure 6.3, the average size of the AuNPs was calculated.<sup>64</sup> The smallest colloidal AuNPs (4.6 nm) were achieved with PVP, while the largest one (11 nm) with P123.<sup>147</sup> For the col-

<sup>146</sup> E. Genty, R. Cousin, S. Capelle, S. Siffert, *Catalysts* **2013**, 3, 966-977.

<sup>147</sup> X. Huang, X. Wang, X. Wang, X. Wang, M. Tan, M. Ding, X. Lu, *J. Catal.* **2013**, 301, 217-226.

loidal Au-PVA the average size calculated from UV-Vis was 6.7 nm, in agreement with data reported in the literature.<sup>141</sup>

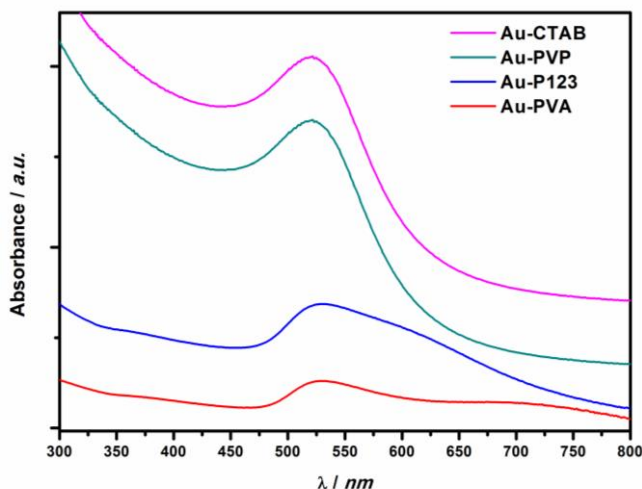


**Figure 6.3:** UV-Vis spectra of different colloidal solutions stabilized with PVA, P123, PVP and CTAB.

The immobilization was successful, except in the case of the colloidal AuNPs-PVP solution. When AuNPs are formed the polar amide groups of PVP are employed in the stabilization of the AuNPs, whereas the hydrophobic main chains are exposed at the surface of polymeric shell.<sup>148</sup> This results in a decrease in solubility of PVP in water. All samples were analysed by means of WAXD analysis (**Figure 6.4**).

After the immobilization, an increase in the AuNPs size was observed for the Au-PVA-PPO and Au-P123-PPO; actually during the immobilization step, the mobility of the AuNPs could be enhanced, favouring their sintering. In the Au-CTAB-PPO sample, a AuNPs average size of 5.9 nm was calculated (**Table 6.1**).

<sup>148</sup> P. Alexandridis, J. F. Holzwarth, T. A. Hatton, *Macromolecules* **1994**, *27*, 2414.

In order to analyse the behaviour of the stabilizers and the immobilization of the gold colloids in PPO, further investigations were carried out with PVA and P123.

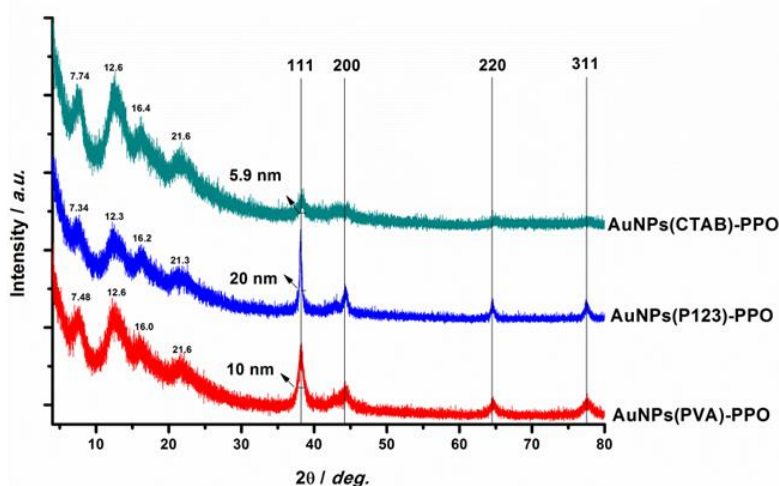


Figure 6.4: WAXD spectra of the immobilized gold colloids.

### **6.2.1: Synthesis of PVA stabilized gold colloids and immobilization on PPO**

PVA is a commercially available polymer with different grade of viscosity; it is soluble in water, and it is used in papermaking, textiles and different coatings for photographic films and food wrappings. Its  $T_m$  and  $T_g$  are 230°C and 85°C, respectively.<sup>149</sup>

In the previous paragraph, it has been demonstrated that it is possible to immobilize in PPO gold colloids stabilized with PVA. Thus, colloids having different gold concentrations have been synthesized and a different

<sup>149</sup> *Polymer Data Handbook*, J. E. Mark, Oxford University Press, 1998.

immobilization procedure has been explored. The data are reported in **Table 6.2**.

**Table 6.2:** Characterization of the colloidal AuNPs sample stabilized with PVA and supported on PPO.

Coll. Sol. (sample)	AuNPs [mM]	Solid Cat. (sample)	Immob. Temp. [°C]	$d_{\text{AuNPs}}$ (UV-Vis) [nm]	$d_{\text{AuNPs}}$ (WAXD) [nm]
Au-PVA(1)	4.6	Au-PVA(1)-PPO(1)	reflux	6.7	10
Au-PVA(2)	2.0	Au-PVA(2)-PPO(1)	reflux	3.9	3.4
Au-PVA(2)	2.0	Au-PVA(2)-PPO(2)	25°C	3.9	14

Reactions conditions: PVA (31000-50000 Da), PPO (100 mg), THF (14 mL), immobilization time=30 min, final gold content= 2 wt%.

The UV-Vis spectra of the samples AuNPs-PVA(1) and AuNPs- PVA(2) are reported in **Figure 6.5**.

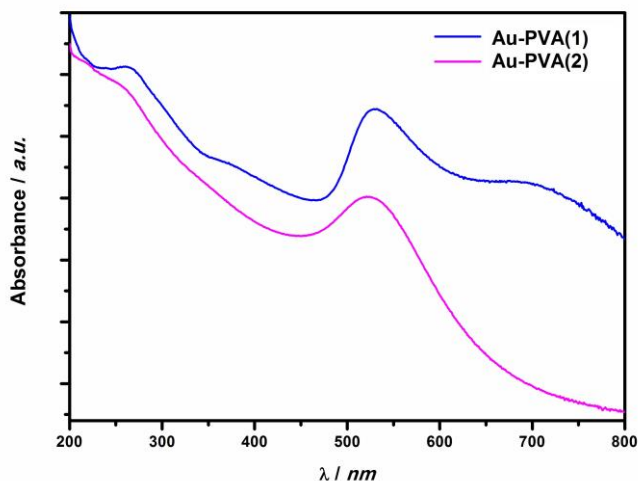


**Figure 6.5:** UV-Vis spectra of the colloidal AuNPs solutions of **Table 6.2**.

The presence of a SPR band at  $\approx 520$  nm confirms the formation of the AuNPs. The AuNPs size resulted of 6.7 nm for Au-PVA(1) and 3.9 nm for Au-PVA(2). The presence in both samples of a band at  $\approx 270$  nm is attributed to the presence of  $\text{Au}^+$  cations.<sup>146</sup> Au-PVA(2) presents spherical nanoparticles, while nanorods are present in AuNPs-PVA(1) for the presence of a SPR band at  $\approx 700$  nm. The WAXD spectra of the immobilized colloids are reported in **Figure 6.6**.

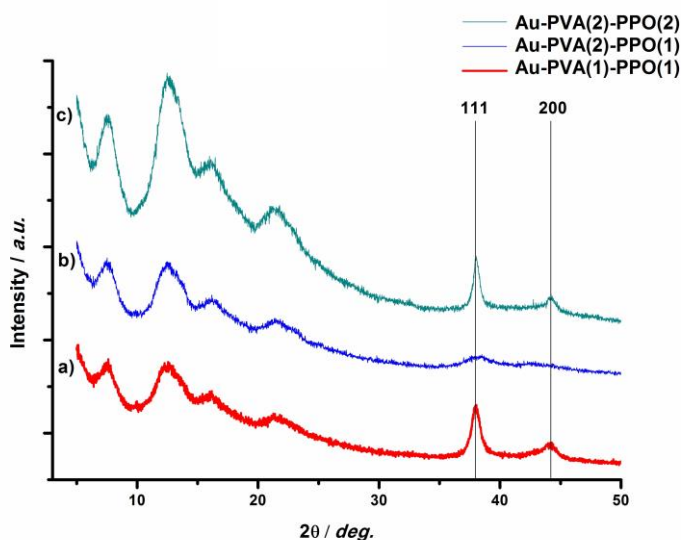


**Figure 6.6:** WAXD spectra of samples described in Table 6.2.

The decrease in the AuNPs concentration from 4.6 to 2.0 mM in the colloidal solution caused a decrease in the AuNPs size from 10 nm to 3.4 nm, respectively for the samples AuNPs-PVA(1)-PPO(1) and AuNPs-PVA(2)-PPO(1). The larger AuNPs were obtained when the addition of the colloidal solution was carried out at 25°C (AuNPs-PVA(2)-PPO(2), **Table 6.2**).

A scale up attempt of the synthetic procedure under the conditions used for the sample AuNPs-PVA(2)-PPO(1) (**Table 6.2**) was unsuccessful probably because THF is not a good solvent for PVA.<sup>149</sup>

### **6.2.2: Synthesis of P123 stabilized gold colloids and immobilization on PPO**

P123 is a poloxamer triblock copolymer consisting of the sequence of poly(ethylene glycol)-poly(propylene glycol)-poly(ethylene glycol) blocks. It is commercially available and the  $T_m$  is generally comprised in the range 34-60°C and changes at variance of the molecular weight.<sup>149</sup>

Two colloidal samples are here described: Au-P123(1) obtained in water using  $\text{NaBH}_4$  as reducing agent, and Au-P123(2) obtained in THF using  $\text{NaBHEt}_3$  as reducing agent. For the immobilization step, THF solutions of PPO were employed. The results are reported in **Table 6.3**.

The UV-Vis spectrum of Au-P123(1) is in **Figure 6.3**, whereas that of AuNPs-P123(2) is in **Figure 6.7**. The average size for the AuNPs-P123(2) is of 7.3 nm, thus slightly lower compared to that size of AuNPs-P123(1) (**Table 6.3**).

**Table 6.3:** Characterization of colloidal AuNPs sample obtained with P123 and the related supported samples on PPO.

Coll. Sol.	Reducing Agent	Supported Catalyst	$d_{\text{AuNPs}}$ (UV-Vis) [nm]	$d_{\text{AuNPs}}$ (WAXD) [nm]
Au-P123(1)	$\text{NaBH}_4$	Au-P123(1)-PPO(1)	11	20
Au-P123(2)	$\text{NaBHEt}_3$	Au-P123(2)-PPO(1)	7.3	8.9

Reaction Conditions: P123 (5800 Da), PPO (100 mg), THF (13.6 mL), Au colloidal concentration= 4.4 mM, final gold content= 2 wt%.

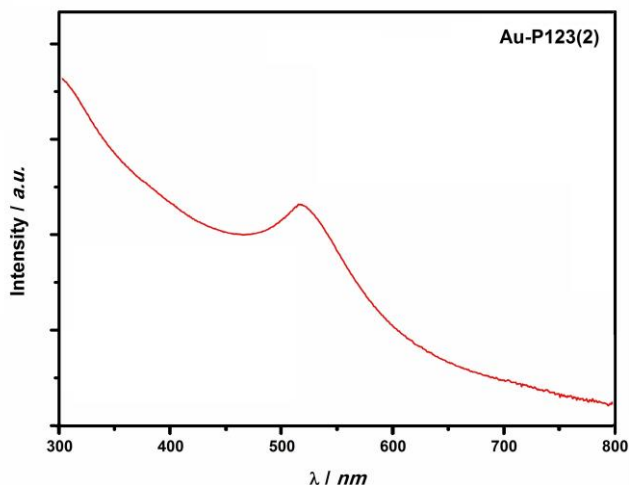


Figure 6.7: UV-Vis spectrum of Au-P123(2), Table 6.3.

After the immobilization of the two solutions onto PPO (Table 6.3) the AuNPs size in the sample Au-P123(2)-PPO(1) calculated from WAXD spectra (Figure 6.8) was 8.9 nm, whereas in AuNPs-P123(1)-PPO(1) was of 20 nm.

Moreover, from the inspection of Figure 6.8, it could be observed that Au-P123(2)-PPO(1) has an amorphous polymeric phase, while this is crystalline in Au-P123(1)-PPO(1). The analysis of the UV-Vis or WAXD spectra doesn't allow understanding if the stabilizer has been removed or not; thus, to demonstrate this, some catalytic tests were carried out.

Au-P123(1)-PPO(1) and Au-P123(2)-PPO(1) were both tested in the aerobic oxidation of benzyl alcohol.<sup>141, 147, 150</sup> The reaction was studied according the conditions already reported in literature,<sup>53, 104</sup> namely: benzyl alco-

<sup>140</sup> **a)** Y. Mikami, A. Dhakshinamoorthy, M. Alvaro, H. García, *Catal. Sci. Technol.* **2013**, 3, 58; **b)** P. Miedziak, M. Sankar, N. Dimitratos, J. A. Lopez-Sanchez, A. F. Carley, D. W. Knight, S. H. Taylor, C. J. Kiely, G. J. Hutchings, *Catal. Tod.* **2011**, 164, 315–319.

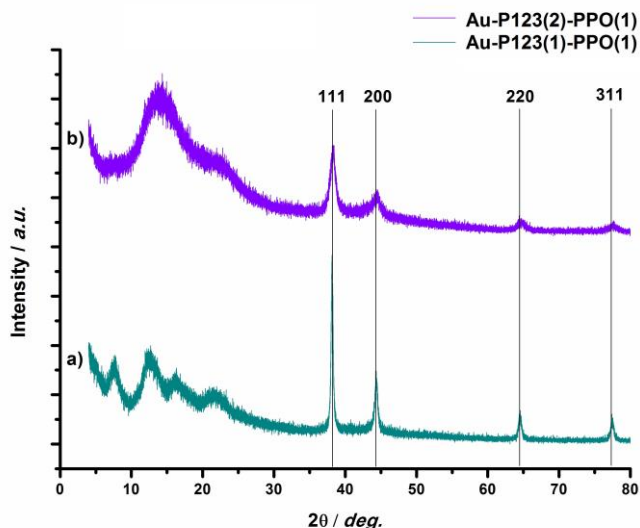


**Figure 6.8:** WAXD spectra of the samples of colloidal AuNPs solutions supported on PPO, described in [table 6.3](#).

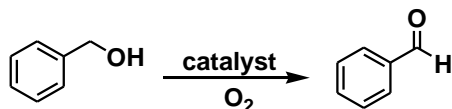
hol/Au molar ratio equal to 100 in  $\text{H}_2\text{O}:\text{CHCl}_3$ ,  $35^\circ\text{C}$  and 20 bar of  $\text{O}_2$ , in the presence of KOH as base. The results are reported in [Table 6.4](#).

Au-P123(1)-PPO(1) showed a modest catalytic activity even if the AuNPs average size was 20 nm (entry 1, [Table 6.4](#)), whereas Au-P123(2)-PPO(1) is substantially inactive

The kinetic plot of entry 1, [Table 6.4](#) is reported in [Figure 6.9](#). Benzyl alcohol was converted in benzaldehyde with a 100 *mol%* selectivity; in 6 h the conversion of benzyl alcohol was 29 *mol%* and it increased up to 52 *mol%* in 24 h.

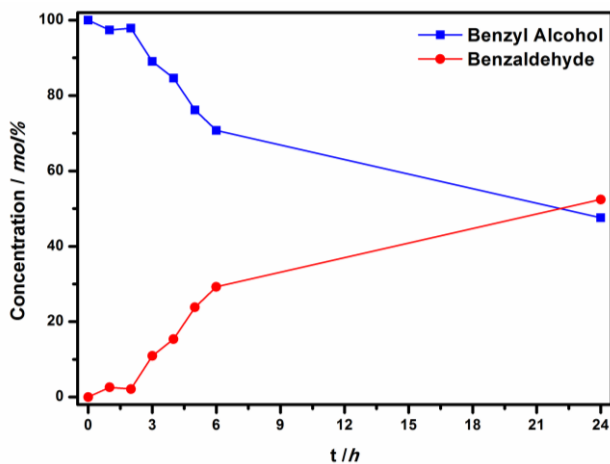
This is an interesting result, since similar catalytic systems, namely AuNPs base catalyst prepared by sol-immobilization technique, suffers of low selectivity in benzaldehyde when the particles were supported on carbon or titania.<sup>138, 141, 142</sup>

## Gold Colloids immobilized on Polymeric Support

**Table 6.4:** Aerobic oxidation of benzyl alcohol with AuNPs-P123(1)-PPO(1) and AuNPs-P123(2)-PPO(1), table 6.3.

Entry <sup>[a]</sup>	Catalyst	t [h]	Conv. <sup>[b]</sup> [mol%]	Selec. <sup>[b]</sup> [mol%]	d <sub>AuNPs</sub> (before) <sup>[c]</sup> [nm]	d <sub>AuNPs</sub> (after) <sup>[c]</sup> [nm]
1	Au-P123(1)-PPO(1)	6	29	100	20	25
		24	52	100		
2	Au-P123(2)-PPO(1)	6	0	0	8.9	9.9
		24	3.9	100		

[a] Reaction Conditions: Benzyl Alcohol (2.54 mmol), 35°C, KOH/Benzyl Alcohol=6, H<sub>2</sub>O:CHCl<sub>3</sub> (v/v=1:1, 30 mL in total), 250 mg of catalyst (2wt% of Au), benzyl alcohol/Au=100, O<sub>2</sub> (20 bar), 700 rpm. [b] Conversions and selectivities evaluated with GC-FID analysis using diglyme as internal standard.

**Figure 6.9:** Kinetic plot of benzyl alcohol oxidation, entry 1, Table 6.4.

### **6.3: Concluding remarks**

In this chapter the sol immobilization technique was explored. This synthetic approach is based on the synthesis of gold colloid and its immobilization onto a polymeric support to allow a good control in the AuNPs size.

This approach was investigated using PVA, CTAB, PVP and P123 as stabilizer for the gold colloids; thereafter these solutions were successfully immobilized onto PPO.

The catalytic tests on benzyl alcohol oxidation carried out with gold colloids stabilized with P123 and immobilized on PPO demonstrated that the stabilizer removal is a critical step in the sol immobilization technique.

Using the Au-P123(1)-PPO(1) catalyst, benzyl alcohol was converted in 52mol% with a 100 mol% in selectivity of benzaldehyde. This is an encouraging result, since catalyst prepared on this same approach but using metal oxides to immobilize the colloidal solutions, generally show lower selectivity in benzaldehyde.

In addition to that, the catalyst was stable under the reaction conditions used for the benzyl alcohol oxidation, and no increase in the AuNPs size was detected.

# CONCLUDING REMARKS

AuNPs supported onto a porous polymeric host phase (AuNPs-sPSB) have been successfully tested in redox reactions under mild conditions.

The AuNPs-sPSB catalyst showed high activity and selectivity both in the aerobic oxidative esterification of cinnamyl alcohol and nitroarenes reduction with  $\text{NaBH}_4$ . The role of the polymeric matrix was to determine which species can have access to the catalytic active site. The catalysts having a nanoporous polymeric phase, e.g. **Au-C $\delta$**  and **Au-C $\epsilon$**  showed high catalytic activities, whereas **Au-C $\gamma$**  and **Au-C $\beta$**  were inactive.

The efficient and selective aerobic oxidation of cinnamyl alcohol and para-substituted derivatives, such as *p*-chloro and *p*-methoxy cinnamyl alcohol to the corresponding aldehydes has been successfully achieved. Cinnamyl alcohols are rapidly oxidized to alkyl cinnamates using a primary or secondary alkyl alcohol. The kinetic investigation of these reactions showed that cinnamyl alcohol oxidation to cinnamaldehyde was a first order reaction respect to the alcohol as result of its fast permeation within the polymeric matrix. The second step of the reaction, namely the esterification of cinnamaldehyde, is diffusion controlled since the alkyl alcohols used don't permeate easily into the polymer matrix.

In order to gain informations on the role of porosity within the polymeric matrix, the polymorphic AuNPs-sPSB catalyst has been synthesized under four different crystalline forms and tested in nitrobenzene reduction to aniline using  $\text{NaBH}_4$  as reductant. The AuNPs-sPSB catalysts having polystyrene moieties in the porous  $\delta$  and  $\epsilon$  form are very effective and selective producing NB reduction to aniline at 35°C in 60 e 45 min, respectively. On the contrary, poor catalytic activity was detected using AuNPs-sPSB catalysts with the polystyrene moieties in the compact  $\beta$  and  $\gamma$  forms, as results of the difficult access of the reagent towards the AuNPs. A *condensation route* was found for the overall transformation of nitrobenzene into aniline, and azoxybenzene and azobenzene were obtained as intermediates. It should be underlined that the azoxybenzene formation can be achieved also outside the polymeric matrix. The reaction pathway is in agreement with a Langmuir–Hinshelwood mechanism where the hydride species and the nitroarene to be reduced compete for the same catalytic site on the surface of the AuNPs.

Gold colloids having nanometric dimensions and synthesized with different stabilizers have been efficiently immobilized on PPO. The effectiveness of the stabilizer removal can be evaluated simply by catalytic tests. Benzyl alcohol oxidation was efficiently oxidized to benzaldehyde with selectivities high compared to the data already reported in literature for similar catalysts.

# CHAPTER 7



## EXPERIMENTAL SECTION



## **7.1: General Procedure and Materials**

The manipulation of air and moisture sensitive compounds was performed under nitrogen atmosphere using Schlenk techniques. THF used for the synthesis of the AuNPs-sPSB was used as received and pre-dried with potassium hydroxide, refluxed 48h over sodium and benzophenone and distilled before use.

The following reagents or solvents were used as received: HAuCl<sub>4</sub>·3H<sub>2</sub>O (Sigma-Aldrich), NaBHET<sub>3</sub> (1M in THF, Sigma-Aldrich), methanol (HPLC grade for catalytic tests, Sigma-Aldrich), water (HPLC grade for catalytic tests, Panreac), acetonitrile (HPLC grade, Sigma-Aldrich), chloroform (HPLC grade for catalytic tests, Romil), 2-butanone (99.5%, Carlo Erba), ethyl acetate (≥99.5%, Sigma-Aldrich), cyclohexanone (≥99.5%, Sigma-Aldrich), toluene (99.5%, Sigma-Aldrich), cinnamyl alcohol (97%, Fluka), cinnamaldehyde (98%, Carlo Erba), *p*-methoxycinnamaldehyde (96%, SAFC), *p*-chlorocinnamaldehyde (96%, Aldrich), *p*-dimethylaminobenzaldehyde (98%, Sigma-Aldrich), potassium hydroxide (99.9%, Sigma-Aldrich), anisole (99%, Sigma-Aldrich), 1-butanol (98%, Labscan), ethanol (99.8%, Fluka), 2-propanol (99.8%, Sigma-Aldrich), 1-hexanol (98%, Sigma-Aldrich), 1-octanol (>99%, Sigma-Aldrich), 2-phenylethanol (≥99.0%, Sigma-Aldrich), linalool (97%, Aldrich), PPO (powder, Aldrich), CTAB (98%, Sigma-Aldrich), PVA (Sigma-Aldrich), PVA (Sigma-Aldrich), P123 (Sigma-Aldrich), NaBH<sub>4</sub> (≥96%, Sigma-Aldrich), water (HPLC grade, Panreac), diglyme (99.5%, Sigma-Aldrich), 1-phenylethanol (98%, Sigma-Aldrich), CCl<sub>4</sub> (99%, Sigma-Aldrich), 1-propanol (≥99.5%), 1-butanol (98%), anisole (99%), nitrobenzene (>99.5%), 4-nitrobenzyl alcohol (99%), 4-nitrobenzaldehyde (98%), 4-nitroaniline (≥99%), 4-nitrotoluene (99%), 4-nitroanisole (99%), 4-chloronitrobenzene (99%), 1,2-dichloro-4-nitrobenzene (99%), 4-nitrobenzoic acid (>98%), 4-nitrophenol (≥99%), *p*-methoxycinnamyl alcohol, *p*-chlorocinnamyl alco-

hol and *p*-dimethylaminobenzyl alcohol were synthesised by reduction of the corresponding aldehydes by literature methods.<sup>151</sup>

Oxygen and nitrogen were supplied by Rivoira and used as received.

## **7.2: Instruments and Samples Preparation**

### **7.2.1: AAS and ICP-OES**

AAS analysis was performed on a PerkinElmer AAnalyst 100 spectrophotometer using an Au hollow cathode lamp (Perkin–Elmer). ICP-OES was performed on a Perkin–Elmer Optima 7000 DV instrument). The sample for the AAS and ICP-OES analysis was prepared as follow.

0.0500 g of the sample were digested in a Kjeldahal apparatus through treatment with 2.5 mL of H<sub>2</sub>SO<sub>4</sub> (98 wt%) at 250°C for 30 min and then with H<sub>2</sub>O<sub>2</sub> (35 wt%) at room temperature. The solution was heated at 250°C producing a colourless solution. 1.5 mL of aqua regia were added at room temperature and the solution was diluted until the final volume of 10 mL with a HCl solution (10 v%). The resulting solution was analysed with AAS and ICP-OES. The calibration was obtained preparing seven solutions having defined concentration through dilutions of a standard solution of Au(III) (1.000±0.002 g/L in water with 2 wt% of HCl) with water and a solution of HCl (10 v%).

### **7.2.2: WAXD analysis**

WAXD patterns were obtained in reflection mode with an automatic Bruker D8 powder diffractometer and nickel-filtered CuK $\alpha$  radiation.

The catalyst samples were prepared by drying at 35°C under vacuum for 12 h.

The average size of AuNPs was obtained by considering the Scherrer equation ( $D=K/\Gamma\cos\theta$ ) where **D** is the weighted average diameter of Au(0) crystallites, **K** is a constant (=1.4476°) which depends from the crys-

---

<sup>151</sup> N. Usami, K. Kitahara, S. Ishikura, M. Nagano, S. Sakai, A. Hara, *Eur. J. Biochem.* **2001**, 268, 5755–5763.

tallite shape and wavelength of the X-Ray,  $\Gamma$  and  $\theta$  are the full width at half maximum and Bragg angle of the (111) peak of Au(0).<sup>67</sup>

### **7.2.3: TEM and SEM analysis**

TEM analysis was carried out with a Tecnai 20 (FEI) microscope operating at 200 kV. The specimens for TEM analysis were sonicated in 2-propanol, then transferred (10 mL) onto a copper grid covered with a lacey carbon film supplied from Assing. The size distribution analysis of the AuNPs was performed with the software Photoshop CS5 Extended. SEM analyses were carried out with a scanning electron microscope (Zeiss). SEM analysis were carried out with a scanning electron microscope (Zeiss).

### **7.2.4: N<sub>2</sub> sorption analysis**

N<sub>2</sub> adsorption at liquid nitrogen temperature (77K) was used to measure surface areas of the AuNPs-SPSB samples with a Nova Quantachrome 4200e instrument.

The powder samples were weighted accurately and degassed at 40°C under vacuum for 24h. The specific surface area of the polymers was calculated using the Brunauer–Emmet–Teller (BET) method.

### **7.2.5: GC analysis**

GC analysis were performed with a GC-MS 7890A/5975C chromatograph, equipped with a HP-Innowax column (polyethylene glycol, 30m, 0.25 mm ID) or Optima 17MS column (1:1 diphenylpolysiloxane/dimethylpolysiloxane, 30m, 0.25mm, ID), a mass-selective detector and a FID detector.

The samples for the GC analysis were taken directly from the reaction medium ( $\approx 0.3$  mL) and diluted in 2 mL of methanol to allow the precipitation of the catalyst. The resulting solution was filtered and 1 mL was effectively used for the final analysis.

The following instrumental parameters were generally used:

- Injector Temperature: 270°C
- Oven: 60°C, 10°C/min to 270°C, 300°C for 10min
- Aux Temperature: 300°C

### **7.2.6: NMR analysis**

NMR spectroscopy was performed on Avance Bruker spectrometers (600, 400, 300 and 250 MHz for  $^1\text{H}$ ). Deuterated solvents were purchase from Euriso-Top or Sigma-Aldrich and used as received.

Considering nitroarenes reduction, the preparation of the samples is reported hereafter.

0.5 mL of solution was taken directly from the reaction medium and filtered.  $\text{CD}_2\text{Cl}_2$  was generally used as deuterated solvent.

### **7.2.7: UV-Vis analysis**

UV-VIS absorbance analyses were performed in 10.0mm quartz cuvette in the range 200-820nm (Instrument Mod. Evolution 220, Thermo Scientific, UK). About 1 mL of the gold colloid was used for the UV-Vis analysis. Instrument settings were: bandwidth 2nm, integration time 0.01s, data interval 0.20nm and scan speed 1200nm.

## **7.3: General procedures for the synthesis of the AuNPs-sPSB catalyst**

Multiblock copolymers syndiotactic polystyrene-*co*-1,4-*cis*-polybutadiene (sPSB)<sup>72</sup> and the AuNPs-sPSB catalysts<sup>53</sup> were synthesized according the procedures already reported in literature. Briefly: a 1 L round-bottomed three-necked flask equipped with a magnetic stirring bar was charged with anhydrous THF (650 mL) and finely grounded sPSB (5.00 g). The mixture was stirred for 24 h at room temperature and then heated to reflux for 1 h to reach the complete swelling of the polymer.  $\text{HAuCl}_4 \cdot 3\text{H}_2\text{O}$  (0.220 g; 0.56 mmol) was added at room temperature and the resulting slurry kept under agitation for 24 h, then refluxed for 1 h. A THF solution of sodium triethylborohydride (10 mL, 1.0 M) was added at 25 °C

producing a rapid change of the colour from pale yellow to red. The polymer was rapidly precipitated in a plenty of methanol, recovered by filtration, washed with fresh methanol and dried in vacuo at room temperature (Au-sPSB catalyst; 2 wt% Au).

### **7.3.1: Synthesis of the AuNPs-sPSB catalyst and Au-C $\delta$ , Au-C $\beta$ , Au-C $\gamma$ and Au-C $\epsilon$**

The thermal annealing on a hot plate of Au-C $\delta$  at 170°C for 5 h afforded Au-C $\beta$  catalyst, while Au-C $\gamma$  was obtained treating Au-C $\delta$  at 135°C for 2 hours. The Au-C $\epsilon$  catalyst was obtained through solvent treatment of Au-C $\beta$  at with CHCl<sub>3</sub>/H<sub>2</sub>O (*v/v*=1/1) solvent mixture for 24 h.

## **7.4 General procedure for the synthesis of the colloidal gold solutions**

To an aqueous HAuCl<sub>4</sub> solution of the desired concentration, the required amount of a stabilizer solution (1 wt %) was added (Stabilizer/Au) (*w/w*=1.2); a freshly prepared solution of NaBH<sub>4</sub> (0.1 M, NaBH<sub>4</sub>/Au=5, molar ratio) was then added to form a dark-brown sol.

## **7.5: General procedure for the immobilization of the gold colloidal solutions on PPO**

PPO solution was stirred for 24 h at r.t., then heated under reflux for 1 h. The right amount of the colloidal solution was added drop to drop, and the whole solution was still stirred for 30 m, then it was cooled down at r.t., coagulated in MeOH, washed deeply with MeOH and water, filtrated and dried under vacuum.

## **7.6: General procedures adopted for the catalytic tests**

### **7.6.1: General procedure for the oxidation of cinnamyl**

## **alcohols**

A round-bottom two-necked flask (50 mL) equipped with a magnetic stirrer bar was charged, in the order noted, with H<sub>2</sub>O (3 mL), KOH (172 mg, 3.06 mmol), anisole (55 mL, 0.51 mmol), cinnamyl alcohol (66 mg, 0.51 mmol), CHCl<sub>3</sub> (3 mL) (3 mL) or other different co-solvent (table 4.3) and catalyst (200 mg). The mixture was stirred at 35 °C under atmospheric pressure of O<sub>2</sub>. Aliquots of the reaction mixture were sampled at the desired reaction time and treated with plenty of acetonitrile. The polymer was separated by filtration and the filtrate was analysed by GC-MS. At the end of the reaction, the polymer was coagulated in plenty of acetonitrile. The catalyst was recovered by filtration and the filtrate analysed by GC-MS.

### **7.6.2: General procedure for direct esterification of cinnamyl alcohol**

A round-bottomed two-necked flask (50 mL) equipped with a magnetic stirrer bar was charged, in the order noted, with H<sub>2</sub>O (3 mL), KOH (172 mg, 3.06 mmol), anisole (55 mL, 0.51 mmol), cinnamyl alcohol (66 mL, 0.51 mmol), 1-butanol (470 mL, 5.1 mmol) or another alkyl alcohol, CHCl<sub>3</sub> (3 mL) and catalyst (200 mg). The mixture was stirred at 35°C under atmospheric pressure of O<sub>2</sub>. Aliquots of the reaction mixture were sampled at the desired reaction time and treated with plenty of acetonitrile. The polymer was separated by filtration and the filtrate was analysed by GC-MS.

At the end of reaction, the polymer was coagulated in plenty of acetonitrile. The catalyst was recovered by filtration and the filtrate analysed by GC-MS.

### **7.6.3: General procedure for direct esterification of cinnamaldehyde**

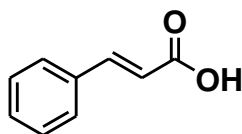
A round-bottomed two-necked flask (50 mL) equipped with a magnetic stirrer bar was charged, in the order noted, with H<sub>2</sub>O (3 mL), KOH (172

mg, 3.06 mmol), anisole (55 mL, 0.51 mmol), freshly distilled cinnamaldehyde (66 mL, 0.51 mmol), alkyl alcohol (5.1 mmol),  $\text{CHCl}_3$  (3 mL) and catalyst (200 mg). The mixture was stirred at  $35^\circ\text{C}$  under atmospheric pressure of  $\text{O}_2$ . Aliquots of the reaction mixture were sampled at the desired reaction time and treated with plenty of acetonitrile. The polymer was separated by filtration and the filtrate was analysed by GC-MS and  $^1\text{H}$  NMR spectroscopy. At the end of reaction, the polymer was coagulated in plenty of acetonitrile. The catalyst was recovered by filtration and the filtrate analysed by GC-MS.

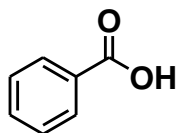
#### 7.6.4: General procedure the aerobic cleavage of double bond of cinnamaldehyde

Cinnamaldehyde (0.260 mL, 2.03 mmol), KOH (3.07 mmol, 172 mg), were added in a high-pressure vessel;  $\text{D}_2\text{O}$  (6 mL) and  $\text{CD}_3\text{CN}$  (1 mL) were added and the vessel was purged with  $\text{O}_2$  (25 bar). An aliquote of the reaction mixture was taken from the vessel, centrifuged and analysed via NMR.

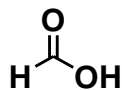
The diagnostic signals of products are here reported.



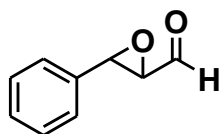
Cinnamic Acid  $^1\text{H}$ -NMR (600 MHz,  $\text{CD}_3\text{CN}$ ): 6.6 (d,  $J=16.0\text{Hz}$ , 1H).  $^{13}\text{C}$ -NMR (150 MHz,  $\text{CD}_3\text{CN}$ ): 177.8 (cinnamate), 176.0, 123.6.



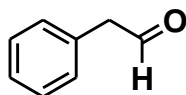
Benzoic Acid  $^1\text{H}$ -NMR (600 MHz,  $\text{CD}_3\text{CN}$ ): 7.9 (m, 2H).  $^{13}\text{C}$ -NMR (150 MHz,  $\text{CD}_3\text{CN}$ ): 180.5 (benzoate), 175.6, 130.4, 129.6, 123.6



Formic Acid  $^1\text{H-NMR}$  (600 MHz,  $\text{CD}_3\text{CN}$ ): 8.5 (s, 1H).  $^{13}\text{C-NMR}$  (150 MHz,  $\text{CD}_3\text{CN}$ ): 166.5.



3-phenyloxirane-2-carbaldehyde.  $^1\text{H-NMR}$  (600 MHz,  $\text{CD}_3\text{CN}$ ): 3.5 (d,  $J=2.16$  Hz, 1H), 4.0 (d,  $J=2.10$  Hz, 1H), 9.5 (d,  $J=8.2$  Hz, 1H).  $^{13}\text{C-NMR}$  (150 MHz,  $\text{CD}_3\text{CN}$ ): 58.1, 59.8, 197.0.

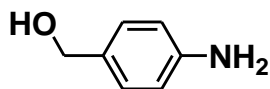


Phenylacetaldehyde.  $^1\text{H-NMR}$  (600 MHz,  $\text{CD}_3\text{CN}$ ): 3.9 (s, 2H), (9.9 (s, 1H).  $^{13}\text{C-NMR}$  (150 MHz,  $\text{CD}_3\text{CN}$ ): 62.2, 199.2.

### **7.6.5: General procedure for nitroarenes reduction**

The catalyst (50 mg), methanol (6 mL), nitrobenzene (2.54 mmol), anisole as internal standard (0.51 mmol) and  $\text{NaBH}_4$  (15.2 mmol) were added in the order in a 50 mL round-bottom flask equipped with a condenser under the protective atmospheric pressure of  $\text{N}_2$ . The mixture was stirred at  $35^\circ\text{C}$  and aliquots of the reaction mixture were sampled at the desired reaction time. The catalyst was separated by filtration and the filtrate analysed by GC-MS and NMR spectroscopy. At the end of reaction, the polymer was coagulated in a plenty of methanol, the catalyst recovered by filtration and the filtrate analysed by GC-MS and  $^1\text{H-NMR}$ .

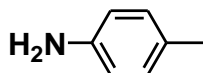
The  $^1\text{H-NMR}$  diagnostic signals of products analysed via NMR are here reported.

4-aminobenzyl alcohol

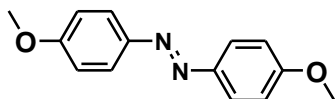
$^1\text{H-NMR}$  (300 MHz,  $\text{CD}_2\text{Cl}_2$ ): 7.04 (d, 2H,  $J=8.0$  Hz), 6.60 (d, 2H,  $J=8.0$  Hz), 4.40 (s, 2H), 3.52 (br s, 2H).

4-aminoaniline

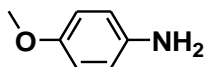
$^1\text{H-NMR}$  (250 MHz,  $\text{CD}_2\text{Cl}_2$ ): 6.55 (s, 4H), 3.77 (br s, 2H).

4-toluidine

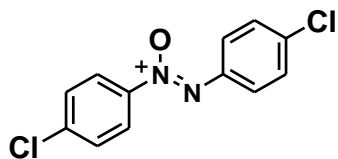
$^1\text{H-NMR}$  (400 MHz,  $\text{CD}_2\text{Cl}_2$ ): 6.86 (d, 2H,  $J=8.0$  Hz), 6.55 (d, 2H,  $J=8.2$  Hz), 3.88 (br s, 2H), 2.14 (s, 2H).

4,4'-dimethoxyazobenzene

$^1\text{H-NMR}$  (300 MHz,  $\text{CD}_2\text{Cl}_2$ ): 8.16 (m, 4H), 6.92 (m, 4H), 3.79 (s, 6H).

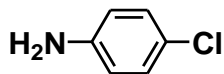
4-anisidine

$^1\text{H-NMR}$  (300 MHz,  $\text{CD}_2\text{Cl}_2$ ): 6.6 (m, 4H), 3.64 (s, 3H), 3.55 (br s, 2H)].



4,4'-dichloroazoxybenzene

$^1\text{H-NMR}$  (300 MHz,  $\text{CD}_2\text{Cl}_2$ ): 8.19 (d, 2H,  $J=8.4$  Hz), 8.10 (d, 2H,  $J=8.8$  Hz), 7.45 (d, 2H,  $J=8.4$  Hz), 7.39 (d, 2H,  $J=8.8$  Hz)].



4-chloroaniline

$^1\text{H-NMR}$  (300 MHz,  $\text{CD}_2\text{Cl}_2$ ): 6.95 (d, 2H,  $J=8.7$  Hz), 6.59 (d, 2H,  $J=8.7$  Hz), 3.55 (br s, 2H)].